

This is an Open Access document downloaded from ORCA, Cardiff University's institutional repository: <https://orca.cardiff.ac.uk/id/eprint/154277/>

This is the author's version of a work that was submitted to / accepted for publication.

Citation for final published version:

Meng, Fanchao, Tian, Yulu, Kerr, Andrew C. , Wang, Wei, Wu, Zhiping, Xu, Qiang, Du, Qing, Zhou, Yaoqi and Liu, Jiaqi 2023. Geochemistry and petrogenesis of Late Permian basalts from the Sichuan Basin, SW China: Implications for the geodynamics of the Emeishan mantle plume. *Journal of Asian Earth Sciences* 241 , 105477. [10.1016/j.jseaes.2022.105477](https://doi.org/10.1016/j.jseaes.2022.105477)

Publishers page: <http://dx.doi.org/10.1016/j.jseaes.2022.105477>

Please note:

Changes made as a result of publishing processes such as copy-editing, formatting and page numbers may not be reflected in this version. For the definitive version of this publication, please refer to the published source. You are advised to consult the publisher's version if you wish to cite this paper.

This version is being made available in accordance with publisher policies. See <http://orca.cf.ac.uk/policies.html> for usage policies. Copyright and moral rights for publications made available in ORCA are retained by the copyright holders.



[Click here to view linked References](#)

1 **Geochemistry and petrogenesis of Late Permian basalts from**  
2 **the Sichuan Basin, SW China: Implications for the**  
3 **geodynamics of the Emeishan mantle plume**

4

5 **Fanchao Meng<sup>a,b,c\*</sup>, Yulu Tian<sup>a,b,c</sup>, Andrew C. Kerr<sup>d\*</sup>, Wei Wang<sup>e</sup>, Zhiping Wu<sup>a,b,c</sup>,**  
6 **Qiang Xu<sup>f</sup>, Qing Du<sup>a,b,c</sup>, Yaoqi Zhou<sup>a,b,c</sup>, Jiaqi Liu<sup>g</sup>**

7

8 a. School of Geosciences, China University of Petroleum (East China), Qingdao 266580, China

9 b. Pilot National Laboratory for Marine Science and Technology (Qingdao), Qingdao 266061,  
10 China

11 c. Shandong Provincial Key Laboratory of Deep Oil and Gas, China University of Petroleum (East  
12 China), Qingdao 266580, China

13 d. School of Earth and Environmental Sciences, Cardiff University, Cardiff, Wales CF10 3AT,  
14 United Kingdom

15 e. Exploration and development Research Institute of Southwest Oil and Gas Field Company,  
16 PetroChina, Chengdu 610041, China

17 f. School of Geoscience and Technology, Southwest Petroleum University, Chengdu 610500, China

18 g. Institute of Geology and Geophysics, Chinese Academy of Sciences, Beijing 100029, China

19

20 **Abstract**

21 Plume-lithosphere interactions are significant in the formation of Large Igneous  
22 Provinces (LIPs). The Permian Emeishan Large Igneous Province (ELIP) is considered  
23 to be the result of a mantle plume. The Emeishan flood basalts comprise a major part  
24 of the ELIP and they define three zones: the inner, intermediate and outer zones. Both  
25 high-Ti and low-Ti basalts are present in the inner zone, whereas only high-Ti basalts  
26 are found in the intermediate zone and outer zone. However, there are only sparse  
27 outcrops in the outer zone, and so geochemical data on basalts from the outer zone are

---

\* Corresponding author.

E-mail address: [mengfc@upc.edu.cn](mailto:mengfc@upc.edu.cn) (Fanchao Meng), [kerra@cf.ac.uk](mailto:kerra@cf.ac.uk) (Andrew C. Kerr).

28 rare and the role of plume-lithosphere interaction in the petrogenesis of volcanic rocks  
29 in the outer zone remains poorly understood. In the Sichuan basin, the Basalt Formation  
30 is found between the Permian Maokou Formation limestone and the Longtan Formation  
31 marl in some drill cores as well as in outcrops in the basin. This relationship  
32 demonstrates that the basaltic layer in the basin is part of the Emeishan flood basalts.  
33 These basalts have  $\text{TiO}_2$  contents of 3.7-4.2 wt.% and Ti/Y ratios of 604-720, being  
34 high-Ti sub-alkaline basalts. They display chondrite-normalized rare earth elements  
35 (REE) patterns enriched in light rare earth elements (LREE) relative to heavy rare earth  
36 elements (HREE) and have elevated large ion lithophile elements (LILE) and high field  
37 strength elements (HFSE). Lead isotope ratios are high ( $^{206}\text{Pb}/^{204}\text{Pb}(t) = 18.102\text{-}18.392$ ,  
38  $^{207}\text{Pb}/^{204}\text{Pb}(t) = 15.578\text{-}15.606$ ,  $^{208}\text{Pb}/^{204}\text{Pb}(t) = 38.410\text{-}38.850$ ), and  $\epsilon_{\text{Nd}}(t)$  values are -  
39 0.38~1.17. Detailed petrology and geochemistry suggest that the high-Ti basalts from  
40 the Sichuan Basin did not experience significant contamination of crustal and  
41 lithospheric mantle material during the ascent of magma. We infer that these basalts  
42 resulted from low-degree melting of the plume mantle source and underwent fractional  
43 crystallization of clinopyroxene. The distribution and petrogenesis of the Sichuan Basin  
44 basalts in the outer zone are different from those of the basalts in the inner zone and  
45 there are clearly different plume-lithosphere interactions in different parts of the ELIP.  
46 In the inner zone, the temperature of the lithosphere mantle was markedly elevated due  
47 to underplating of the mantle plume, causing a substantial quantity of lithosphere  
48 mantle melting and the initial formation of low-Ti basalts. This was followed by melting  
49 of the mantle plume and the formation of high-Ti basalts. In the outer zone, lower  
50 temperatures further from the plume centre were insufficient to generate extensive  
51 melting of the lithospheric mantle. Consequently, only the mantle plume melted in the  
52 outer zone, resulting in the formation of high-Ti basalts with minimal lithospheric input.

53 **Keywords:** Emeishan mantle plume, outer zone, Sichuan Basin basalts, petrogenesis  
54 of high-Ti basalts, plume-lithosphere interaction

55

## 56 **1. Introduction**

57 The Emeishan Large Igneous Province (ELIP) in the Upper Yangtze craton,  
58 Southwest China is composed mainly of Late Permian flood basalts, mafic-ultramafic  
59 intrusions and mafic dykes, along with lesser amounts of felsic volcanic rocks,  
60 pyroclastic counterparts, and alkaline rocks. The stratigraphy, chronology,  
61 geochemistry and geophysics of the ELIP has been studied in detail for many years and  
62 has been proposed to have formed by melting of a mantle plume (Chen et al., 2015; Liu  
63 et al., 2017; Shellnutt, 2014; Xiao et al., 2003; Xu et al., 2020; Xu et al., 2021; Zhang  
64 et al., 2008; Zhou et al., 2022). The Emeishan continental flood basalts have been  
65 broadly divided into two groups: a high-Ti series ( $\text{TiO}_2 > 2.5 \text{ wt.}\%$  and  $\text{Ti/Y} > 500$ ) and  
66 a low-Ti series (He et al., 2007; Song et al., 2008).

67 Geographically, the ELIP has been divided into inner, intermediate and outer  
68 zones based on geochemical, sedimentological, and biostratigraphic characteristics of  
69 the rock units (He et al., 2003; Xiao et al., 2004; Xu et al., 2014). The rocks in the inner  
70 zone include both the high-Ti and low-Ti series, which are widely distributed in the  
71 Binchuan, Jianchuan, Lijiang and Ertan areas, whereas rocks in the intermediate and  
72 outer zones are dominated by high-Ti basalts (Li et al., 2017a; Liao, et al., 2012; Xiao  
73 et al., 2004; Xu et al., 2001, 2004). Basalts are much more extensively exposed in the  
74 intermediate zone (in Zhaotong, Qiaojia and Dongchuan) than in the outer zone (Tian  
75 et al., 2021; Xu et al., 2001; Zhang et al., 2011). The outer zone does have some well-  
76 developed outcrops in Guangxi and Guizhou provinces (Liao et al., 2012; Xiao et al.,

77 2004; Xu et al., 2001, 2004).

78 There are three major petrogenetic models for the Emeishan basalts: 1) High-Ti  
79 basalts were derived from low-degree partial melting of the mantle plume (Cheng et al.,  
80 2019; Liang et al., 2021; Wang et al., 2007; Xiao et al., 2004; Xu et al., 2001), whereas  
81 the low-Ti basalts were generated from the sub-continental lithosphere mantle (SCLM),  
82 possibly with assimilation of some upper crust (Fan et al., 2008; Kamenetsky et al.,  
83 2012; Li et al., 2010; Song et al., 2008; Wang et al., 2007; Xiao et al., 2004); 2) High-  
84 Ti basalts were derived from the SCLM or mixed with lithospheric mantle materials  
85 during magma ascent, whereas the low-Ti basalts were generated from the mantle  
86 plume (Xu et al., 2007); 3) High-Ti and low-Ti basalts have the same mantle source  
87 and may represent different degrees of partial melting, fractional crystallization and/or  
88 crustal contamination (Dong et al., 2009; Hou et al., 2011; Ren et al., 2017; Zhang et  
89 al., 2019). A common feature of all models is that the lithosphere is most influential at  
90 the centre of the Emeishan mantle plume (Li et al., 2015; Song et al., 2001, 2008; Xiao  
91 et al., 2004; Xu et al., 2001, 2014; Zhang et al., 2006).

92 These previous studies, however, have mainly focused on the inner and  
93 intermediate zones and although there have been some more recent studies of igneous  
94 rocks in the outer zone (Li et al., 2017a; Liu et al., 2017; Liu et al., 2022), there is still  
95 a lack of information on the source of the Emeishan high-Ti basalts and comparison  
96 between the inner and outer zones. For instance, it is still unclear whether there was  
97 plume-lithosphere interaction in the outer zone of the ELIP.

98 In this paper, we investigate the petrology, major and trace elements, and Sr-Nd-  
99 Pb isotope systematics of eighteen samples from three boreholes (twelve samples) and  
100 three outcrops (six samples) within and around the Sichuan Basin belonging to the outer  
101 zone of the ELIP in order to assess their petrogenesis. This data is combined with

102 previously published data from the inner and outer zones in order to ascertain the nature  
103 of plume-lithosphere interaction and the influence of the Emeishan mantle plume over  
104 the whole province, especially the difference between the inner and outer zones.

105

## 106 **2. Geological background**

107 The ELIP is located on the western Yangtze Plate and to the east of the Qinghai-  
108 Tibet Plateau, and mainly erupted in 260~257 Ma (Fan et al., 2008; Huang et al., 2022;  
109 Li et al., 2015; Shellnutt et al., 2012; Zhong et al., 2014). Traditionally, the ELIP has  
110 been thought to be bounded on the northeast and southeast by the Baoxing-Yibin fault  
111 and the Mile-Shizong fault, respectively. The eastern boundary is situated in the  
112 Fuquan-Weng'an areas, eastern Guiyang, China. The northwestern and southwestern  
113 boundaries are the Longmenshan belt and the Jinshajiang-Ailaoshan-Red River fault,  
114 respectively (Chung et al., 1998; Li et al., 2016a; Xiao et al., 2003). Tectonic  
115 movements occur in the region, with a series of well-developed north-trending faults,  
116 such as the Anninghe fault, the Longmenshan fault and the Xianshuihe fault (Song et  
117 al., 2001; Yan et al., 2018a; Yan et al., 2018b) (Fig. 1). The basement of the ELIP is  
118 dominated by Mesoproterozoic metamorphic rocks (Zhai et al., 1986), overlying Pre-  
119 Sinian-Cenozoic strata.

120 The Emeishan volcanic sequence is mainly composed of flood basalts and  
121 contemporaneous ultramafic-felsic plutons, layered mafic-ultramafic intrusions and  
122 radiating mafic dyke swarms (Li et al., 2015; Liu et al., 2022; Shellnutt, 2014; Xu et al.,  
123 2001; Zhou et al., 2022). The Emeishan flood basalts range from a few hundred to five  
124 thousand meters in thickness (Xiao et al., 2003; Xu et al., 2001; Zhang et al., 2001) and  
125 the areal extent of the basalts may well be larger than  $1 \times 10^6$  km<sup>2</sup> (Li et al., 2017a; Liu

126 et al., 2022). The thickness of the basalts gradually decreases from the inner zone to the  
127 outer zone (Chung et al., 1998; Xu et al., 2001; Zhu et al., 2018). The inner zone consists  
128 of a variety of lavas and pyroclastic rocks, including picrites, basalts, basaltic andesites  
129 and basaltic pyroclastic rocks, with trachytic and rhyolite tuff in the uppermost part of  
130 the sequence (Xiao et al., 2004; Xu et al., 2001, 2004). A more-restricted range of rocks  
131 is found in the intermediate and outer zones and includes tholeiites and alkaline basalts  
132 (He et al., 2010).

133 The Sichuan Basin, located in the northeast (outer zone) of the ELIP in the  
134 northwestern Yangtze Craton in the South China Block, is a typical superimposed basin  
135 common in southwestern China (Liu et al., 2021a). The Late Permian basalt outcrops  
136 of the ELIP have only been found in a few places (Jinding, Huayingshan and Yanghe)  
137 in the Sichuan Basin (e.g., Li et al., 2017a; Liang et al., 2021; Liu et al., 2021a). The  
138 lack of volcanic outcrops in this region can be attributed to the complex burial history  
139 of the Sichuan Basin, and this has made geochemical research difficult on the Emeishan  
140 basalts in the basin. However, abundant drill cores from the Sichuan Basin indicate that  
141 the Emeishan basalts are widely distributed between the Middle and Upper Permian  
142 strata (Liang et al., 2021). Based on seismic and drilling data, it has been proposed that  
143 basalts are mainly distributed in the western Sichuan Basin with a thickness of 40-500  
144 m, which thins from the southwest to northeast (Fig. 2) (Liu et al., 2021a; Tian et al.,  
145 2017). However, the geochemistry and petrogenesis of the basalts in the Sichuan Basin  
146 are still unclear. Therefore, in this study we have sampled the drill cores and available  
147 outcrops from the Sichuan Basin.

148

### 149 **3. Samples and geochronology**

150 All samples in this study were collected from six areas within and around the  
151 southwest of the Sichuan Basin (Fig. 2) , including the borehole samples from ST1  
152 (ST1-2, ST1-5) (Fig. 3a), YT1 (YT1-1, YT1-3, YT1-4, YT1-5, YT1-6, YT1-7) (Fig.  
153 3b) and ZG2 (ZG2-4, ZG2-5, ZG2-7, ZG2-8) (Fig. 3c, d), as well as outcrops  
154 Longmendong in Leshan City (20LMD04, 20LMD05) (Fig. 3e, f), Longchi in  
155 Emeishan City (20LC04, 20LC06) (Fig. 3g) and Xinlin in Leshan City (20XL01,  
156 20XL02) (Fig. 3h). Boreholes YT1 and ST1 are located around the Longquanshan fault,  
157 Longchi outcrop is close to the Longmenshan fault, while outcrops Xinlin and  
158 Longmendong, and borehole ZG2 border the Emei-Yibin fault in the western Sichuan  
159 Basin (Fig. 2b). All the samples were analysed for whole-rock major and trace elements,  
160 and eleven samples were analysed for Sr, Nd and Pb isotopes. All samples were  
161 collected from the central part of the massive lava flows with little amygdales and crack  
162 fillings. The basalts contain 2% to 15% phenocrysts of clinopyroxene, plagioclase, and  
163 minor olivine, set in a matrix comprising mostly plagioclase. The clinopyroxene  
164 phenocrysts are generally subhedral, occasionally euhedral, whereas the plagioclase  
165 phenocrysts are euhedral grains. The phenocrysts range in size from 700  $\mu\text{m}$  to 1800  
166  $\mu\text{m}$  in samples YT1-6 and YT1-7, while they are about 60~400  $\mu\text{m}$  in size in ZG2 Well,  
167 Longchi and Xinlin (Fig. 3b, d).

168 Stratigraphally, the Sichuan Basin volcanic rocks lie between the Permian Maokou  
169 Formation limestone and the Longtan Formation marl (Fig. 4), indicating that the  
170 Sichuan Basin basalts erupted in the Mid-Late Permian. This eruption time is consistent  
171 with the formation time of the ELIP, which suggests the Sichuan Basin basalts belong  
172 to the ELIP (Li et al., 2017a; Liu et al., 2022). Based on chronological data (Table 1),  
173 the main duration of the ELIP eruption is 260~257 Ma (e.g., Fan et al., 2008; Lai et al.,  
174 2012; Li et al., 2016a; Li et al., 2016b; Zhou et al., 2006; Zi et al., 2010).



175

176 **4. Analytical methods**

177 Fresh rocks were selected based on the characteristics of rock thin sections.  
178 Following the removal of amygdales and minor veins, the samples were crushed to 200  
179 mesh by an agate mortar. The pre-treatment ensures the accuracy of whole-rock  
180 geochemical analyses.

181 The major and trace elements and Sr-Nd-Pb isotopes of the samples were  
182 determined at the Wuhan Sample Solution Analytical Technology Co., Ltd., Wuhan,  
183 China. International reference material values are listed in the appendix.

184 Major elements were analysed by a Primus II X-ray fluorescence spectrometer  
185 (XRF) with wave-length dispersive X-ray fluorescence spectrometry. The major  
186 element data are corrected by the theoretical  $\alpha$  coefficient method, and relative standard  
187 deviations (RSD) for most major element oxides are within  $\pm 1-3\%$ . The contents of  
188 trace elements were analysed by Agilent 7700e ICP-MS. The analytical precision and  
189 accuracy for trace elements are mostly better than 10%. The detailed sample-  
190 preparation procedure for ICP-MS analyses can be found in Rudnick et al. (2004) and  
191 Liu et al. (2008).

192 Sr-Nd-Pb isotopic analyses of whole-rock samples were carried out on a Neptune  
193 Plus MC-ICP-MS (Thermo Fisher Scientific, Dreieich, Germany). All chemical  
194 preparations were performed on class 100 work benches within a class 1000 over-  
195 pressured clean laboratory. The sample powders were acid-leached before isotopic  
196 analysis (Weis et al., 2005). The data was processed by "Iso-Compass" software (Zhang  
197 et al., 2020a). Detailed analytical procedures are described in Chen et al. (2002) and Li  
198 et al. (2012).

199 The analysed  $^{87}\text{Sr}/^{86}\text{Sr}$  of NBS 987 standard solution is  $0.710242\pm 14$  (2SD,  $n=345$ ),  
200 which is consistent with the published values ( $0.710248\pm 12$ , Zhang and Hu, 2020). In  
201 addition, analysis of USGS reference materials BCR-2 (basalt) yielded ratios of  
202  $0.705012\pm 22$  (2SD,  $n=63$ ) for  $^{87}\text{Sr}/^{86}\text{Sr}$ , which are identical within error to their  
203 published results (Li et al. 2012). The Sr isotope standard precision (2SE) =  $0.000010$ -  
204  $0.000020$  (0.01‰-0.03‰, 2RSE), and the accuracy is better than  $0.000020$  ( $\sim 0.03\%$ ).  
205 For standard GSB 04-3258-2015, a  $^{143}\text{Nd}/^{144}\text{Nd}$  of  $0.512440\pm 6$  (2SD,  $n=31$ ) was  
206 obtained which is identical, within error, to its published value ( $0.512438\pm 6$  (2SD), Li  
207 et al., 2017b). In addition, the measurement results of  $^{143}\text{Nd}/^{144}\text{Nd}$  for USGS reference  
208 materials BCR-2 (basalt) are  $0.512641\pm 11$  (2SD,  $n=82$ ), which are identical, within  
209 error, to their published values (Li et al. 2012). The precision of Nd isotope analyses  
210 (2SE) =  $0.000005$ - $0.000025$  (0.01‰-0.05‰, 2RSE), and the analytical accuracy is  
211 better than  $0.000025$  ( $\sim 0.05\%$ ). The external precision of  $^{20x}\text{Pb}/^{204}\text{Pb}$  ratios for the  
212 reference material NBS 981 is 0.03% (2RSD). Furthermore, the USGS reference  
213 material BCR-2 (basalt) had analysed ratios of  $^{208}\text{Pb}/^{204}\text{Pb}=38.736\pm 17$ ,  
214  $^{207}\text{Pb}/^{204}\text{Pb}=15.628\pm 3$ , and  $^{206}\text{Pb}/^{204}\text{Pb}=18.756\pm 10$  (2SD,  $n=22$ ), which are consistent  
215 within error of 0.03% with the published results ( $^{208}\text{Pb}/^{204}\text{Pb}=38.725\pm 22$ ,  
216  $^{207}\text{Pb}/^{204}\text{Pb}=15.621\pm 4$ ,  $^{206}\text{Pb}/^{204}\text{Pb}=18.753\pm 8$ , Zhang and Hu 2020). The internal  
217 precision of  $^{20x}\text{Pb}/^{204}\text{Pb}$  ratio is 0.002‰-0.025‰, and the analytical accuracy is better  
218 than 0.03%.

219

## 220 **5. Results**

### 221 **5.1 Major elements**

222 The major element compositions of the volcanic rock samples from different

223 regions of the Sichuan Basin are listed in Table 2. The samples have all experienced  
224 some degree of hydrothermal alteration, and so the whole-rock raw data has been  
225 normalised on a volatile-free basis. Samples ST1-2 and ST1-5 have high LOI values of  
226 5.9 wt.% and 6.0 wt.% respectively and so their major element compositions were not  
227 used in this study.

228 The samples of the Sichuan Basin show large variations in SiO<sub>2</sub> (45.6-49.2 wt.%)  
229 and MgO (4.3-7.1 wt.%). The rocks have total alkalis (Na<sub>2</sub>O+K<sub>2</sub>O) that range from 3.0  
230 to 5.8 wt.% and have K<sub>2</sub>O/Na<sub>2</sub>O ratios of ~1.7. They have high TiO<sub>2</sub> contents of 3.7 to  
231 4.2 wt.% and Ti/Y ratios of 604 to 720, indicating that the basin basalts belong to the  
232 high-Ti series (Fig. 5a). The analysed samples mainly plot in the sub-alkaline field on  
233 the Ol'-Ne'-Q' diagram (Fig. 5b). The concentrations of the Al<sub>2</sub>O<sub>3</sub> and CaO are  
234 positively correlated with MgO, whereas K<sub>2</sub>O, TiO<sub>2</sub>, P<sub>2</sub>O<sub>5</sub>, Fe<sub>2</sub>O<sub>3</sub><sup>T</sup>, La and Nb are  
235 negatively correlated with MgO (Fig. 6). Compared with the outer zone of the ELIP,  
236 the inner zone has variable volcanic rock types, ranging from low-Ti series to high-Ti  
237 series (Fig. 5a).

238

## 239 **5.2 Trace elements**

240 The trace element contents of the basalts in the Sichuan Basin are listed in Table  
241 2. Chondrite-normalised REE patterns are enriched in the LREE ((La/Yb)<sub>N</sub> = 9.8-13.2)  
242 and depleted in the HREE ((Dy/Yb)<sub>N</sub> = 1.8-2.0), with only slight negative Eu anomalies  
243 (δEu = 0.83-0.95) (Fig. 7a). On primitive mantle-normalised trace element diagrams  
244 (Fig. 7b), the large ion lithophile elements (LILE) are quite variable, especially the large  
245 negative anomalies of Rb and K, as well as positive anomalies of Ba and Pb, which  
246 may result from sub-solidus hydrothermal alteration. However, alteration-resistant

247 immobile high field strength elements (HFSE, e.g., Nb, Ta, Zr, Hf, Th) of the samples  
248 are much more consistent, with slightly negative Zr anomalies and positive Th  
249 anomalies (Fig. 7b). The trace element compositions of the samples ST1-2 and ST1-5  
250 have not been affected considerably except for some mobile elements, therefore, they  
251 are still used in the following discussion. Overall, the Sichuan basalts have OIB (ocean  
252 island basalt)-like REE and trace element signatures, which are similar to compositions  
253 of the Emeishan high-Ti basalts from other regions.

254

### 255 **5.3 Sr-Nd-Pb isotopes**

256 The isotopic data of the basalts in the Sichuan Basin are presented in Table 3. The  
257 initial Sr-Nd-Pb isotopic compositions have been age-corrected to 258.5 Ma based on  
258 the age range of the Emeishan basalts in this paper. The initial Sr isotopic compositions  
259 of the high-Ti basalts in the Sichuan Basin range from 0.705230 to 0.706935 and the  
260  $\epsilon_{\text{Nd}}(t)$  values range from -0.38 to 1.17 (Fig. 8a). The Sichuan Basin basalts show a  
261 relatively wide range in  $^{208}\text{Pb}/^{204}\text{Pb}(t)$  ratios between 38.403 and 38.845, whereas  
262  $^{206}\text{Pb}/^{204}\text{Pb}(t)$  (18.097-18.388) and  $^{207}\text{Pb}/^{204}\text{Pb}(t)$  (15.578-15.606) compositions are  
263 more uniform (Fig. 8c, d). Compared with low-Ti basalts in the inner zone, the  
264 compositional range of high-Ti basalts in the ELIP is relatively constant with typical  
265 OIB-like Sr-Nd-Pb isotopic characteristics. The Sichuan Basin samples have slightly  
266 higher  $^{87}\text{Sr}/^{86}\text{Sr}(t)$  ratios than the high-Ti samples in other areas of the ELIP, and show  
267 the characteristics of the EMII end-member. However, in general, the basin samples  
268 overlap with the field of high-Ti basalts in the outer zone, which indicates the Sichuan  
269 Basin basalts belong to the outer zone of the ELIP.

270 These data plot above the LoNd (low Nd) array, close to OIB and EMII, in distinct

271 contrast to the DM (depleted mantle) and MORB (mid-ocean ridge basalt) (Fig. 8a, b).  
272 The samples lie above the North Hemisphere Reference Line (NHRL) and overlap with  
273 the field of OIB (Fig. 8c, d). In terms of  $^{206}\text{Pb}/^{204}\text{Pb}(t)$  vs.  $^{208}\text{Pb}/^{204}\text{Pb}(t)$ , the Sichuan  
274 Basin samples data have similar compositions to the high-Ti basalts in the ELIP and  
275 overlap with alkaline lavas from the Kerguelen Plateau (Fig. 8d) (Fan et al., 2008). The  
276 Kerguelen Plateau in the South Indian Ocean (which comprises a large amount of  
277 alkaline basalts, (Zhu et al., 2007)) is one of the largest LIPs in the world, which is  
278 related to the Kerguelen plume activity from the Early Cretaceous.

279

## 280 **6. Discussion**

### 281 **6.1 Crustal contamination and fractional crystallization**

282 As previously noted fluid-mobile elements (LILE) such as Rb, Ba, K, Pb and Sr  
283 show large variations and both positive and negative peaks, which are most likely to be  
284 caused by sub-solidus hydrothermal alteration, however, the REE, Th and HFSE (e.g.,  
285 Hf, Nb and Ta) are relatively alteration-resistant and so are essentially immobile.  
286 Therefore, in the following discussion, only immobile elements are used to assess the  
287 petrogenesis of these rocks.

288 It is necessary to evaluate the role of crustal contamination and fractional  
289 crystallization during magma ascent before we discuss potential mantle sources of  
290 volcanic rocks. Importantly, the proxies for crustal contamination, Th/Nb, La/Nb,  
291 Th/Ta and Nb/U ratios are not changed by partial melting or fractional crystallization  
292 in magma. Crustal contamination usually results in high Th/Nb (>5), La/Nb (>12) and  
293 Th/Ta ratios, and low Nb/U ratios (Neal et al., 2002; Pearce, 2008; Rudnick and Gao,  
294 2003). The basalts in the present study have low La/Nb (1.01-1.23), Th/Nb (0.15-0.22)

295 and Th/Ta (2.41-3.27), and high Nb/U (21.48-28.00). These characteristics reveal that  
296 they were derived from mantle source without significant continental crust  
297 contamination. In addition, there is no clear mixing trend between the Sichuan Basin  
298 samples and average continental crust on a Ce vs. Nb/Th diagram (Fig. 9a). The  
299 analysed samples are broadly similar to primitive mantle (PM) values, and are close to  
300 the field of Kerguelen alkaline OIB, as well as plotting far from the values of middle  
301 and upper continental crust (MC and UC) (Fig. 9b). Moreover, slightly positive Th  
302 anomalies, and slightly negative Nb and Ta anomalies (Fig. 7b) also confirm that the  
303 Sichuan Basin basalts have not been significantly contaminated by crustal materials,  
304 because continental crust is enriched in Th and strongly depleted in Nb and Ta.  
305 Furthermore,  $(^{87}\text{Sr}/^{86}\text{Sr})_i$  and  $\epsilon_{\text{Nd}}(t)$  do not correlate with increasing  $\text{SiO}_2$  (Fig. 9c, d),  
306 which also suggests little crustal contamination occurred. Therefore, the magmatic  
307 evolution of basalts in the Sichuan Basin is dominated by fractional crystallization or  
308 partial melting.

309 Basalts from Sichuan Basin have low MgO values (4.3-7.1 wt.%) and display good  
310 correlations between MgO and other major oxides ( $\text{Al}_2\text{O}_3$ ,  $\text{K}_2\text{O}$ ,  $\text{Fe}_2\text{O}_3^{\text{T}}$ ) as well as trace  
311 elements (La, Nb) (Fig. 6), which indicates the likely occurrence of fractional  
312 crystallization. The basalts in the Sichuan Basin have lower Ni, Cr and MgO than  
313 primitive magma (Hirajima et al., 1990) (Fig. 6), further suggesting that the magma  
314 experienced a substantial amount of fractional crystallization (e.g., olivine,  
315 clinopyroxene) during ascent.

316 The basalts are characterised by a positive correlation between MgO and CaO (Fig.  
317 6b), indicating that the magma underwent the fractional crystallization of clinopyroxene  
318 (Wei et al., 2013). A slight negative Eu anomaly (Fig. 7b) suggests the magma also  
319 experienced slight fractional crystallization of plagioclase. As illustrated in Fig. 10a,

320 the Sichuan Basin basalts exhibit a positive correlation between  $\text{CaO}/\text{Al}_2\text{O}_3$  ratios and  
321  $\text{Mg}\#$  values, similar to other Emeishan basalts. The calculated effects of fractional  
322 crystallization are shown in mineral vector diagrams in Figs. 10b and c. The data mostly  
323 plot near the clinopyroxene crystallization vector (Fig. 10b, c), further suggesting that  
324 clinopyroxene is the most significant mineral phase in the fractional crystallization.  
325 This is consistent with the petrographic features (Fig. 3), as there are more  
326 clinopyroxene phenocrysts than plagioclase in YT1-7 (Fig. 3b) and ZG2-5 (Fig. 3d).  
327 Moreover, the Sichuan basalts have enriched Fe and Ti, and  $\text{MgO}$  vs.  $\text{Fe}_2\text{O}_3^{\text{T}}$  and  $\text{TiO}_2$   
328 show negative correlations (Fig. 6d, e). These characteristics may be induced by the  
329 early fractional crystallization of Ti and Fe-poor silicate minerals, which indicates little  
330 crystallization of titanomagnetite in low oxygen fugacity conditions (Li et al., 2017;  
331 Zhang et al., 2011). Furthermore, low oxygen fugacity may also have promoted the  
332 fractional crystallization of clinopyroxene and plagioclase in the Sichuan Basin basalts  
333 (Fig. 3) (Li et al., 2017).

334

## 335 **6.2 Magma Source and Petrogenesis**

336 The Sichuan Basin basalts have high  $\text{TiO}_2$  contents ( $>3.5$  wt.%), relative  
337 enrichment of alkalis (3.1-5.9 wt.%), LILE and HFSE, and significant REE  
338 fractionation with  $(\text{La}/\text{Yb})_{\text{N}}$  ratios ranging from 9.8 to 13.2. The trace element and Sr-  
339 Nd-Pb isotope signatures are OIB-like with  $\epsilon_{\text{Nd}}(t)$  values ranging from -0.38 to 1.17,  
340 (Fig. 7, 8). However, the origin of the Emeishan basalts with these characteristics is still  
341 controversial, and has been variously ascribed to the melting of either a mantle plume  
342 (Cheng et al., 2019; Liang et al., 2021; Wang et al., 2007; Xiao et al., 2004; Zhang et  
343 al., 2019) or lithospheric mantle (Lai et al., 2012; Xu et al., 2007). Alternatively, some  
344 authors propose that these basalts result from the interaction of mantle plume melts with

345 the lithospheric mantle (Cheng et al., 2019; Fan et al., 2008; He et al., 2010; Xu et al.,  
346 2007).

347 Like the high-Ti basalts in other regions of the ELIP, REEs, trace elements (except  
348 some LILEs) and incompatible element ratios of the Sichuan Basin high-Ti basalts are  
349 very similar to OIB and Kerguelen alkaline OIB-like basalts (Fig. 7, 11). Furthermore,  
350 the Sichuan Basin samples have OIB-like initial Sr-Nd-Pb isotopic characteristics,  
351 broadly fall in the field of OIB and Kerguelen basalts (Fig. 8). These geochemical  
352 signatures suggest the high-Ti basalts from the Sichuan Basin might have originated  
353 from a plume source, compositionally similar to other regions in the ELIP (e.g., Cheng  
354 et al., 2019; He et al., 2010; Liu et al., 2017; Song et al., 2008). It is proposed that the  
355 high-Ti basaltic magma from the Sichuan Basin is probably the product of partial  
356 melting of the head of the mantle plume, because the outer zone is further from the  
357 plume centre, and lower temperatures would have resulted in less lithospheric melting  
358 (Cheng et al., 2019).

359 In terms of incompatible trace element ratios, the Sichuan Basin basalts show  
360 broadly constant  $(La/Yb)_N$  ratios as  $\epsilon_{Nd}(t)$  values increase (Fig. 12a), and La/Yb ratios  
361 have a negative correlation with Yb compositions (Fig. 12b). These characteristics  
362 reveal that the Emeishan high-Ti basalts did not originate from partial melting of a  
363 homogeneous plume source. The samples from the Sichuan Basin define a linear array  
364 on Th/La vs. Nb/U (Fig. 12c) and  $^{206}Pb/^{204}Pb$  vs.  $\epsilon_{Nd}(t)$  (Fig. 12d) plots similar to other  
365 Emeishan high-Ti basalts, which would support this inference. In addition, it is  
366 generally argued that metasomatic melts derived from the primitive mantle have La/Nb  
367 ratios of  $\sim 0.53$ , whereas those from MORB source have values of  $\sim 1.02$  (McKenzie  
368 and O’Nions, 1995). The Sichuan Basin basalts have high La/Nb ratios of 1.01-1.23,  
369 with OIB-like Sr-Nd isotopes signatures significantly different from MORB (Fig. 8a),



370 indicating that they were likely derived from OIB-like enriched mantle source that was  
371 previously metasomatized. Moreover, the Sichuan Basin high-Ti samples plot around  
372 the field of OIB (Fig. 8c, d) and have an EMII-type signature (Fig. 8a, b) in terms of  
373 Sr-Nd-Pb isotope space. These features indicate the mantle plume may have been  
374 metasomatized by enriched materials before the eruption of the Late Permian basalts  
375 (Xu et al., 2021).

376 It is still unclear whether such enriched components originate from the  
377 asthenosphere, SCLM, crust, or recycled materials. The asthenosphere is ruled out since  
378 the trace elements and Sr-Nd-Pb isotopes of the Emeishan high-Ti basalts have OIB-  
379 like rather than MORB-like characteristics (Fig. 8) (Liu et al., 2017; Song et al., 2001;  
380 Wang et al., 2007; Xiao et al., 2004). Like the Emeishan high-Ti basalts in other regions,  
381 the basalts in the Sichuan Basin have relatively high Ti/Yb ratios, distant from OIB-  
382 SCLM and OIB-crust mixing lines. They are also significantly different from the  
383 Sangxiu Formation basalts which have a contribution from both continental lithospheric  
384 mantle materials and the Kerguelen mantle plume (Fig. 11b) (Zhu et al., 2007).  
385 Furthermore, the Sichuan Basin samples have high Ce, unlike continental lithosphere  
386 (Fig. 9a), which indicates minimal involvement of SCLM. As shown in Section 6.1, the  
387 samples were not significantly contaminated by crust. Therefore, the enriched  
388 components are unlikely to be related to either SCLM or crust.

389 It has been argued that the enriched signature in the OIB-like source is related to  
390 ancient recycled oceanic crust (Sobolev et al., 2000, 2007) or subducted terrigenous  
391 sediments (Eisele et al., 2002; Hofmann, 1997; Weaver, 1991). The Sichuan Basin  
392 basalts display  $(\text{Ta/La})_N$  ratios of 0.8-1.1, with an average of 0.94. Ta is depleted  
393 relative to La, and Th/Yb and Nb/Yb ratios are high (Fig. 11a), suggesting the  
394 involvement of crustal components during ascent or the contribution of subduction

395 component. The Sichuan Basin basalts have not experienced crustal contamination, so  
396 it is more likely that the Emeishan mantle plume has undergone metasomatism,  
397 accompanied by mixing of enriched components during subduction. Many studies on  
398 volcanic and sedimentary rocks in southwestern China and the Ailaoshan Region  
399 propose that the Ailaoshan Ocean crust (Paleotethyan slab) subducted eastward into the  
400 upper mantle beneath the western South China Block during the Permian-Middle  
401 Triassic (Hou et al., 2017; Qin et al., 2011; Wang et al., 2013; Xu et al., 2019, 2021;  
402 Yang et al., 2012; Yang and He, 2012; Zhong et al., 2013).

403       Based on a study of the Late Permian and Early Triassic A-type granites in the  
404 Yuanyang area of Yunnan, South China, Xu et al. (2021) proposed a geodynamic model  
405 of the interaction between the Emeishan mantle plume and the subducted Paleotethyan  
406 oceanic crust. According to the model, the Ailaoshan Ocean subducted eastward  
407 beneath the western South China Block, and the adjacent Emeishan mantle plume  
408 rapidly entrained the recycled lithospheric fragments (Xu et al., 2021). This model  
409 provides a mechanism for the metasomatism of the Emeishan mantle plume, and further  
410 explains why the composition of the Emeishan mantle plume is heterogeneous. In  
411 addition, many authors have proposed that the Emeishan mantle plume is likely to be  
412 intrinsically related to recycled ancient oceanic materials (Ren et al., 2017; Zhu et al.,  
413 2018). Zhu et al. (2018) proposed that the amount of recycled materials may be 10~20%  
414 in the Emeishan plume, which is broadly consistent with the view of Ren et al. (2017).  
415 In summary, we propose that the high-Ti basalts in the outer zone were derived from  
416 an OIB-like Emeishan mantle plume, which was modified by enriched materials  
417 derived from a subducted slab before the Late Permian.

418       The high-Ti basalts in the Sichuan Basin, which are located in the outer zone of  
419 the ELIP, are a similar age to the Emeishan basalts. Reconstruction of the thermal

420 history of the Sichuan Basin with a high paleogeothermal gradient of 23.0-42.6 °C/km  
421 in 259 Ma, indicates that the Sichuan Basin suffered an intensive thermal event related  
422 to the Emeishan mantle plume (Zhu et al., 2010, 2016). The basalts in Guangxi and  
423 Guizhou provinces that are relevant to the ELIP imply an extension of magmatism at  
424 the periphery (the outer zone) of the plume (Fan et al., 2008; Lai et al., 2012; Liu et al.,  
425 2017). This evidence indicates that the Sichuan Basin high-Ti basalts are related to the  
426 Emeishan mantle plume.

427 Rare-earth element ratios of the Sichuan Basin basalts (Fig. 13a) suggest they were  
428 derived from a mantle source containing garnet. The Emeishan high-Ti basalts lie  
429 between the melting curves for garnet and spinel lherzolites, indicating that they are  
430 derived from the spinel-garnet transition zone (Fig. 13b). In contrast, the low-Ti basalts  
431 in the inner zones have lower La/Sm, Sm/Yb and Dy/Yb ratios, revealing a higher  
432 degree of mantle melting at a shallower melting depth (Wang et al., 2007; Xiao et al.,  
433 2004). The low-Ti basalts also plot closer to SCLM end members than high-Ti basalts  
434 (Fig. 11b) We therefore argue that low-Ti magma might be generated from, or contain,  
435 a greater proportion of material from the SCLM (Fan et al., 2008; Xiao et al., 2004).

436

### 437 **6.3 Spatial and temporal distribution of the Emeishan basalts and tectonic** 438 **significance**

439 Chronological data give precise constraints on the duration of the ELIP eruption  
440 as 260~257 Ma (Table 1) (e.g., Fan et al., 2008; Lai et al., 2012; Li et al., 2016a; Li et  
441 al., 2016b; Zhou et al., 2006; Zi et al., 2010). Magnetostratigraphic studies of the  
442 Emeishan basalts indicate that a substantial number of basalts were formed during a  
443 period of normal polarity, with the main eruption lasting ~1-2 Ma (Zheng et al., 2010).

444 It has been proposed that the major eruption phase lasted less than 1 Ma (Xu et al., 2017;  
445 Zhu et al., 2018). Therefore, it is difficult to give the exact eruptive ages of high-Ti and  
446 low-Ti basalts, although most low-Ti basalts are stratigraphically below high-Ti basalts  
447 in most field profiles (Fig.14).

448 As summarised in Fig. 14, both high-Ti and low-Ti series are exposed in the inner  
449 zone (e.g. Binchuan, Ertan, and Miyi areas), with high-Ti basalts overlying low-Ti  
450 basalts, whereas only high-Ti basalts erupted in the outer zone, i.e., a greater distance  
451 from the centre of the mantle plume (Table 4) (Fan et al., 2008; He et al., 2010; Song  
452 et al., 2001, 2008; Xiao et al., 2004; Xu et al., 2001, 2007; Zhang et al., 2006). Overall,  
453 the Permian basalts are distributed from northeast (the Sichuan Basin) to southwest (the  
454 centre of the mantle plume) in the ELIP, and the thickness of basalts gradually decreases  
455 from the inner zone to the outer zone (Fig. 14). This distribution trend not only is  
456 consistent with the hotspot track of the Emeishan mantle plume (Fig. 1b) (Liu et al.,  
457 2021b), but also overlaps the seismic anomaly trends and residual gravity anomaly  
458 (Deng et al., 2014; Liu et al., 2021b; Xie et al., 2013).

459 Our petrogenetic model is shown in Fig. 15 and builds on previous models (e.g.,  
460 Feng et al., 2022; Liu et al., 2021b; Liu et al., 2022; Xiao et al., 2004; He et al., 2010).  
461 Based on our new data, we further consider the petrology, geochemistry, and  
462 distribution characteristics of the Sichuan Basin basalts in the outer zone of the ELIP,  
463 and consider the influence of subduction of the paleo-oceanic crust (Hou et al., 2017;  
464 Xu et al., 2019, 2021), the movement of the South China block (Liu et al., 2021b; Liu  
465 et al., 2022), and the successive eruptions of the late Permian low-Ti and high-Ti basalts  
466 (He et al., 2010; Xiao et al., 2004; Xu et al., 2001).

467 Paleomagnetic studies suggest that the Yangtze Craton moved northward between  
468 300 and ~260 Ma and experienced an overall ~27° clockwise rotation from Permian to

469 present (Huang et al., 2018; Liu et al., 2021b). The Western Yangtze block experienced  
470 Ailaoshan slab eastward subduction from the early-Guadalupian (~269 Ma) (Xu et al.,  
471 2021), and the adjacent Emeishan mantle plume was modified by the recycled  
472 lithospheric fragments (Fig. 15a) (e.g. Hou et al., 2017; Qin et al., 2011; Wang et al.,  
473 2013; Xu et al., 2019, 2021). Paleotethyan subduction resulted in an extensional  
474 tectonic setting in the Sichuan Basin during Middle-Late Permian (Xu et al., 2021; Liu  
475 et al., 2022). Before the eruption of the Emeishan basalts, mantle upflow reached the  
476 lithosphere (Liu et al., 2021b), resulting in plume-lithosphere interactions, and crustal  
477 uplift. The magnitude of uplift is greater than 1000 m at its core (the inner zone) (He et  
478 al., 2003), and the uplift range of the Sichuan Basin in the outer zone is relatively low.  
479 The upper part of the Maokou Formation was exposed at the surface, resulting in  
480 different degrees of weathering, denudation, and a paleo-karst landscape (Hu et al.,  
481 2012; Xiao et al., 2014; Zhang et al., 2020b). This resulted in variable degrees of uplift  
482 in the Sichuan Basin. As the South China block drifted northward, major eruptions  
483 including low-Ti and high-Ti series occurred throughout the ELIP during the end-  
484 Guadalupian (260~257 Ma) (Fig. 15b, c) (Liu et al., 2021b, Feng et al., 2022).

485 We propose that from 260 to ~257 Ma, the temperature of the lithosphere mantle  
486 in the inner zone rose dramatically due to underplating of the mantle plume, causing  
487 partial melting of lithosphere mantle and forming the low-Ti basalts (Fig. 15b). As the  
488 lithospheric mantle gradually became refractory, OIB-like high-Ti basalts derived from  
489 the plume became the predominant magma type that erupted over the low-Ti basalts  
490 (Fig. 14, 15d). In contrast, at the periphery of the plume, the lithospheric mantle was  
491 cooler due to the distance from the centre of the mantle plume. As a result, the  
492 temperature would have been insufficient to generate extensive melting of the  
493 lithospheric mantle (Xu et al., 2001; Xiao et al., 2004; He et al. al., 2010). Therefore,

494 only the mantle plume melted in the outer zone, forming high-Ti basalts (Fig. 15c). As  
495 discussed in Section 6.2, the geochemical evidence also indicates that the source of the  
496 high-Ti basalts did not involve melts from SCLM.

497 The coexistence of high-Ti and low-Ti magma in the inner zone of the Emeishan  
498 mantle plume could be attributed to plume-lithosphere interaction. Geochemical  
499 modeling suggests that the Emeishan high-Ti basalts are formed at a higher melting  
500 pressure than the low-Ti basalts (Liu et al., 2017; Zhang et al., 2019). Continuous  
501 polybaric melting of the mantle source might account for compositional variations of  
502 the rock types in the inner zone. Furthermore, Dy/Yb and La/Yb ratios of the high-Ti  
503 basalts in the outer zone are lower than those in the inner zone, indicating a shallower  
504 source and higher melting degree of mantle peridotite for the high-Ti basalts in the outer  
505 zone (Tian et al., 2021). It is proposed that melting generally happens beneath thin  
506 lithosphere rather than thickened lithosphere, i.e., lid-effect, and the extent of melting  
507 beneath the thin lithosphere is likely very low (no more than ~5%) (Fram and Leshner,  
508 1993; Niu et al., 2021). The lithosphere in the outer zone is thicker than that in the inner  
509 zone in the ELIP (Tian et al., 2021). The magmatic activity in the outer zone is more  
510 limited than that in the inner zone, which is consistent with the “lid effect” model.

511 Therefore, the high-Ti basalts from the Sichuan Basin are the result of partial  
512 melting of the plume in the outer zone of the ELIP. In contrast, relatively few low-Ti  
513 basalts derived from the lithosphere mantle have been discovered in the outer zone,  
514 because it is more distant from the centre of the mantle plume and so has a cooler  
515 lithosphere.

516

517 **7. Conclusions**

518 Based on petrography and geochemistry of the basalts in the Sichuan Basin, and  
519 combined with published data from the inner and outer zones of the Emeishan mantle  
520 plume, it is concluded that.

521 (1) In the outer zone of the ELIP, the volcanic rocks from the Sichuan Basin are  
522 part of the Emeishan flood basalts. Based on chronological data, the main duration of  
523 the basalt in outer zone eruption is 260~257 Ma.

524 (2) Unlike the inner zone, the volcanic rocks in Sichuan Basin of the outer zone  
525 are predominantly high-Ti sub-alkaline basalts. The Sichuan Basin basalts with OIB-  
526 like geochemical signatures originated from the Emeishan mantle plume, which was  
527 modified by enriched materials derived from a subducted slab before the Late Permian.  
528 The samples have compositions consistent with low degrees of partial mantle melting  
529 and fractional crystallization dominated by clinopyroxene during magma evolution.

530 (3) During the early-Guadalupian (~269 Ma), Western Yangtze Block experienced  
531 Ailaoshan slab (Paleotethys Ocean) eastward subduction, and the adjacent Emeishan  
532 mantle plume was modified by the recycled lithospheric fragments. During the end-  
533 Guadalupian (260~257 Ma), the Emeishan mantle plume underplated the lithosphere  
534 mantle in the Yangtze Continent.

535 (4) In the inner zone, the lithosphere mantle and the mantle plume melted  
536 successively, forming low-Ti basalts and overlying high-Ti basalts respectively.  
537 However, in the outer zone, only high-Ti basalts derived from the mantle plume were  
538 able to form.

539

#### 540 **Acknowledgements**

541 We are grateful to two anonymous reviewers, handle editor Liang Qiu and chief

542 editor Meifu Zhou for their constructive comments and suggestions. We thank  
543 Hongfang Chen for help with major and trace elements and Sr-Nd-Pb isotopic  
544 composition analyses at the Wuhan Sample Solution Analytical Technology Co., Ltd.,  
545 Wuhan, China. This study was supported by Marine S&T Fund of Shandong Province  
546 for Pilot National Laboratory for Marine Science and Technology (Qingdao)  
547 (2021QNLM020001-1), National Natural Science Foundation of China Project  
548 (42272225; 42072169) and Shandong Provincial Natural Science Foundation, China  
549 (ZR2021MD083).

550

## 551 **References**

- 552 Aldanmaz, E., Pearce, J.A., Thirlwall, M.F., Mitchell, J.G., 2000. Petrogenetic  
553 evolution of late Cenozoic, post-collision volcanism in western Anatolia, Turkey.  
554 *J. Volcanol. Geotherm. Res.* 102(1-2), 67-95.
- 555 Barling, J., Goldstein, S.L., 1990. Extreme isotopic variations in Heard Island lavas and  
556 the nature of mantle reservoirs. *Nature* 348, 59-62.
- 557 Carlson, R.W., 1995. Isotopic inferences on the chemical structure of the mantle. *J.*  
558 *Geodyn.* 20, 365-386.
- 559 Chen, F., Satir, M., Ji, J., Zhong, D., 2002. Nd-Sr-Pb isotopes of Tengchong Cenozoic  
560 volcanic rocks from western Yunnan, China: evidence for an enriched-mantle  
561 source. *J. Asian Earth Sci.* 21, 39-45.
- 562 Chen, J.F., Jahn, B.M., 1998. Crustal evolution of southeastern China: Nd and Sr  
563 isotopic evidence. *Tectonophysics* 284, 101-133.
- 564 Chen, Y., Xu, Y.G., Xu, T., Si, S.K., Liang, X.F., Tian, X.B., Deng, Y.F., Chen, L., Wang,  
565 P., Xu, Y.H., Lan, H.Q., Xiao, F.H., Li, W., Zhang, X., Yuan, X.H., Badal, J., Teng,  
566 J.W., 2015. Magmatic underplating and crustal growth in the Emeishan Large



567 Igneous Province, SW China, revealed by a passive seismic experiment. Earth  
568 Planet. Sci. Lett. 432, 103-114.

569 Cheng, W.B., Dong, S.Y., Jin, C.H., Zhao, B., Zhang, Y., Wang, C., 2019.  
570 Characteristics of elemental geochemistry and petrogenesis discussion of the  
571 Emeishan basalts in Muchuan area, Sichuan province. J. Mineral. Petrol. 39(4),  
572 49-60. In Chinese with English abstract.

573 Chung, S.L., Jahn, B.M., Wu, G.Y., Lo, C.H., Cong, S.L., 1998. The Emeishan flood  
574 basalt in SW China: A mantle plume initiation model and its connection with  
575 continental breakup and mass extinction at the Permian-Triassic Boundary. Mantle  
576 Dynamics and Plate Interactions in East Asia. American Geophysical Union (AGU)  
577 798(12), 47-58.

578 Deng, Y., Zhang, Z., Mooney, W., Badal, J., Fan, W., Zhong, Q., 2014. Mantle origin of  
579 the Emeishan large igneous province (South China) from the analysis of residual  
580 gravity anomalies. Lithos 204, 4-13.

581 Deniel, C., 1998. Geochemical and isotopic (Sr, Nd, Pb) evidence for plume-lithosphere  
582 interactions in the genesis of Grande Comore magmas (Indian Ocean). Chem. Geol.  
583 144, 281-303.

584 Dong, S.Y., Zhang, Z.C., 2009. Geochemical Behavior of Yttrium in Fe-Ti Oxides - An  
585 Example Inferred from the Emeishan Large Igneous Province. Geol. Rev. 55(3),  
586 355-360. In Chinese with English abstract.

587 Eisele, J., Sharma, M., Galer, S.J.G., Blichert-Toft, J., Devey, C.W., Hofmann, A.W.,  
588 2002. The role of sediment recycling in EM-1 inferred from Os, Pb, Hf, Nd, Sr  
589 isotope and trace element systematics of the Pitcairn hotspot. Earth Planet. Sci.  
590 Lett. 196, 197-212.

591 Fan, W.M., Zhang, C.H., Wang, Y.J., Guo, F., Peng, T.P., 2008. Geochronology and

592 geochemistry of Permian basalts in western Guangxi Province, Southwest China:  
593 evidence for plume–lithosphere interaction. *Lithos* 102 (1-2), 218-236.

594 Feigenson, M.D., Patino, L.C., Carr, M.J., 1996. Constraints on partial melting imposed  
595 by rare earth element variations in Mauna Kea basalts. *J. Geophys. Res.* 101(B5),  
596 11815-11829.

597 Feng, Q.Q., Qiu, N.S., Fu, X.D., Li, W.Z., Liu, X., Ji, R.Y., 2022. Maturity evolution of  
598 Permian source rocks in the Sichuan Basin, southwestern China: The role of the  
599 Emeishan mantle plume. *J. Asian Earth Sci.* 229, 105180.

600 Fram, M.S., Leshner, C.E., 1993. Geochemical constraints on mantle melting during  
601 creation of the North Atlantic basin. *Nature* 363(6431), 712-715.

602 Gao, S., Ling, W., Qiu, Y., Lian, Z., Hartmann, G., Simon, K., 1999. Contrasting  
603 geochemical and Sm-Nd isotopic compositions of Archean metasediments from  
604 the Kongling high-grade terrain of the Yangtze craton: evidence for cratonic  
605 evolution and redistribution of REE during crustal anatexis. *Geochim. Cosmochim.*  
606 *Acta* 63(13-14), 2071-2088.

607 Hamelin, B., Allègre, C.J., 1985. Large scale regional units in the depleted upper mantle  
608 revealed by an isotopic study of the south-west India ridge. *Nature* 315, 196-198.

609 Hart, S.R., 1984. The Dupal anomaly: a large-scale isotopic anomaly in the southern  
610 hemisphere. *Nature* 309, 753-756.

611 Hao, Y.L., Zhang, Z.C., Wang, F.S., Mahoney, J.J., 2004. Petrogenesis of high-Ti and  
612 low-Ti basalts from the Emeishan large igneous province. *Geol. Rev.* 50(6), 587-  
613 592. In Chinese with English abstract.

614 Hawkesworth, C.J., Rogers, N.W., van Calsteren, P.W.C., Menzies, M.A., 1984. Mantle  
615 enrichment processes. *Nature* 311 (27), 331-335.

616 He, B., Xu, Y.G., Chung, S.L., Xiao, L., Wang, Y.M., 2003. Sedimentary evidence for

617 a rapid, kilometer-scale crustal doming prior to the eruption of the Emeishan flood  
618 basalts, *Earth Planet. Sci. Lett.* 213, 391-405.

619 He, B., Xu, Y.G., Huang, X.L., Luo, Z.Y., Shi, Y.R., Yang, Q.J., Yu, S.Y., 2007. Age  
620 and duration of the Emeishan flood volcanism, SW China: Geochemistry and  
621 SHRIMP zircon U–Pb dating of silicic ignimbrites, post-volcanic Xuanwei  
622 Formation and clay tuff at the Chaotian section. *Earth Planet. Sci. Lett.* 255, 306-  
623 323.

624 He, Q., Xiao, L., Balta, B., Gao, R., Chen, J.Y., 2010. Variety and complexity of the  
625 Late-Permian Emeishan basalts: Reappraisal of plume-lithosphere interaction  
626 processes. *Lithos* 119, 91-107.

627 Hirajima, T., Ishiwatari, A., Gong, B., Zhang, R.Y., Nozaka, A.T., 1990. Coesite from  
628 Mengzhong eclogite at Dhonghai county, northeastern Jiangsu province, China.  
629 *Mineral. Mag.* 54(377), 579-583.

630 Hofmann, A.W., 1997. Mantle geochemistry: The message from oceanic volcanism.  
631 *Nature* 385, 219-229.

632 Hofmann, A.W., Jochum, K.P., Seufert, M., White, W.M., 1986. Nb and Pb in oceanic  
633 basalts: new constraints on mantle evolution. *Earth Planet. Sci. Lett.* 79, 33-45.

634 Hou, T., Zhang, Z.C., Kusky, T., Du, Y.S., Liu, J.L., Zhao, Z.D., 2011. A reappraisal of  
635 the high-Ti and low-Ti classification of basalts and petrogenetic linkage between  
636 basalts and mafic-ultramafic intrusions in the Emeishan Large Igneous Province,  
637 SW China. *Ore Geol. Rev.* 41, 133-143.

638 Hou, Y.L., Zhong, Y.T., Xu, Y.G., He, B., 2017. The provenance of late Permian karstic  
639 bauxite deposits in SW China, constrained by the geochemistry of interbedded  
640 clastic rocks, and U-Pb-Hf-O isotopes of detrital zircons. *Lithos* 278-281, 240-254.

641 Hu, M.Y., Hu, Z.G., Wei, G.Q., Yang, W., Liu, M.C., 2012. Sequence lithofacies

642 paleogeography and reservoir prediction of the Maokou Formation in Sichuan  
643 Basin. *Petrol. Explor. Dev.* 39(1), 45-55. In Chinese with English abstract.

644 Huang, B., Yan, Y., Piper, J.D.A., Zhang, D., Yi, Z., Yu, S., Zhou, T., 2018.  
645 Paleomagnetic constraints on the paleogeography of the East Asian blocks during  
646 Late Paleozoic and Early Mesozoic times. *Earth-Sci. Rev.* 186, 8-36.

647 Huang, H., Huyskens, M.H., Yin, Q.Z., Cawood, P.A., Hou, M.C., Yang, J.H., Xiong,  
648 F.H., Du, Y.S., Yang, C.C., 2022. Eruptive tempo of Emeishan large igneous  
649 province, southwestern China and northern Vietnam: Relations to biotic crises and  
650 paleoclimate changes around the Guadalupian-Lopingian boundary. *Geology* doi:  
651 <https://doi.org/10.1130/G50183.1>.

652 Kamenetsky, V.S., Chung, S.L., Kamenetsky, M., Kuzmin, D.V., 2012. Picrites from  
653 the Emeishan Large Igneous Province, SW China: a Compositional Continuum in  
654 Primitive Magmas and their Respective Mantle Sources. *J. Petrol.* 53(10), 2095-  
655 2113.

656 LaFlèche, M.R., Camiré, G., Jenner, G.A., 1998. Geochemistry of post-Acadian,  
657 Carboniferous continental intraplate basalts from the Maritimes basin, Magdalen  
658 islands, Québec, Canada. *Chem. Geol.* 148, 115-136.

659 Lai, S.C., Qin, J.F., Li, Y.F., Li, S.Z., Santosh, M., 2012. Permian high-Ti/Y basalts  
660 from the eastern part of the Emeishan Large Igneous Province, Southwestern  
661 China: Petrogenesis and tectonic implications. *J. Asian Earth Sci.* 47, 216-230.

662 Lassiter J.C., Depaolo, D.J., 1997. Plume/lithosphere interaction in the generation of  
663 continental and oceanic flood basalts: Chemical and isotopic constraints. Large  
664 igneous provinces: Continental, oceanic, and planetary flood volcanism.  
665 *Geophysical Monograph* 100, 335-355.

666 Li, C., Ripley, E.M., Tao, Y., Hu, R.Z., 2016b. The significance of PGE variations with

667 Sr-Nd isotopes and lithophile elements in the Emeishan flood basalt province from  
668 SW China to northern Vietnam. *Lithos* 248-251, 1-11.

669 Li, C.F., Li, X.H., Li, Q.L., Guo, J.H., Yang, Y.H., 2012. Rapid and precise  
670 determination of Sr and Nd isotopic ratios in geological samples from the same  
671 filament loading by thermal ionization mass spectrometry employing a single-step  
672 separation scheme. *Anal. Chim. Acta* 727(10), 54-60.

673 Li, H.B., Zhang, Z.C., Ernst, R., Lu, L.S., Santosh, M., Zhang, D.Y., Cheng, Z.G., 2015.  
674 Giant radiating mafic dyke swarm of the Emeishan Large Igneous Province,  
675 Identifying the mantle plume centre. *Terra Nova* 27(4), 247-257.

676 Li, H.B., Zhang, Z.C., Santosh, M., Lü, L.S., Han, L., Liu, W., 2017a. Late Permian  
677 basalts in the Yanghe area, eastern Sichuan Province, SW China, Implications for  
678 the geodynamics of the Emeishan flood basalt province and Permian global mass  
679 extinction. *J. Asian Earth Sci.* 134, 293-308.

680 Li, H.B., Zhang, Z.C., Santosh, M., Lü, L.S., Han, L., Liu, W., Cheng, Z.G., 2016a.  
681 Late Permian basalts in the northwestern margin of the Emeishan Large Igneous  
682 Province, Implications for the origin of the Songpan-Ganzi terrane. *Lithos* 256-  
683 257, 75-87.

684 Li, J., Zhong, H., Zhu, W.G., Bai, Z.J., Hu, W.J., 2017c. Elemental and Sr–Nd isotopic  
685 geochemistry of Permian Emeishan flood basalts in Zhaotong, Yunnan Province,  
686 SW China. *Int. J. Earth Sci.* 106, 617-630.

687 Li, J., Tang, S.H., Zhu, X.K., Pan, C.X., 2017b. Production and Certification of the  
688 Reference Material GSB 04-3258-2015 as a  $^{143}\text{Nd}/^{144}\text{Nd}$  Isotope Ratio Reference.  
689 *Geostand. Geoanal. Res.* 41, 255-262.

690 Li, J., Xu, J.F., Suzuki, K., He, B., Xu, Y.G., Ren, Z.Y., 2010. Os, Nd and Sr isotope  
691 and trace element geochemistry of the Muli picrites: Insights into the mantle

692 source of the Emeishan Large Igneous Province. *Lithos* 119(1-2), 108-122.

693 Liang, Y.X., Li, H., Zhang, D.D., Yang, K., Zhou, D.W., Zheng, T.Y., Dong, Y.K., Zhai,  
694 L.G., 2021. Geochemical characteristics and genetic analysis of Huayingshan  
695 Emeishan basalt in Sichuan Basin. *Chin. J. Geol.* 56(1), 288-302. In Chinese with  
696 English abstract.

697 Liao, B.L., Zhang, Z.C., Kou, C.H., Li, H.B., 2012. Geochemistry of the Shuicheng  
698 Permian sodium trachybasalts in Guizhou Province and constraints on the mantle  
699 sources. *Acta Petrol. Sin.* 28(4), 1238-1250. In Chinese with English abstract.

700 Liu, R., Luo, B., Li, Y., Qiu, N.S., Wang, W., Zhang, Y., He, Q.L., Pei, S.Q., 2021a.  
701 Relationship between Permian volcanic rocks distribution and karst  
702 paleogeomorphology of Maokou Formation and its significance for petroleum  
703 exploration in western Sichuan Basin, SW China. *Petrol. Explor. Dev.* 48(3), 575-  
704 585. In Chinese with English abstract.

705 Liu, X.J., Liang, Q.D., Li, Z.L., Castillo, P.R., Shi Y., Xu, J.F., Huang, X.L., Liao, S.A.,  
706 Huang, W.L., Wu, W.N., 2017. Origin of Permian extremely high-Ti/Y mafic lavas  
707 and dykes from Western Guangxi, SW China: Implications for the Emeishan  
708 mantle plume magmatism. *J. Asian Earth Sci.* 141, 97-111.

709 Liu, X.Y., Qiu, N.S., Søger, N., Fu, X.D., Liu, R., 2022. Geochemistry of Late Permian  
710 basalts from boreholes in the Sichuan Basin, SW China: Implications for an  
711 extension of the Emeishan large igneous province. *Chem. Geol.* 588, 120636.

712 Liu, Y.D., Li, L., van Wijk, J., Li, A.B., Fu, Y. V., 2021b. Surface-wave tomography of  
713 the Emeishan large igneous province (China): Magma storage system, hidden  
714 hotspot track, and its impact on the Capitanian mass extinction. *Geology* 49(9),  
715 1032-1037.

716 Liu, Y.S., Zong, K.Q., Kelemen, P.B., Gao, S., 2008. Geochemistry and magmatic

717 history of eclogites and ultramafic rocks from the Chinese continental scientific  
718 drill hole: subduction and ultrahigh-pressure metamorphism of lower crustal  
719 cumulates. *Chem. Geol.* 247, 133-153.

720 Ma, C.Q., Ehlers, C., Xu, C.H., 2000. The roots of the Dabieshan ultrahigh-pressure  
721 metamorphic terrain: constraints from geochemistry and Nd-Sr isotope  
722 systematics. *Precambrian Res.* 102, 279-301.

723 McDonough, W.F., 1990. Constraints on the composition of the continental lithosphere  
724 mantle. *Earth Planet. Sci. Lett.* 101, 1-18.

725 McKenzie, D., O’Nions, R.K., 1991. Partial melt distributions from inversion of rare  
726 earth element concentrations. *J. Petrol.* 32, 1021-1091.

727 McKenzie, D., O’Nions, R.K., 1995. The Source Regions of Ocean Island Basalts. *J.*  
728 *Petrol.* 36(1), 133-159.

729 Neal, G.R., Mahoney, J.J., Chazey III, W.J., 2002. Mantle sources and the highly  
730 variable role of the continental lithosphere in basalt petrogenesis of the Kerguelen  
731 Plateau and the broken ridge LIP: results from ODP Leg 183. *J. Petrol.* 43, 1177-  
732 1205.

733 Niu, Y.L., 2021. Lithosphere thickness controls the extent of mantle melting, depth of  
734 melt extraction and basalt compositions in all tectonic settings on Earth-A review  
735 and new perspectives. *Earth-Sci. Rev.* 217, 103614.

736 Norman, M.D., 1998. Melting and metasomatism in the continental lithosphere: laser  
737 ablation ICPMS analysis of minerals in spinel lherzolites from eastern Australia.  
738 *Contrib. Mineral. Petrol.* 130(3-4), 240-255.

739 Palacz, Z.A., Saunders, A.D., 1986. Coupled trace element and isotope enrichment in  
740 the Cook–Austral– Samoa islands, southwest Pacific. *Earth Planet. Sci. Lett.* 79,  
741 270-280.

742 Pearce, J.A., 2008. Geochemical fingerprinting of oceanic basalts with applications to  
743 ophiolite classification and the search for Archean oceanic crust. *Lithos* 100(1–4),  
744 14-48.

745 Qin, X. F., Wang, Z. Q., Zhang, Y. L., Pan, L. Z., Hu, G. A., Zhou, F. S., 2011.  
746 Geochronology and geochemistry of early Mesozoic acid volcanic rocks from  
747 Southwest Guangxi: Constraints on tectonic evolution of the southwestern  
748 segment of Qinzhou- Hangzhou joint belt. *Acta Petrol. Sin.* 27(3), 794-808.

749 Ren, Z.Y., Wu, Y.D., Zhang, L., Nichols, A.R.L., Hong, L.B., Zhang, Y.H., Zhang, Y.,  
750 Liu, J.Q., Xu, Y.G., 2017. Primary magmas and mantle sources of Emeishan  
751 basalts constrained from major element, trace element and Pb isotope  
752 compositions of olivine-hosted melt inclusions. *Geochim. Cosmochim. Acta*  
753 208(2), 63-85.

754 Rudnick, R.L., Gao, S., 2003. Composition of the Continental Crust. *Treatise Geochem.*  
755 3, 1-64.

756 Rudnick, R.L., Gao, S., Ling, W.L., Liu, Y.S., McDonough, W.F., 2004. Petrology and  
757 geochemistry of spinel peridotite xenoliths from Hannuoba and Qixia, North  
758 China Craton. *Lithos* 77, 609-637.

759 Shellnutt, J. G., 2014. The Emeishan large igneous province: a synthesis. *Geosci. Front.*  
760 5(3), 369-394.

761 Shellnutt, J.G., Denyszyn, S.W., Mundil, R., 2012. Precise age determination of mafic  
762 and felsic intrusive rocks from the Permian Emeishan large igneous province (SW  
763 China). *Gondwana Res.* 22, 118-126.

764 Sobolev, A.V., Hofmann, A.W., Kuzmin, D.V., Yaxley, G.M., Arndt, N.T., Chung, S.L.,  
765 Danyushevsky, L.V., Elliott, T., Frey, F.A., Garcia, M.O., 2007. The amount of  
766 recycled crust in sources of mantle-derived melts. *Science* 316, 412-417.



767 Sobolev, A.V., Hofmann, A.W., Nikogosian, I.K., 2000. Recycled oceanic crust  
768 observed in “ghost plagioclase” within the source of Mauna Loa lavas. *Nature* 404,  
769 986-990.

770 Song, X.Y., Qi, H.W., Robinson, P.T., Zhou, M.F., Cao, Z.M., Chen, L.M., 2008.  
771 Melting of the subcontinental lithosphere mantle by the Emeishan mantle plume:  
772 evidence from the basal alkaline basalts in Dongchuan, Yunnan, Southwestern  
773 China. *Lithos* 100, 93-111.

774 Song, X.Y., Zhou, M.F., Hou, Z.Q., Cao, Z.M., Wang, Y.L., Li, Y.G., 2001.  
775 Geochemical constraints on the mantle source of the Upper Permian Emeishan  
776 continental flood basalts, southwestern China. *Int. Geol. Rev.* 43, 213-225.

777 Stanley, C.R., Russel, J.K., 1989. Petrologic hypothesis testing with Pearce element  
778 ration diagrams derivation of diagram axes. *Contrib. Mineral. Petrol.* 103, 78-89.

779 Sun, S.S., McDonough, W.F., 1989. Chemical and isotopic systematics of oceanic  
780 basalt: Implications for mantle composition and processes. *Geo. Soc. London*  
781 *Special Pub.* 42, 313-345.

782 Tao, Y., Ma, Y., Miao, L., Zhu, F., 2009. SHRIMP U-Pb zircon age of the Jinbaoshan  
783 ultramafic intrusion, Yunnan Province, SW China. *Chin. Sci. Bull.* 54, 168-172.

784 Thirlwall, M.F., Upton, B.G.J., Jenkins, C., 1994. Interaction between continental  
785 lithosphere and the Iceland plume—Sr-Nd-Pb isotope geochemistry of Tertiary  
786 basalts, NE Greenland. *J. Petrol.* 35(3), 839-879.

787 Thompson, G.M., Ali, J.R., Song, X.Y., Jolley, D.W., 2001. Emeishan basalts, SW  
788 China: Reappraisal of the formation’s type area stratigraphy and a discussion of its  
789 significance as a large igneous province. *J. Geol. Soc.* 158(4), 593-599.

790 Tian, J.C., Lin, X.B., Guo, W., Zhang, X., Huang, P.H., 2017. Geological significance  
791 of oil and gas in the Permian basalt eruption event in Sichuan Basin, China. *J.*

792 Chengdu University Technology (Sci. Technology Edition) 44(1), 14-20. In  
793 Chinese with English abstract.

794 Tian, Y.L., Li, Y., Meng, F.C., Zhao, L.K., Wu, Z.P., Du, Q., 2021. A study of the  
795 petrogenesis and spatial difference of the Emeishan large igneous province: Based  
796 on geochemical analysis and simulation of the high-Ti basalts in the whole region.  
797 *Acta Petrol. Mineral.* 40(4), 687-703. In Chinese with English abstract.

798 Wang, C.Y., Zhou, M.F., 2006. Genesis of the Permian Baimazhai magmatic Ni-Cu-  
799 (PGE) sulfide deposit, Yunnan, SW China. *Miner. Deposita* 41, 771-783.

800 Wang, C.Y., Zhou, M.F., Qi, L., 2007. Permian flood basalts and mafic intrusions in the  
801 Jinping (SW China)-Song Da (northern Vietnam) district: Mantle sources, crustal  
802 contamination and sulfide segregation. *Chem. Geol.* 243, 317-343.

803 Wang, Z. L., Xu, D.R., WU, C.J., Fu, W.W., Wang, L., Wu, J., 2013. Discovery of the  
804 late Paleozoic ocean island basalts (OIB) in Hainan Island and their geodynamic  
805 implications. *Acta Petrol. Sin.* 29(3), 875-886.

806 Weaver, B.L., 1991. The origin of ocean island basalt end-member compositions: trace  
807 element and isotopic constraints. *Earth Planet. Sci. Lett.* 104, 381-397.

808 Wei, X., Xu, Y.G., 2013. Petrogenesis of the mafic dykes from Bachu and implications  
809 for the magma evolution of the Tarim large igneous province, SW China. *Acta*  
810 *Petrol. Sin.* 29(10), 3323-3335.

811 Weis, D., Kieffer, B., Maerschalk, C., Pretorius, W., Barling, J., 2005. High-precision  
812 Pb-Sr-Nd-Hf isotopic characterization of USGS BHVO-1 and BHVO-2 reference  
813 materials. *Geochem. Geophys. Geosyst.* 6(2), 1-10.

814 Xiao, D., Tan, X.C., Shan, S.J., Chen, Y.Q., Xia, J.W., Yang, J., Zhou, T., Cheng, Y.,  
815 2014. The restoration of palaeokarst geomorphology of middle Permian Maokou  
816 Formation and its petroleum geological significance in southern Sichuan Basin.

817 Acta Geol. Sin. 88(10), 1992-2002. In Chinese with English abstract.

818 Xiao, L., Xu, Y.G., Chung, S.L., He, B., Mei, H.J., 2003. Chemostratigraphic  
819 correlation of Upper Permian lavas from Yunnan province, China: extent of the  
820 Emeishan large igneous province. *Int. Geol. Rev.* 45, 753-766.

821 Xiao, L., Xu, Y.G., Mei, H.J., Zheng, Y.F., He, B., Pirajno, F., 2004. Distinct mantle  
822 sources of low-Ti and high-Ti basalts from the Eastern Emeishan Large Igneous  
823 Province, SW China: implications for plume-lithosphere interaction. *Earth Planet.*  
824 *Sci. Lett.* 228(3-4), 525-546.

825 Xie, J., Ritzwoller, M.H., Shen, W., Yang, Y., Zheng, Y., Zhou, L., 2013. Crustal radial  
826 anisotropy across eastern Tibet and the western Yangtze craton. *J. Geophys. Res.*  
827 *- Sol. Ea.* 118(8), 4226-4252.

828 Xu, J., Xia, X.P., Lai, C.K., Zhou, M., Ma, P., 2019. First identification of Late Permian  
829 Nb- enriched basalts in Ailaoshan region (SW Yunnan, China): Contribution from  
830 Emeishan plume to subduction of eastern Paleotethys. *Geophys. Res. Lett.* 46,  
831 2511-2523.

832 Xu, J., Xia, X.P., Wang, Q., Spencer, C.J., He, B., Lai, C.K., 2021. Low- $\delta^{18}\text{O}$  A-type  
833 granites in SW China: Evidence for the interaction between the subducted  
834 Paleotethyan slab and the Emeishan mantle plume. *Geol Soc. Am. Bull.*  
835 <https://doi.org/10.1130/B35929.1>.

836 Xu, J.F., Suzuki K., Xu Y.G., Mei H.J., Li J., 2007. Os, Pb, and Nd isotope geochemistry  
837 of the Permian Emeishan continental flood basalts: Insights into the source of a  
838 large igneous province. *Geochim. Cosmochim. Acta* 71, 2104-2119.

839 Xu, R., Liu, Y., Lambart, S., 2020. Melting of a hydrous peridotite mantle source under  
840 the Emeishan large igneous province. *Earth-Sci. Rev.* 207, 103253.

841 Xu, Y.G., Chung, S.L., Jahn, B.M., Wu, G.Y., 2001. Petrologic and geochemical

842 constraints on the petrogenesis of Permian-Triassic Emeishan flood basalts in  
843 southern China. *Lithos* 58, 145-168.

844 Xu, Y.G., He, B., Chung, S.L., Menzies, M.A., Frey, F.A., 2014. Geologic, geochemical  
845 and geophysical consequences of plume involvement in the Emeishan flood-basalt  
846 province. *Geology* 32, 917-920.

847 Xu, Y.G., He, B., Luo, Z.Y., Liu, H.Q., 2013. Study on mantle plume and Large igneous  
848 provinces in China: An overview and perspectives. *Bull. Mineral. Petrol.*  
849 *Geochem.* 32(1), 25-39. In Chinese with English abstract.

850 Xu, Y.G., Luo, Z.Y., Huang, X.L., He, B., Xiao, L., Xie, L.W., Shi, Y.R., 2008. Zircon  
851 U-Pb and Hf isotope constraints on crustal melting associated with the Emeishan  
852 mantle plume. *Geochim. Cosmochim. Acta* 72(13), 3084-3104.

853 Xu, Y.G., Zhong, Y.T., Wei, X., Chen, J., Liu, H.Q., Xie, W., Luo, Z.Y., Li, H.Y., He,  
854 B., Huang, X.L., Wang, Y., Chen, Y., 2017. Permian Mantle Plumes and Earth's  
855 Surface System Evolution. *Bull. Mineral. Petrol. Geochem.* 36(3), 359-373+358.  
856 In Chinese with English abstract.

857 Yan, D.P., Qiu, L., Wells, M.L., Zhou, M.F., Meng, X., Lu, S., Zhang, S., Wang, Y., Li,  
858 S.B., 2018a. Structural and Geochronological constraints on the early Mesozoic  
859 North Longmen Shan Thrust Belt: Foreland fold- thrust propagation of the SW  
860 Qinling Orogenic Belt, Northeastern Tibetan plateau. *Tectonics* 37(12), 4595-4624.

861 Yan, D.P., Zhou, Y., Qiu, L., Wells, M.L., Mu, H., Xu, C.G., 2018b. The Longmenshan  
862 tectonic complex and adjacent tectonic units in the eastern margin of the Tibetan  
863 Plateau: a review. *J. Asian Earth Sci.* 164, 33-57.

864 Yang, J., Cawood, P. A., Du, Y., Huang, H., Hu, L., 2012. Detrital record of Indosinian  
865 mountain building in SW China: Provenance of the middle Triassic turbidites in  
866 the Youjiang Basin. *Tectonophysics* 574- 575, 105-117.

867 Yang, Z., He, B., 2012. Geochronology of detrital zircons from the middle Triassic  
868 sedimentary rocks in the Nanpanjiang Basin: Provenance and its geological  
869 significance. *Geotectonica et Metallogenia* 36(4), 581-596. In Chinese with  
870 English abstract.

871 Zhai, M.G., Yang, R.Y., 1986. Early Precambrian gneiss basement in the Panxi area,  
872 Southwest China. *Acta Petrol. Sin.* 2(3), 22-37. In Chinese with English abstract.

873 Zhang, J., Cao, X.M., Wang, J.L., Zhang, Z.C., 2011. Petrology of the Permian  
874 Langmao Basaltic Porphyry, Luquan County, Yunnan Province: Implications for  
875 the Petrogenesis of High-Ti Basalts. *Geoscience* 25(4), 692-702. In Chinese with  
876 English abstract.

877 Zhang, L., Ren, Z.Y., Handler, M.R., Wu, Y.D., Xu, Y.G., 2019. The origins of high-Ti  
878 and low-Ti magmas in large igneous provinces, insights from melt inclusion trace  
879 elements and Sr-Pb isotopes in the Emeishan large Igneous Province. *Lithos* 344-  
880 345, 122-133.

881 Zhang, L., Ren, Z.Y., Zhang, L., Wu, Y.D., Qian, S.P., Xia, X.P., Xu, Y.G., 2021. Nature  
882 of the mantle plume under the Emeishan large igneous province: Constraints from  
883 olivine-hosted melt inclusions of the Lijiang picrites. *J. Geophys. Res. Sol. Ea.*  
884 126, e2020JB021022.

885 Zhang, W., Hu Z.C., 2020. Estimation of isotopic reference values for pure materials  
886 and geological reference materials. *At. Spectrosc.* 41(3), 93-102.

887 Zhang, W., Hu, Z.C., Liu, Y.S., 2020a. Iso-Compass: new freeware software for isotopic  
888 data reduction of LA-MC-ICP-MS. *J. Anal. At. Spectrom.* 35, 1087-1096.

889 Zhang, Y., Chen, S.L., Zhang, X.L., Zhang, X.H., Xie, C., Chen, C., Yang, Y.R., Gao,  
890 Y.L., 2020b. Restoration of paleokarst geomorphology of Lower Permian Maokou  
891 Formation and its petroleum exploration implication in Sichuan Basin. *Lithologic*

892 Reservoirs 32(3), 44-55. In Chinese with English abstract.

893 Zhang, Y.X. 1988. Panxi rift. Beijing: Geological Press.

894 Zhang, Z.C., Mahoney, J.J., Mao, J.W., Wang, F.S., 2006. Geochemistry of picritic and  
895 associated basalt flows of the western Emeishan flood basalt province, China. J.  
896 Petrol. 47, 1997-2019.

897 Zhang, Z.C., Wang, F.S., 2003. Sr, Nd and Pb Isotopic Characteristics of Emeishan  
898 Basalt Province and Discussion on Their Source Region. Earth Sci.- J. China  
899 University of Geosciences 28(4), 431-439. In Chinese with English abstract.

900 Zhang, Z.C., Wang, F.S., Fan, W.M., Deng, H.L., Xu, Y.G., Xu, J.F., Wang, Y.J., 2001.  
901 A Discussion on Some Problems Concerning the Study of the Emeishan Basalts.  
902 Acta Petrol. Mineral. 20(3), 239-246. In Chinese with English abstract.

903 Zhang, Z.C., Zhi, X.C., Chen, L., Saunders, A.D., Reichow, M.K., 2008. Re-Os isotopic  
904 compositions of picrites from the Emeishan flood basalt province, China. Earth  
905 Planet. Sci. Lett. 276, 30-39.

906 Zheng, L.D., Yang, Z.Y., Tong, Y.B., Yuan, W., 2010. Magnetostratigraphic constraints  
907 on two-stage eruptions of the Emeishan continental flood basalts. Geochem.  
908 Geophys. Geosy. 11(12), 1-19.

909 Zhong, H., Zhu, W.G., 2006. Geochronology of layered mafic intrusions from the Pan-  
910 Xi area in the Emeishan large igneous province, SW China. Miner. Deposita 41,  
911 599-606.

912 Zhong, Y.T., He, B., Mundil, R., Xu, Y.G., 2014. CA-TIMS zircon U-Pb dating of felsic  
913 ignimbrite from the Binchuan section: implications for the termination age of  
914 Emeishan large igneous province. Lithos 204, 14-19.

915 Zhong, Y.T., He, B., Xu, Y.G., 2013. Mineralogy and geochemistry of claystones from  
916 the Guadalupian– Lopingian boundary at Penglaitan, South China: Insights into

917 the pre- Lopingian geological events. *J. Asian Earth Sci.* 62, 438-462.

918 Zhou, M.F., Chen, W.T., Wang, C.Y., Prevec, S.A., Liu, P.P., Howarth, G.H., 2013. Two  
919 stages of immiscible liquid separation in the formation of Panzhihua-type Fe-Ti-  
920 V oxide deposits, SW China. *Geosci. Front.* 4, 481-502.

921 Zhou, M.F., Malpas, J.G., Song, X.Y., Robinson, P.T., Sun, M., Kennedy, A., Leshner,  
922 M., Keays, R.R., 2002. A temporal link between the Emeishan large igneous  
923 province (SW China) and the end-Guadalupian mass extinction. *Earth Planet. Sci.*  
924 *Lett.* 196(3-4), 113-122.

925 Zhou, M.F., Wang, Z.C., Zhao, W.W., Qi, L., Zhao, Z., Zhou, J.X., Huang, Z.L., Chen,  
926 W.T., 2022. A reconnaissance study of potentially important scandium deposits  
927 associated with carbonatite and alkaline igneous complexes of the Permian  
928 Emeishan Large Igneous Province, SW China. *J. Asian Earth Sci.* 236, 105309.

929 Zhou, M.F., Zhao, J.H., Qi, L., Su, W.C., Hu, R.Z., 2006. Zircon U-Pb geochronology  
930 and elemental and Sr-Nd isotope geochemistry of Permian mafic rocks in the  
931 Funing area, SW China. *Contrib. Mineral. Petrol.* 151, 1-19.

932 Zhu, C.Q., Hu, S.B., Qiu, N.S., Rao, S., Yuan, Y.S., 2016. The thermal history of the  
933 Sichuan Basin, SW China: evidence from the deep boreholes. *Sci. China, Ser. D:*  
934 *Earth Sci.* 59, 70-82.

935 Zhu, C.Q., Xu, M., Yuan, Y.S., Zhao, Y.Q., Shan, J.N., He, Z.G., Tian, Y.T., Hu, S.B.,  
936 2010. Palaeogeothermal response and record of the effusing of Emeishan basalts  
937 in the Sichuan basin. *Chin. Sci. B* 55, 949-956.

938 Zhu, D.C., Mo, X.X., Wang, L.Q., Zhao, Z.D., Liao, Z.L., 2008. Hotspot-ridge  
939 interaction of the evolution of Neo-Tethys: insights from the Late Jurassic-Early  
940 Cretaceous magmatism in southern Tibet. *Acta Petrol. Sin.* 24(2), 225-237.

941 Zhu, D.C., Pan, G.T., Mo, X.X., Liao, Z.L., Jiang, X.S., Wang, L.Q., Zhao, Z.D., 2007.

942 Petrogenesis of volcanic rocks in the sangxiu formation, central segment of  
943 Tethyan Himalaya: a probable example of plume-lithosphere interaction. *J. Asian*  
944 *Earth Sci.* 29(2-3), 320-335.

945 Zhu, J., 2019. A study of mantle plume dynamics and its environmental effect in the  
946 Emeishan large igneous province. Beijing: China University of Geosciences  
947 (Beijing). In Chinese with English abstract.

948 Zhu, J., Zhang, Z.C., Reichow, M.K., Li, H.B., Cai, W.C., Pan, R.H., 2018. Weak  
949 vertical surface movement caused by the ascent of the Emeishan mantle anomaly.  
950 *J. Geophys. Res. Sol. Ea.* 123(2), 1018-1034.

951 Zi, J.W., Fan, W.M., Wang, Y.J., Cawood, P.A., Peng, T.P., Sun, L.H., Xu, Z.Q., 2010.  
952 U-Pb geochronology and geochemistry of the Dashibao Basalts in the Songpan-  
953 Ganzi Terrane, SW China, with implications for the age of Emeishan volcanism.  
954 *Am. J. Sci.* 310(9), 1054-1080.



955 **Fig. 1.** Simplified geological map showing the inner, intermediate and outer zones of  
956 the ELIP and sampling locations (modified after He et al., 2003; Zi et al., 2010).

957 The inner, intermediate, and outer zones in the ELIP area were defined by He et al.,  
958 2003. The hotspot track was obtained from Liu et al., 2021b. The ELIP eruption centre  
959 was obtained from He et al., 2010.

960 CAO = Central Asia Orogen; TM = Tarim Block; AHO = Alpine–Himalaya Orogen;  
961 QKO = Qinling-Qilian-Kunlun Orogen; NCC = North China Craton; YC = Yangtze  
962 Craton; CC = Cathaysia Craton.

963

964 **Fig. 2.** Schematic map of southwestern China showing the distribution of volcanic rocks  
965 in the Late Permian (a), and geological map of the Sichuan Basin showing the  
966 distribution of the Late Permian volcanic rocks (b) (modified after Liu et al., 2021a).

967

968 **Fig. 3.** Representative photos of field geology and petrographic features of the volcanic  
969 rocks from the drill cores and outcrops in and around the Sichuan Basin.

970 a. ST1-2, stomata almond basalt; b. YT1-7, massive basalt (cross-polarised light); c.  
971 ZG2-5, massive basalt; d. ZG2-5, massive basalt (cross-polarised light); e.  
972 Longmendong section; f. Longmendong basalt outcrop; g. Longchi basalt outcrop; h.  
973 Xinlin basalt outcrop.

974 Pl-plagioclase, Cpx-clinopyroxene.

975

976 **Fig. 4.** The connecting well section of boreholes ZG2-YT1-TF2-ZJ2-ST1 in the  
977 Sichuan Basin (based on logging data from Southwest Oil and Gas Field Company,

978 PetroChina).

979 The location of the connecting well section is shown in Fig. 2

980

981 **Fig. 5.**  $\text{TiO}_2$  vs.  $\text{Ti/Y}$  (a), and  $\text{O}'\text{-Ne}'\text{-Q}'$  (b) classification diagrams for the basalts in  
982 Sichuan Basin (LT and HT data from the inner zone in the ELIP were obtained from  
983 Song et al., 2001; Xiao et al., 2004; Xu et al., 2001; Zhang et al., 2006; data of HT from  
984 the outer zone were obtained from Fan et al., 2008; Lai et al., 2012; Li et al., 2016b;  
985 Wang et al., 2007; Xu et al., 2007).

986 (a) LT-low Ti series, HT-high low series. (b). A-Alkaline, S-Sub-alkaline.

987

988 **Fig. 6.** Selected elements plotted vs. MgO for the basalts from the Sichuan Basin

989

990 **Fig. 7.** Chondrite-normalised REE (a), and primitive mantle-normalised trace element  
991 (b) for the basalts in the Sichuan Basin (data for chondrite, primitive mantle and OIB  
992 are from Sun and McDonough, 1989; sources of geochemical data from other regions  
993 in the ELIP as for Fig. 5).

994

995 **Fig. 8.** Plots of  $^{87}\text{Sr}/^{86}\text{Sr}(t)$  vs.  $\epsilon_{\text{Nd}}(t)$  (a),  $^{206}\text{Pb}/^{204}\text{Pb}(t)$  vs.  $^{87}\text{Sr}/^{86}\text{Sr}(t)$  (b),  $^{206}\text{Pb}/^{204}\text{Pb}(t)$   
996 vs.  $^{207}\text{Pb}/^{204}\text{Pb}(t)$  (c), and  $^{206}\text{Pb}/^{204}\text{Pb}(t)$  vs.  $^{208}\text{Pb}/^{204}\text{Pb}(t)$  (d) for the basalts in the  
997 Sichuan Basin (Sources of geochemical data from other regions in the ELIP as for Fig.  
998 5. The fields of DM, MORB, Atlantic-Pacific MORB, Indian Ocean MORB, FOZO  
999 (focal zone), OIB, Dupal OIB, BSE (bulk silicate earth), HIMU (mantle with high U/Pb  
1000 ratios), EMI and EMII (enriched mantle), Kerguelen are from Barling and Goldstein,  
1001 1990; Deniel, 1998; Hamelin and Allègre, 1985; Hart, 1984; Hawkesworth et al., 1984;

1002 and Weaver, 1991. The LoNd (low Nd) array and NHRL (Northern Hemisphere  
1003 Reference Line) are from Hart, 1984. The Yangtze Block crustal compositions are from  
1004 Chen and Jahn, 1998; Gao et al., 1999; Ma et al., 2000 and Zhang et al., 2008.)

1005

1006 **Fig. 9.** Plots of Ce vs. Nb/Th (a),  $(Th/Ta)_P$  vs.  $(La/Nb)_P$  (b),  $SiO_2$  vs.  $^{87}Sr/^{86}Sr(t)$  (c), and  
1007  $SiO_2$  vs.  $\epsilon_{Nd}(t)$  (d) for the basalts in the Sichuan Basin (The fields of PM, N-MORB and  
1008 E-MORB are from Sun and McDonough, 1989; SCLM are from McDonough, 1990;  
1009 UC (upper crust), MC (middle crust) and LC (lower crust) are from Rudnick and Gao,  
1010 2003; Kerguelen alkaline basalts are from [http://georoc.mpch-](http://georoc.mpch-mainz.gwdg.de/georoc/Entry.html)  
1011 [mainz.gwdg.de/georoc/Entry.html](http://georoc.mpch-mainz.gwdg.de/georoc/Entry.html).)

1012

1013 **Fig. 10.** Plots of Mg# vs.  $CaO/Al_2O_3$  (a),  $Eu_N/Eu^*$  vs. Th+U (b), and  $Eu_N/Eu^*$  vs.  $\sum REE$   
1014 (c) for the basalts in the Sichuan Basin (sources of geochemical data from other regions  
1015 in the ELIP as for Fig. 5; the sample 20LMD05 is assumed as the initial melt of  
1016 fractional crystallization, mineral fractionation vectors are calculated using Rayleigh  
1017 fractionation law, and partition coefficients are from McKenzie and O'Nions, 1991).  
1018 Pl-plagioclase, Cpx-clinopyroxene and Opx-orthopyroxene.

1019

1020 **Fig. 11.** Diagrams of Nb/Yb vs. Th/Yb (a), and Ti/Yb vs. Nb/Th (b) for the basalts in  
1021 the Sichuan Basin (sources of geochemical data from other regions in the ELIP as for  
1022 Fig. 5. (a) MORB-OIB array, subduction component adding models are from Pearce,  
1023 2008. The arrow in the Figure represents the trend of adding subduction component. (b)  
1024 SCLM are from McDonough, 1990; UC, MC and LC are from Rudnick et al., 2003;  
1025 Hawaiian OIB mean was obtained from Feigenson et al., 1996; Kerguelen alkaline

1026 basalts are from <http://georoc.mpch-mainz.gwdg.de/georoc/Entry.html>; Sangxiu  
1027 Formation basalts were obtained from Zhu et al., 2007).

1028

1029 **Fig. 12.** Plots of  $\epsilon_{Nd}(t)$  vs.  $(La/Yb)_N$  (a), Yb vs. La/Yb (b), Th/La vs. Nb/U (c), and  
1030  $^{206}Pb/^{204}Pb$  vs.  $\epsilon_{Nd}(t)$  (d) for the basalts in the Sichuan Basin (sources of geochemical  
1031 data from other regions in the ELIP as for Fig. 5).

1032

1033 **Fig. 13.** Diagrams of  $(La/Sm)_N$  vs.  $(Tb/Yb)_N$  (a), and Sm/Yb vs. La/Sm (b) for the  
1034 basalts in the Sichuan Basin (sources of geochemical data from other regions in the  
1035 ELIP as for Fig. 5; (b) batch melting trends for garnet and spinel lherzolite were  
1036 obtained from Lassiter and Depaolo, 1997).

1037

1038 **Fig. 14.** Stratigraphic variation of the representative lava successions in the ELIP  
1039 (modified after Xiao et al., 2004; Xu et al., 2001, 2014).

1040

1041 **Fig. 15.** Evolution model of EILP during the Middle Permian. (The framework for the  
1042 plumbing system of ELIP associated with the Emeishan mantle plume was modified  
1043 from Feng et al. (2022) and Liu et al. (2021b). The boundaries of the inner-intermediate-  
1044 outer zones in the ELIP was defined by He et al. (2003) and Xiao et al. (2004). LQF,  
1045 HYF and QYF represent the Longquanshan fault, Huayingshan fault and Longquanshan  
1046 fault, respectively. LT and HT represent low-Ti basalts and high-Ti basalts, respectively.  
1047 The NE (northeastward) arrows show the direction of movement of the South China  
1048 Block (Liu et al., 2021b).)

1049 a. During the early-Guadalupian (~269 Ma), Western Yangtze Block experienced  
1050 Ailaoshan slab (Paleotethys Ocean) eastward subduction, and the adjacent Emeishan  
1051 mantle plume was modified by the recycled lithospheric fragments. b. In the first stage  
1052 of end-Guadalupian (260~257 Ma), lithosphere mantle melted and formed the low-Ti  
1053 basalts (LT) in the inner zone. c. In the second stage of end-Guadalupian (260~257 Ma),  
1054 the mantle plume melted and formed the high-Ti basalts (HT) in the inner-intermediate-  
1055 outer zones, with high-Ti basalts overlying low-Ti basalts in the inner zone.

**Table 1** Zircon U-Pb dating results of the Emeishan large igneous province

|                 | Locality                   | Rock type          | Analytical method     | Age/Ma              | Reference               |                      |                    |
|-----------------|----------------------------|--------------------|-----------------------|---------------------|-------------------------|----------------------|--------------------|
|                 | Dali-Jiangwei              | acid volcanic rock | ID-TIMS zircon U-Pb   | 258.9±0.5           | Xu et al. (2013)        |                      |                    |
|                 | Midu-Jinbaoshan            | wehrlite           | Shrimp zircon U-Pb    | 260.6±3.5           | Tao et al. (2009)       |                      |                    |
|                 |                            | hornblendite       | Shrimp zircon U-Pb    | 260.7±5.6           |                         |                      |                    |
|                 | Binchuan                   | acid tuff          | ID-TIMS zircon U-Pb   | 259.1±0.5           | Zhong et al. (2014)     |                      |                    |
|                 |                            | basalt             | Shrimp zircon U-Pb    | 256.2±1.4           | Li et al. (2016a)       |                      |                    |
|                 | Panxi-Daheishan            | syenite            | ID-TIMS zircon U-Pb   | 259.1±0.5           | Shellnutt et al. (2012) |                      |                    |
|                 | Panxi-Baima                | granite            | ID-TIMS zircon U-Pb   | 259.2±0.4           |                         |                      |                    |
|                 | Panxi-Huangcao             | syenite            | ID-TIMS zircon U-Pb   | 258.9±0.7           |                         |                      |                    |
| Inner Zone      | Panxi-Cida                 | granite            | ID-TIMS zircon U-Pb   | 258.4±0.6           | Xu et al. (2008)        |                      |                    |
|                 | Panxi-Maomaogou            | syenite            | Shrimp zircon U-Pb    | 261.6 ± 4.4         |                         |                      |                    |
|                 | Panxi-Miyi                 | syenite            | Shrimp zircon U-Pb    | 259.8 ± 3.5         |                         |                      |                    |
|                 | Panxi-Salian               | diorite            | Shrimp zircon U-Pb    | 260.4 ± 3.6         |                         |                      |                    |
|                 | Panxi-Taihe                | granite            | Shrimp zircon U-Pb    | 261.4 ± 2.3         |                         |                      |                    |
|                 | Panxi-Hongge               | gabbro             | Shrimp zircon U-Pb    | 259.3±1.3           |                         | Zhong and Zhu (2006) |                    |
|                 |                            | gabbro             | Shrimp zircon U-Pb    | 259.3 ± 1.3         |                         |                      |                    |
|                 |                            | Panxi-Binggu       | gabbro                | Shrimp zircon U-Pb  |                         | 260.7 ± 0.8          |                    |
|                 |                            | Xinjie             | gabbro                | Shrimp zircon U-Pb  |                         | 259±3                | Zhou et al. (2002) |
|                 | Intermediate Zone          | Guizhou-Weining    | boundary clay rock    | ID-TIMS zircon U-Pb |                         | 258.1±0.6            | Xu et al. (2013)   |
| Panxian-Zhudong |                            | ignimbrite         | ID-TIMS zircon U-Pb   | 258.3±1.4           | Zhu (2019)              |                      |                    |
| Xingyi-Xiongwu  |                            | tuff               | ID-TIMS zircon U-Pb   | 258.5±0.9           |                         |                      |                    |
| Puan-Louxia     |                            | tuff               | ID-TIMS zircon U-Pb   | 258.1±1.1           |                         |                      |                    |
|                 |                            | Baimazhai          | pyroxenite            | Shrimp zircon U-Pb  | 258.5±3.5               | Wang et al. (2006)   |                    |
| Outer Zone      | Tubagou                    | basalt             | Shrimp zircon U-Pb    | 257.3±2.0           | Li et al. (2016b)       |                      |                    |
|                 | Baise-Yangxu               | basalt             | Shrimp zircon U-Pb    | 259.1 ± 4.0         | Fan et al. (2008)       |                      |                    |
|                 | Bama-Minan                 | basalt             | Shrimp zircon U-Pb    | 259.6±5.9           |                         |                      |                    |
|                 | Nayong-Xilin-Tianyang Area | basalt             | LA-ICP-MS zircon U-Pb | 257.0±9.0           | Lai et al. (2012)       |                      |                    |

|                        |                       |                          |           |                     |
|------------------------|-----------------------|--------------------------|-----------|---------------------|
| Guangyuan-<br>Chaotian | boundary clay<br>rock | ID-TIMS<br>zircon U-Pb   | 258.6±1.4 | Xu et al. (2013)    |
|                        |                       |                          | 259.2±0.3 | Zhong et al. (2014) |
| Funing                 | diabase               | Shrimp zircon<br>U-Pb    | 260±3     | Zhou et al. (2006)  |
|                        | diorite               | Shrimp zircon<br>U-Pb    | 258±3     |                     |
| Mianhuadi              | metagabbro            | MC-ICP-MS<br>zircon U-Pb | 259.6±0.8 | Zhou et al. (2013)  |

1058 **Table 2** Major elements (wt.%) and trace elements ( $\times 10^{-6}$ ) contents for the analysed volcanic rocks in the Sichuan Basin

| Samples                                     | ST1<br>-2 | ST1<br>-5 | YT1<br>-1 | YT1<br>-3 | YT1<br>-4 | YT1<br>-5 | YT1<br>-6 | YT1<br>-7 | ZG2<br>-4 | ZG2<br>-5 | ZG2<br>-7   | ZG2<br>-8 | 20L<br>MD0<br>4 | 20L<br>MD0<br>5 | 20LC<br>04 | 20LC<br>06 | 20XL<br>01 | 20XL<br>02 | 20XL02<br>(replicate) |
|---|-----------|-----------|-----------|-----------|-----------|-----------|-----------|-----------|-----------|-----------|-------------|-----------|-----------------|-----------------|------------|------------|------------|------------|-----------------------|
| Locality                                    | ST1 Well  |           | YT1 Well  |           |           |           | ZG2 Well  |           |           |           | Longmendong |           | Longchi         |                 | Xinlin     |            |            |            |                       |
| SiO <sub>2</sub>                            | 49.64     | 48.78     | 48.62     | 47.55     | 46.69     | 47.67     | 48.67     | 48.96     | 46.59     | 47.64     | 48.74       | 45.59     | 45.99           | 48.99           | 45.94      | 49.08      | 49.21      | 48.12      | 48.32                 |
| TiO <sub>2</sub>                            | 4.01      | 3.87      | 4.06      | 3.91      | 4.17      | 4.19      | 3.83      | 3.71      | 4.01      | 3.98      | 4.05        | 4.14      | 3.69            | 3.73            | 4.08       | 3.69       | 4.24       | 3.82       | 3.84                  |
| Al <sub>2</sub> O <sub>3</sub>              | 13.75     | 13.66     | 13.69     | 13.66     | 13.64     | 13.82     | 14.99     | 14.96     | 13.07     | 12.98     | 13.30       | 13.70     | 13.44           | 13.90           | 13.91      | 13.88      | 13.57      | 13.08      | 13.06                 |
| Fe <sub>2</sub> O <sub>3</sub> <sup>T</sup> | 12.92     | 13.82     | 13.86     | 15.65     | 16.91     | 16.10     | 13.41     | 13.60     | 18.43     | 17.46     | 14.02       | 16.27     | 15.44           | 12.75           | 15.75      | 12.40      | 14.32      | 14.16      | 14.23                 |
| MnO   | 0.21      | 0.17      | 0.18      | 0.16      | 0.17      | 0.17      | 0.16      | 0.16      | 0.20      | 0.19      | 0.20        | 0.19      | 0.21            | 0.16            | 0.17       | 0.17       | 0.18       | 0.17       | 0.17                  |
| MgO   | 3.43      | 3.68      | 4.92      | 4.81      | 4.38      | 4.47      | 4.99      | 5.08      | 4.69      | 4.33      | 4.69        | 4.89      | 7.12            | 5.28            | 5.24       | 5.41       | 4.65       | 5.06       | 5.10                  |
| CaO   | 4.88      | 4.27      | 6.53      | 8.26      | 6.03      | 7.39      | 7.22      | 7.21      | 6.99      | 7.87      | 7.01        | 7.40      | 6.79            | 9.09            | 7.20       | 6.75       | 9.15       | 8.08       | 8.13                  |
| Na <sub>2</sub> O                           | 4.38      | 3.91      | 3.82      | 2.29      | 3.44      | 2.39      | 2.78      | 2.75      | 4.32      | 2.14      | 2.38        | 2.34      | 2.81            | 1.97            | 2.47       | 3.52       | 2.05       | 2.78       | 2.76                  |
| K <sub>2</sub> O                            | 0.22      | 0.56      | 1.96      | 1.73      | 2.36      | 1.98      | 1.92      | 1.93      | 0.85      | 1.94      | 2.21        | 2.03      | 1.51            | 1.42            | 1.17       | 2.15       | 0.99       | 1.83       | 1.85                  |
| P <sub>2</sub> O <sub>5</sub>               | 0.45      | 0.45      | 0.40      | 0.40      | 0.42      | 0.42      | 0.40      | 0.43      | 0.44      | 0.43      | 0.43        | 0.43      | 0.37            | 0.39            | 0.43       | 0.39       | 0.45       | 0.40       | 0.40                  |
| LOI   | 5.87      | 6.04      | 1.89      | 1.70      | 1.33      | 1.12      | 1.15      | 1.21      | 0.54      | 0.77      | 2.59        | 2.68      | 2.89            | 2.03            | 3.03       | 1.99       | 1.38       | 2.25       | 2.24                  |
| Total                                       | 99.76     | 99.20     | 99.94     | 100.1     | 99.56     | 99.70     | 99.51     | 99.99     | 100.1     | 99.71     | 99.61       | 99.66     | 100.2           | 99.71           | 99.37      | 99.41      | 100.1      | 99.75      | 100.12                |
| Mg#   | 34.45     | 34.49     | 41.29     | 37.85     | 33.92     | 35.47     | 42.42     | 42.53     | 33.53     | 32.93     | 39.85       | 37.33     | 47.74           | 45.09           | 39.72      | 46.36      | 39.15      | 41.42      | 39.12                 |
| La  | 45.2      | 45.1      | 47.9      | 46.8      | 47.1      | 49.4      | 45.2      | 45.8      | 49.5      | 48.7      | 44.2        | 44.8      | 37.4            | 47.2            | 43.3       | 44.3       | 48.4       | 42.0       | 41.9                  |
| Ce  | 96.3      | 95.6      | 98.3      | 97.5      | 99.4      | 103       | 93.6      | 95.6      | 99.1      | 101       | 95.0        | 97.6      | 85.9            | 104             | 98.0       | 101        | 106        | 94.9       | 93.4                  |
| Pr  | 12.4      | 12.2      | 12.8      | 12.7      | 12.9      | 13.0      | 11.8      | 12.4      | 12.9      | 13.4      | 12.8        | 12.8      | 11.3            | 13.2            | 12.8       | 13.1       | 13.8       | 12.5       | 12.3                  |
| Nd  | 52.6      | 51.9      | 52.1      | 52.0      | 52.9      | 52.7      | 49.5      | 50.4      | 51.4      | 56.0      | 52.8        | 54.0      | 48.7            | 54.3            | 53.4       | 53.7       | 56.8       | 52.8       | 51.5                  |
| Sm  | 11.7      | 11.0      | 11.0      | 10.6      | 10.6      | 10.6      | 9.41      | 9.91      | 9.99      | 11.6      | 10.6        | 11.4      | 10.8            | 11.5            | 11.4       | 11.6       | 12.0       | 11.3       | 10.7                  |
| Eu  | 3.00      | 2.82      | 2.97      | 3.06      | 3.01      | 2.98      | 2.87      | 2.95      | 2.94      | 3.01      | 2.96        | 3.04      | 2.84            | 3.08            | 3.06       | 3.02       | 3.30       | 3.11       | 3.03                  |
| Gd  | 9.72      | 9.91      | 9.55      | 9.83      | 9.58      | 9.51      | 9.05      | 9.25      | 9.67      | 10.3      | 9.80        | 10.3      | 9.48            | 10.0            | 9.69       | 9.69       | 10.4       | 9.64       | 9.46                  |
| Tb  | 1.36      | 1.31      | 1.26      | 1.28      | 1.26      | 1.27      | 1.13      | 1.22      | 1.29      | 1.33      | 1.33        | 1.39      | 1.32            | 1.41            | 1.35       | 1.41       | 1.43       | 1.34       | 1.31                  |
| Dy  | 8.07      | 7.36      | 7.47      | 7.50      | 7.80      | 7.51      | 6.90      | 7.02      | 7.90      | 8.13      | 7.83        | 8.02      | 7.28            | 7.65            | 7.47       | 7.79       | 7.91       | 7.64       | 7.38                  |
| Ho  | 1.45      | 1.26      | 1.29      | 1.26      | 1.30      | 1.35      | 1.16      | 1.15      | 1.37      | 1.35      | 1.29        | 1.39      | 1.31            | 1.40            | 1.33       | 1.44       | 1.42       | 1.35       | 1.28                  |



|    |      |      |      |      |      |      |      |      |      |      |      |      |      |      |      |      |      |      |      |
|----|------|------|------|------|------|------|------|------|------|------|------|------|------|------|------|------|------|------|------|
| Er | 3.61 | 3.36 | 3.45 | 3.41 | 3.42 | 3.38 | 3.12 | 3.08 | 3.51 | 3.59 | 3.51 | 3.61 | 3.36 | 3.61 | 3.49 | 3.70 | 3.55 | 3.47 | 3.44 |
| Tm | 0.47 | 0.46 | 0.44 | 0.45 | 0.46 | 0.46 | 0.41 | 0.44 | 0.50 | 0.49 | 0.50 | 0.51 | 0.45 | 0.47 | 0.46 | 0.48 | 0.47 | 0.47 | 0.45 |
| Yb | 2.93 | 2.73 | 2.73 | 2.70 | 2.77 | 2.69 | 2.48 | 2.53 | 2.93 | 2.75 | 2.86 | 2.98 | 2.74 | 2.91 | 2.80 | 2.97 | 2.84 | 2.81 | 2.73 |
| Lu | 0.38 | 0.36 | 0.36 | 0.37 | 0.37 | 0.35 | 0.35 | 0.36 | 0.40 | 0.40 | 0.39 | 0.41 | 0.39 | 0.40 | 0.40 | 0.42 | 0.40 | 0.39 | 0.38 |
| V  | 355  | 346  | 369  | 366  | 351  | 342  | 307  | 298  | 403  | 388  | 379  | 389  | 382  | 348  | 382  | 329  | 388  | 389  | 375  |
| Cr | 345  | 437  | 406  | 76.1 | 81.6 | 73.0 | 346  | 332  | 123  | 111  | 459  | 543  | 197  | 302  | 222  | 271  | 337  | 184  | 166  |
| Co | 48.4 | 45.6 | 47.5 | 45.8 | 46.1 | 45.3 | 49.9 | 50.6 | 43.3 | 46.7 | 49.9 | 57.8 | 48.1 | 41.4 | 48.7 | 40.1 | 46.6 | 44.9 | 43.6 |
| Ni | 226  | 265  | 257  | 139  | 158  | 131  | 247  | 246  | 302  | 257  | 255  | 293  | 136  | 172  | 132  | 163  | 195  | 120  | 107  |
| Cu | 254  | 284  | 284  | 249  | 304  | 266  | 259  | 267  | 364  | 541  | 193  | 412  | 257  | 241  | 234  | 64.4 | 247  | 332  | 326  |
| Zn | 128  | 124  | 141  | 133  | 134  | 131  | 116  | 118  | 150  | 123  | 140  | 146  | 136  | 120  | 145  | 120  | 142  | 136  | 132  |
| Ga | 25.8 | 23.1 | 26.2 | 25.8 | 25.2 | 25.7 | 25.4 | 25.5 | 24.5 | 25.7 | 25.4 | 26.5 | 27.9 | 25.5 | 27.3 | 23.5 | 26.0 | 26.6 | 25.7 |
| Rb | 3.82 | 13.3 | 43.4 | 38.5 | 52.1 | 45.7 | 53.5 | 53.1 | 22.6 | 65.1 | 70.6 | 68.9 | 58.5 | 38.8 | 46.9 | 70.3 | 23.1 | 59.7 | 58.6 |
| Sr | 882  | 870  | 830  | 580  | 1027 | 639  | 661  | 672  | 457  | 484  | 742  | 785  | 451  | 511  | 448  | 569  | 586  | 546  | 539  |
| Y  | 38.3 | 36.9 | 36.5 | 36.0 | 36.2 | 35.4 | 32.7 | 33.6 | 37.1 | 37.0 | 36.7 | 37.7 | 34.4 | 36.9 | 35.4 | 37.6 | 37.2 | 36.1 | 35.0 |
| Zr | 365  | 350  | 350  | 348  | 360  | 349  | 327  | 324  | 366  | 352  | 356  | 377  | 304  | 349  | 352  | 353  | 370  | 341  | 335  |
| Nb | 40.8 | 40.4 | 42.0 | 42.2 | 41.8 | 43.3 | 42.0 | 40.2 | 43.0 | 39.4 | 41.8 | 44.3 | 33.3 | 39.0 | 39.9 | 38.7 | 41.9 | 37.1 | 36.3 |
| Ba | 239  | 424  | 1306 | 405  | 1621 | 524  | 472  | 498  | 239  | 741  | 1065 | 1003 | 627  | 479  | 578  | 697  | 407  | 510  | 490  |
| Hf | 9.47 | 8.78 | 8.81 | 8.56 | 8.79 | 8.66 | 7.74 | 7.91 | 8.65 | 8.50 | 8.55 | 9.19 | 7.74 | 8.96 | 8.96 | 9.22 | 9.51 | 8.76 | 8.67 |
| Ta | 2.38 | 2.38 | 2.54 | 2.52 | 2.55 | 2.58 | 2.48 | 2.52 | 2.56 | 2.34 | 2.57 | 2.83 | 2.20 | 2.57 | 2.62 | 2.57 | 2.69 | 2.46 | 2.38 |
| Pb | 8.48 | 8.92 | 7.42 | 7.74 | 12.4 | 8.94 | 6.61 | 5.97 | 5.63 | 7.64 | 6.95 | 8.15 | 6.54 | 11.9 | 7.80 | 7.64 | 6.64 | 8.62 | 8.95 |
| Th | 7.12 | 6.90 | 6.84 | 6.77 | 7.03 | 6.97 | 6.70 | 6.63 | 6.58 | 6.61 | 6.57 | 6.81 | 7.21 | 8.12 | 6.49 | 8.35 | 6.97 | 6.47 | 6.25 |
| U  | 1.60 | 1.58 | 1.69 | 1.60 | 1.74 | 1.69 | 1.52 | 1.58 | 1.55 | 1.48 | 1.49 | 1.68 | 1.52 | 1.82 | 1.50 | 1.76 | 1.65 | 1.47 | 1.46 |

1059 LOI: weight loss on ignition to 1000 °C. Mg# =  $Mg^{2+}/(Mg^{2+}+Fe^{2+})$  in atomic ratio, assuming 15% of total iron oxide is ferric.

1060

**Table 3** Sr-Nd-Pb isotope ratios for the analysed volcanic rocks in the Sichuan Basin

| Sample                               | ST1-5    | YT1-1    | YT1-3    | YT1-6    | YT1-7    | ZG2-5    | ZG2-7    | ZG2-8    | 20LMD05     | 20LC06   | 20XL01   |
|--------------------------------------|----------|----------|----------|----------|----------|----------|----------|----------|-------------|----------|----------|
| Locality                             | ST1 Well | YT1 Well |          |          |          |          | ZG2 Well |          | Longmendong | Longchi  | Xinlin   |
| Rb( $\times 10^{-6}$ )               | 13.3     | 43.4     | 38.5     | 53.5     | 53.1     | 65.1     | 70.6     | 68.9     | 38.8        | 70.3     | 23.1     |
| Sr( $\times 10^{-6}$ )               | 870      | 830      | 580      | 661      | 672      | 484      | 742      | 785      | 511         | 569      | 586      |
| $^{87}\text{Rb}/^{86}\text{Sr}$      | 0.044372 | 0.151194 | 0.192215 | 0.234105 | 0.228342 | 0.389072 | 0.275352 | 0.254148 | 0.219834    | 0.357378 | 0.113896 |
| $^{87}\text{Sr}/^{86}\text{Sr}$      | 0.706884 | 0.707491 | 0.707355 | 0.706681 | 0.706694 | 0.706661 | 0.707085 | 0.707075 | 0.706865    | 0.707546 | 0.705942 |
| $^{26}\text{Al}$                     | 0.000008 | 0.000007 | 0.00001  | 0.000008 | 0.000008 | 0.000008 | 0.000006 | 0.000007 | 0.000007    | 0.00001  | 0.000009 |
| $^{87}\text{Sr}/^{86}\text{Sr}(t)$   | 0.706721 | 0.706935 | 0.706648 | 0.705820 | 0.705854 | 0.705230 | 0.706072 | 0.706140 | 0.706057    | 0.706232 | 0.705523 |
| Sm( $\times 10^{-6}$ )               | 11.0     | 11.0     | 10.6     | 9.41     | 9.91     | 11.6     | 10.6     | 11.4     | 11.5        | 11.6     | 12.0     |
| Nd( $\times 10^{-6}$ )               | 51.9     | 52.1     | 52.0     | 49.5     | 50.4     | 56.0     | 52.8     | 54.0     | 54.3        | 53.7     | 56.8     |
| $^{147}\text{Sm}/^{144}\text{Nd}$    | 0.128166 | 0.127908 | 0.123307 | 0.114987 | 0.118988 | 0.125756 | 0.121209 | 0.128019 | 0.128721    | 0.130854 | 0.127975 |
| $^{143}\text{Nd}/^{144}\text{Nd}$    | 0.512530 | 0.512533 | 0.512526 | 0.512528 | 0.512528 | 0.512567 | 0.512570 | 0.512573 | 0.512507    | 0.512507 | 0.512561 |
| $^{26}\text{Al}$                     | 0.000005 | 0.000008 | 0.000005 | 0.000006 | 0.000005 | 0.000004 | 0.000006 | 0.000013 | 0.000004    | 0.000004 | 0.000008 |
| $^{143}\text{Nd}/^{144}\text{Nd}(t)$ | 0.512313 | 0.512317 | 0.512317 | 0.512333 | 0.512327 | 0.512354 | 0.512365 | 0.512356 | 0.512289    | 0.512286 | 0.512344 |
| $\epsilon_{\text{Nd}}(t)$            | 0.16     | 0.22     | 0.24     | 0.55     | 0.42     | 0.96     | 1.17     | 1.00     | -0.31       | -0.38    | 0.77     |
| $T_{\text{DM}}(\text{Ma})$           | 1106     | 1098     | 1054     | 962      | 1002     | 1012     | 958      | 1028     | 1154        | 1184     | 1049     |
| $f_{\text{Sm}/\text{Nd}}$            | -0.35    | -0.35    | -0.37    | -0.42    | -0.40    | -0.36    | -0.38    | -0.35    | -0.35       | -0.33    | -0.35    |
| $^{206}\text{Pb}/^{204}\text{Pb}$    | 18.715   | 18.751   | 18.728   | 18.757   | 18.789   | 18.800   | 18.888   | 18.867   | 18.789      | 18.881   | 18.899   |
| $^{26}\text{Al}$                     | 0.001    | 0.001    | 0.001    | 0.001    | 0.001    | 0.001    | 0.001    | 0.001    | 0.000       | 0.001    | 0.000    |
| $^{207}\text{Pb}/^{204}\text{Pb}$    | 15.609   | 15.613   | 15.612   | 15.611   | 15.613   | 15.617   | 15.620   | 15.621   | 15.626      | 15.629   | 15.614   |
| $^{26}\text{Al}$                     | 0.001    | 0.001    | 0.001    | 0.001    | 0.001    | 0.001    | 0.001    | 0.001    | 0.000       | 0.001    | 0.000    |
| $^{208}\text{Pb}/^{204}\text{Pb}$    | 39.236   | 39.292   | 39.271   | 39.310   | 39.357   | 39.276   | 39.356   | 39.316   | 39.432      | 39.628   | 39.349   |
| $^{26}\text{Al}$                     | 0.002    | 0.002    | 0.002    | 0.002    | 0.002    | 0.002    | 0.001    | 0.002    | 0.001       | 0.002    | 0.001    |
| $^{206}\text{Pb}/^{204}\text{Pb}(t)$ | 18.251   | 18.154   | 18.185   | 18.156   | 18.097   | 18.293   | 18.323   | 18.325   | 18.388      | 18.272   | 18.245   |
| $^{207}\text{Pb}/^{204}\text{Pb}(t)$ | 15.585   | 15.582   | 15.584   | 15.580   | 15.578   | 15.592   | 15.591   | 15.593   | 15.606      | 15.598   | 15.581   |
| $^{208}\text{Pb}/^{204}\text{Pb}(t)$ | 38.572   | 38.500   | 38.520   | 38.440   | 38.403   | 38.533   | 38.542   | 38.597   | 38.845      | 38.685   | 38.446   |

1062

Notes:

1063

1.  $^{87}\text{Rb}/^{86}\text{Sr}$  and  $^{147}\text{Sm}/^{144}\text{Nd}$  ratios are calculated using Rb, Sr, Sm and Nd contents by ICP-MS and measured  $^{87}\text{Sr}/^{86}\text{Sr}$  and  $^{143}\text{Nd}/^{144}\text{Nd}$  ratios by MC-ICP-MS.

1064

2. In  $T_{\text{DM}}$  calculation, ratios of  $(^{143}\text{Nd}/^{144}\text{Nd})_{\text{DM}}$  and  $(^{147}\text{Sm}/^{144}\text{Nd})_{\text{DM}}$  took values of 0.51315 and 0.225, respectively.

1065

3. In  $\epsilon_{\text{Nd}}(t)$  calculations, ratios of  $(^{87}\text{Sr}/^{86}\text{Sr})_{\text{CHUR}}$ ,  $(^{87}\text{Rb}/^{86}\text{Sr})_{\text{CHUR}}$ ,  $(^{143}\text{Nd}/^{144}\text{Nd})_{\text{CHUR}}$  and  $(^{147}\text{Sm}/^{144}\text{Nd})_{\text{CHUR}}$  are 0.7045, 0.0847, 0.512638 and 0.1967, respectively,

1066

while  $t = 258.5$  Ma.

**Table 4** Distribution of the Emeishan basalts in the ELIP

| Zone              | Locality                        | Rock type                       | Reference   |
|-------------------|---------------------------------|---------------------------------|---|
| Inner zone        | Dali                            | High-Ti basalts, low Ti basalts | Hanski et al. (2010)  |
|                   | Lijiang                         | High-Ti basalts, low Ti basalts | Song et al. (2001), Zhang et al. (2006)                                       |
|                   | Binchuan                        | High-Ti basalts, low Ti basalts | Song et al. (2001), Xiao et al. (2004),<br>Xu et al. (2007), Xu et al. (2001) |
|                   | Ertan                           | High-Ti basalts, low Ti basalts | Song et al. (2001), Xu et al. (2001)  |
|                   | Jianchuan                       | High-Ti basalts, low Ti basalts | Song et al. (2001)  |
|                   | Pingchuan                       | Low Ti basalts                  | Xu et al. (2014)  |
|                   | Miyi                            | High-Ti basalts                 | Xu et al. (2014)  |
|                   | Kangsi                          | High-Ti basalts                 | He et al. (2010)  |
|                   | Wanmachang                      | High-Ti basalts                 | He et al. (2010)  |
|                   | Shuidiqiao                      | High-Ti basalts                 | He et al. (2010)  |
|                   | Longzhoushan                    | High-Ti basalts                 | Xu et al. (2007)  |
| Yongsheng         | High-Ti basalts, low Ti basalts | Hao et al. (2004)               |   |
| Intermediate zone | Dongchuan                       | High-Ti basalts                 | Song et al. (2008), Xu et al. (2001)  |
|                   | Qingyin                         | High-Ti basalts                 | Xu et al. (2014)  |
|                   | Qiaojia                         | High-Ti basalts                 | Xu et al. (2014)  |
|                   | Weining                         | High-Ti basalts                 | Xu et al. (2014)  |
|                   | Duge                            | High-Ti basalts                 | Xu et al. (2014)  |
|                   | Zhaotong                        | High-Ti basalts                 | Li et al. (2017c)   |
| Outer zone        | Zhijin                          | High-Ti basalts                 | Lai et al. (2012), Xu et al. (2007)   |
|                   | Jinding                         | High-Ti basalts                 | Xu et al. (2007)  |
|                   | Tubagou                         | High-Ti basalts                 | Li et al. (2016b)   |
|                   | Baise                           | High-Ti basalts                 | Fan et al. (2008)   |
|                   | Bama                            | High-Ti basalts                 | Fan et al. (2008), Lai et al. (2012), Liu<br>et al. (2017)                    |
|                   | Tianyang                        | High-Ti basalts                 | Fan et al. (2008), Liu et al. (2017)  |
|                   | Sichuan Basin                   | High-Ti basalts                 | This study  |

[Click here to view linked References](#)

1 **Geochemistry and petrogenesis of Late Permian basalts from**  
2 **the Sichuan Basin, SW China: Implications for the**  
3 **geodynamics of the Emeishan mantle plume**

4

5 **Fanchao Meng<sup>a,b,c\*</sup>, Yulu Tian<sup>a,b,c</sup>, Andrew C. Kerr<sup>d\*</sup>, Wei Wang<sup>e</sup>, Zhiping Wu<sup>a,b,c</sup>,**  
6 **Qiang Xu<sup>f</sup>, Qing Du<sup>a,b,c</sup>, Yaoqi Zhou<sup>a,b,c</sup>, Jiaqi Liu<sup>g</sup>**

7

8 a. School of Geosciences, China University of Petroleum (East China), Qingdao 266580, China

9 b. Pilot National Laboratory for Marine Science and Technology (Qingdao), Qingdao 266061,  
10 China

11 c. Shandong Provincial Key Laboratory of Deep Oil and Gas, China University of Petroleum (East  
12 China), Qingdao 266580, China

13 d. School of Earth and Environmental Sciences, Cardiff University, Cardiff, Wales CF10 3AT,  
14 United Kingdom

15 e. Exploration and development Research Institute of Southwest Oil and Gas Field Company,  
16 PetroChina, Chengdu 610041, China

17 f. School of Geoscience and Technology, Southwest Petroleum University, Chengdu 610500, China

18 g. Institute of Geology and Geophysics, Chinese Academy of Sciences, Beijing 100029, China

19

20 **Abstract**

21 **Plume-lithosphere interactions are significant in the formation of Large Igneous**  
22 **Provinces (LIPs). The Permian Emeishan Large Igneous Province (ELIP) is considered**  
23 **to be the result of a mantle plume. The Emeishan flood basalts comprise a major part**  
24 **of the ELIP and they define three zones: the inner, intermediate and outer zones. Both**  
25 **high-Ti and low-Ti basalts are present in the inner zone, whereas only high-Ti basalts**  
26 **are found in the intermediate zone and outer zone. However, there are only sparse**  
27 **outcrops in the outer zone, and so geochemical data on basalts from the outer zone are**

---

\* Corresponding author.

E-mail address: [mengfc@upc.edu.cn](mailto:mengfc@upc.edu.cn) (Fanchao Meng), [kerra@cf.ac.uk](mailto:kerra@cf.ac.uk) (Andrew C. Kerr).

28 rare and the role of plume-lithosphere interaction in the petrogenesis of volcanic rocks  
29 in the outer zone remains poorly understood. In the Sichuan basin, the Basalt Formation  
30 is found between the Permian Maokou Formation limestone and the Longtan Formation  
31 marl in some drill cores as well as in outcrops in the basin. This relationship  
32 demonstrates that the basaltic layer in the basin is part of the Emeishan flood basalts.  
33 These basalts have  $\text{TiO}_2$  contents of 3.7-4.2 wt.% and Ti/Y ratios of 604-720, being  
34 high-Ti sub-alkaline basalts. They display chondrite-normalized rare earth elements  
35 (REE) patterns enriched in light rare earth elements (LREE) relative to heavy rare earth  
36 elements (HREE) and have elevated large ion lithophile elements (LILE) and high field  
37 strength elements (HFSE). Lead isotope ratios are high ( $^{206}\text{Pb}/^{204}\text{Pb}(t) = 18.102\text{-}18.392$ ,  
38  $^{207}\text{Pb}/^{204}\text{Pb}(t) = 15.578\text{-}15.606$ ,  $^{208}\text{Pb}/^{204}\text{Pb}(t) = 38.410\text{-}38.850$ ), and  $\epsilon_{\text{Nd}}(t)$  values are -  
39 0.38~1.17. Detailed petrology and geochemistry suggest that the high-Ti basalts from  
40 the Sichuan Basin did not experience significant contamination of crustal and  
41 lithospheric mantle material during the ascent of magma. We infer that these basalts  
42 resulted from low-degree melting of the plume mantle source and underwent fractional  
43 crystallization of clinopyroxene. The distribution and petrogenesis of the Sichuan Basin  
44 basalts in the outer zone are different from those of the basalts in the inner zone and  
45 there are clearly different plume-lithosphere interactions in different parts of the ELIP.  
46 In the inner zone, the temperature of the lithosphere mantle was markedly elevated due  
47 to underplating of the mantle plume, causing a substantial quantity of lithosphere  
48 mantle melting and the initial formation of low-Ti basalts. This was followed by melting  
49 of the mantle plume and the formation of high-Ti basalts. In the outer zone, lower  
50 temperatures further from the plume centre were insufficient to generate extensive  
51 melting of the lithospheric mantle. Consequently, only the mantle plume melted in the  
52 outer zone, resulting in the formation of high-Ti basalts with minimal lithospheric input.

53 **Keywords:** Emeishan mantle plume, outer zone, Sichuan Basin basalts, petrogenesis  
54 of high-Ti basalts, plume-lithosphere interaction

55

## 56 **1. Introduction**

57 The Emeishan Large Igneous Province (ELIP) in the Upper Yangtze craton,  
58 Southwest China is composed mainly of Late Permian flood basalts, mafic-ultramafic  
59 intrusions and mafic dykes, along with lesser amounts of felsic volcanic rocks,  
60 pyroclastic counterparts, and alkaline rocks. The stratigraphy, chronology,  
61 geochemistry and geophysics of the ELIP has been studied in detail for many years and  
62 has been proposed to have formed by melting of a mantle plume (Chen et al., 2015; Liu  
63 et al., 2017; Shellnutt, 2014; Xiao et al., 2003; Xu et al., 2020; Xu et al., 2021; Zhang  
64 et al., 2008; Zhou et al., 2022). The Emeishan continental flood basalts have been  
65 broadly divided into two groups: a high-Ti series ( $\text{TiO}_2 > 2.5 \text{ wt.}\%$  and  $\text{Ti/Y} > 500$ ) and  
66 a low-Ti series (He et al., 2007; Song et al., 2008).

67 Geographically, the ELIP has been divided into inner, intermediate and outer  
68 zones based on geochemical, sedimentological, and biostratigraphic characteristics of  
69 the rock units (He et al., 2003; Xiao et al., 2004; Xu et al., 2014). **The rocks in the inner  
70 zone include both the high-Ti and low-Ti series, which are widely distributed in the  
71 Binchuan, Jianchuan, Lijiang and Ertan areas, whereas rocks in the intermediate and  
72 outer zones are dominated by high-Ti basalts (Li et al., 2017a; Liao, et al., 2012; Xiao  
73 et al., 2004; Xu et al., 2001, 2004).** Basalts are much more extensively exposed in the  
74 intermediate zone (in Zhaotong, Qiaojia and Dongchuan) than in the outer zone (Tian  
75 et al., 2021; Xu et al., 2001; Zhang et al., 2011). The outer zone does have some well-  
76 developed outcrops in Guangxi and Guizhou provinces (Liao et al., 2012; Xiao et al.,

77 2004; Xu et al., 2001, 2004).

78 There are three major petrogenetic models for the Emeishan basalts: 1) High-Ti  
79 basalts were derived from low-degree partial melting of the mantle plume (Cheng et al.,  
80 2019; Liang et al., 2021; Wang et al., 2007; Xiao et al., 2004; Xu et al., 2001), whereas  
81 the low-Ti basalts were generated from the sub-continental lithosphere mantle (SCLM),  
82 possibly with assimilation of some upper crust (Fan et al., 2008; Kamenetsky et al.,  
83 2012; Li et al., 2010; Song et al., 2008; Wang et al., 2007; Xiao et al., 2004); 2) High-  
84 Ti basalts were derived from the SCLM or mixed with lithospheric mantle materials  
85 during magma ascent, whereas the low-Ti basalts were generated from the mantle  
86 plume (Xu et al., 2007); 3) High-Ti and low-Ti basalts have the same mantle source  
87 and may represent different degrees of partial melting, fractional crystallization and/or  
88 crustal contamination (Dong et al., 2009; Hou et al., 2011; Ren et al., 2017; Zhang et  
89 al., 2019). A common feature of all models is that the lithosphere is most influential at  
90 the centre of the Emeishan mantle plume (Li et al., 2015; Song et al., 2001, 2008; Xiao  
91 et al., 2004; Xu et al., 2001, 2014; Zhang et al., 2006).

92 These previous studies, however, have mainly focused on the inner and  
93 intermediate zones and although there have been some more recent studies of igneous  
94 rocks in the outer zone (Li et al., 2017a; Liu et al., 2017; Liu et al., 2022), there is still  
95 a lack of information on the source of the Emeishan high-Ti basalts and comparison  
96 between the inner and outer zones. For instance, it is still unclear whether there was  
97 plume-lithosphere interaction in the outer zone of the ELIP.

98 In this paper, we investigate the petrology, major and trace elements, and Sr-Nd-  
99 Pb isotope systematics of eighteen samples from three boreholes (twelve samples) and  
100 three outcrops (six samples) within and around the Sichuan Basin belonging to the outer  
101 zone of the ELIP in order to assess their petrogenesis. This data is combined with

102 previously published data from the inner and outer zones in order to ascertain the nature  
103 of plume-lithosphere interaction and the influence of the Emeishan mantle plume over  
104 the whole province, especially the difference between the inner and outer zones.

105

## 106 **2. Geological background**

107 The ELIP is located on the western Yangtze Plate and to the east of the Qinghai-  
108 Tibet Plateau, and mainly erupted in 260~257 Ma (Fan et al., 2008; Huang et al., 2022;  
109 Li et al., 2015; Shellnutt et al., 2012; Zhong et al., 2014). Traditionally, the ELIP has  
110 been thought to be bounded on the northeast and southeast by the Baoxing-Yibin fault  
111 and the Mile-Shizong fault, respectively. The eastern boundary is situated in the  
112 Fuquan-Weng'an areas, eastern Guiyang, China. The northwestern and southwestern  
113 boundaries are the Longmenshan belt and the Jinshajiang-Ailaoshan-Red River fault,  
114 respectively (Chung et al., 1998; Li et al., 2016a; Xiao et al., 2003). Tectonic  
115 movements occur in the region, with a series of well-developed **north-trending faults**,  
116 such as the Anninghe fault, the Longmenshan fault and the Xianshuihe fault (Song et  
117 al., 2001; Yan et al., 2018a; Yan et al., 2018b) (Fig. 1). The basement of the ELIP is  
118 dominated by Mesoproterozoic metamorphic rocks (Zhai et al., 1986), overlying Pre-  
119 Sinian-Cenozoic strata.

120 The Emeishan volcanic sequence is mainly composed of flood basalts and  
121 contemporaneous ultramafic-felsic plutons, layered mafic-ultramafic intrusions and  
122 radiating mafic dyke swarms (Li et al., 2015; Liu et al., 2022; Shellnutt, 2014; Xu et al.,  
123 2001; Zhou et al., 2022). The Emeishan flood basalts range from a few hundred to five  
124 thousand meters in thickness (Xiao et al., 2003; Xu et al., 2001; Zhang et al., 2001) and  
125 the areal extent of the basalts may well be larger than  $1 \times 10^6 \text{ km}^2$  (Li et al., 2017a; Liu



126 et al., 2022). The thickness of the basalts gradually decreases from the inner zone to the  
127 outer zone (Chung et al., 1998; Xu et al., 2001; Zhu et al., 2018). The inner zone consists  
128 of a variety of lavas and pyroclastic rocks, including picrites, basalts, basaltic andesites  
129 and basaltic pyroclastic rocks, with trachytic and rhyolite tuff in the uppermost part of  
130 the sequence (Xiao et al., 2004; Xu et al., 2001, 2004). A more-restricted range of rocks  
131 is found in the intermediate and outer zones and includes tholeiites and alkaline basalts  
132 (He et al., 2010).

133 The Sichuan Basin, located in the northeast (outer zone) of the ELIP in the  
134 northwestern Yangtze Craton in the South China Block, is a typical superimposed basin  
135 common in southwestern China (Liu et al., 2021a). The Late Permian basalt outcrops  
136 of the ELIP have only been found in a few places (Jinding, Huayingshan and Yanghe)  
137 in the Sichuan Basin (e.g., Li et al., 2017a; Liang et al., 2021; Liu et al., 2021a). The  
138 lack of volcanic outcrops in this region can be attributed to the complex burial history  
139 of the Sichuan Basin, and this has made geochemical research difficult on the Emeishan  
140 basalts in the basin. However, abundant drill cores from the Sichuan Basin indicate that  
141 the Emeishan basalts are widely distributed between the Middle and Upper Permian  
142 strata (Liang et al., 2021). Based on seismic and drilling data, it has been proposed that  
143 basalts are mainly distributed in the western Sichuan Basin with a thickness of 40-500  
144 m, which thins from the southwest to northeast (Fig. 2) (Liu et al., 2021a; Tian et al.,  
145 2017). However, the geochemistry and petrogenesis of the basalts in the Sichuan Basin  
146 are still unclear. Therefore, in this study we have sampled the drill cores and available  
147 outcrops from the Sichuan Basin.

148

### 149 **3. Samples and geochronology**

150 All samples in this study were collected from six areas within and around the  
151 southwest of the Sichuan Basin (Fig. 2) , including the borehole samples from ST1  
152 (ST1-2, ST1-5) (Fig. 3a), YT1 (YT1-1, YT1-3, YT1-4, YT1-5, YT1-6, YT1-7) (Fig.  
153 3b) and ZG2 (ZG2-4, ZG2-5, ZG2-7, ZG2-8) (Fig. 3c, d), as well as outcrops  
154 Longmendong in Leshan City (20LMD04, 20LMD05) (Fig. 3e, f), Longchi in  
155 Emeishan City (20LC04, 20LC06) (Fig. 3g) and Xinlin in Leshan City (20XL01,  
156 20XL02) (Fig. 3h). Boreholes YT1 and ST1 are located around the Longquanshan fault,  
157 Longchi outcrop is close to the Longmenshan fault, while outcrops Xinlin and  
158 Longmendong, and borehole ZG2 border the Emei-Yibin fault in the western Sichuan  
159 Basin (Fig. 2b). All the samples were analysed for whole-rock major and trace elements,  
160 and eleven samples were analysed for Sr, Nd and Pb isotopes. All samples were  
161 collected from the central part of the massive lava flows with little amygdales and crack  
162 fillings. The basalts contain 2% to 15% phenocrysts of clinopyroxene, plagioclase, and  
163 minor olivine, set in a matrix comprising mostly plagioclase. The clinopyroxene  
164 phenocrysts are generally subhedral, occasionally euhedral, whereas the plagioclase  
165 phenocrysts are euhedral grains. The phenocrysts range in size from 700  $\mu\text{m}$  to 1800  
166  $\mu\text{m}$  in samples YT1-6 and YT1-7, while they are about 60~400  $\mu\text{m}$  in size in ZG2 Well,  
167 Longchi and Xinlin (Fig. 3b, d).

168 Stratigraphally, the Sichuan Basin volcanic rocks lie between the Permian Maokou  
169 Formation limestone and the Longtan Formation marl (Fig. 4), indicating that the  
170 Sichuan Basin basalts erupted in the Mid-Late Permian. This eruption time is consistent  
171 with the formation time of the ELIP, which suggests the Sichuan Basin basalts belong  
172 to the ELIP (Li et al., 2017a; Liu et al., 2022). Based on chronological data (Table 1),  
173 the main duration of the ELIP eruption is 260~257 Ma (e.g., Fan et al., 2008; Lai et al.,  
174 2012; Li et al., 2016a; Li et al., 2016b; Zhou et al., 2006; Zi et al., 2010).

175

176 **4. Analytical methods**

177 Fresh rocks were selected based on the characteristics of rock thin sections.  
178 Following the removal of amygdales and minor veins, the samples were crushed to 200  
179 mesh by an agate mortar. The pre-treatment ensures the accuracy of whole-rock  
180 geochemical analyses.

181 The major and trace elements and Sr-Nd-Pb isotopes of the samples were  
182 determined at the Wuhan Sample Solution Analytical Technology Co., Ltd., Wuhan,  
183 China. International reference material values are listed in the appendix.

184 Major elements were analysed by a Primus II X-ray fluorescence spectrometer  
185 (XRF) with wave-length dispersive X-ray fluorescence spectrometry. The major  
186 element data are corrected by the theoretical  $\alpha$  coefficient method, and relative standard  
187 deviations (RSD) for most major element oxides are within  $\pm 1-3\%$ . The contents of  
188 trace elements were analysed by Agilent 7700e ICP-MS. The analytical precision and  
189 accuracy for trace elements are mostly better than 10%. The detailed sample-  
190 preparation procedure for ICP-MS analyses can be found in Rudnick et al. (2004) and  
191 Liu et al. (2008).

192 Sr-Nd-Pb isotopic analyses of whole-rock samples were carried out on a Neptune  
193 Plus MC-ICP-MS (Thermo Fisher Scientific, Dreieich, Germany). All chemical  
194 preparations were performed on class 100 work benches within a class 1000 over-  
195 pressured clean laboratory. The sample powders were acid-leached before isotopic  
196 analysis (Weis et al., 2005). The data was processed by "Iso-Compass" software (Zhang  
197 et al., 2020a). Detailed analytical procedures are described in Chen et al. (2002) and Li  
198 et al. (2012).

199 The analysed  $^{87}\text{Sr}/^{86}\text{Sr}$  of NBS 987 standard solution is  $0.710242\pm 14$  (2SD,  $n=345$ ),  
200 which is consistent with the published values ( $0.710248\pm 12$ , Zhang and Hu, 2020). In  
201 addition, analysis of USGS reference materials BCR-2 (basalt) yielded ratios of  
202  $0.705012\pm 22$  (2SD,  $n=63$ ) for  $^{87}\text{Sr}/^{86}\text{Sr}$ , which are identical within error to their  
203 published results (Li et al. 2012). The Sr isotope standard precision (2SE) =  $0.000010$ -  
204  $0.000020$  (0.01‰-0.03‰, 2RSE), and the accuracy is better than  $0.000020$  ( $\sim 0.03\%$ ).  
205 For standard GSB 04-3258-2015, a  $^{143}\text{Nd}/^{144}\text{Nd}$  of  $0.512440\pm 6$  (2SD,  $n=31$ ) was  
206 obtained which is identical, within error, to its published value ( $0.512438\pm 6$  (2SD), Li  
207 et al., 2017b). In addition, the measurement results of  $^{143}\text{Nd}/^{144}\text{Nd}$  for USGS reference  
208 materials BCR-2 (basalt) are  $0.512641\pm 11$  (2SD,  $n=82$ ), which are identical, within  
209 error, to their published values (Li et al. 2012). The precision of Nd isotope analyses  
210 (2SE) =  $0.000005$ - $0.000025$  (0.01‰-0.05‰, 2RSE), and the analytical accuracy is  
211 better than  $0.000025$  ( $\sim 0.05\%$ ). The external precision of  $^{20x}\text{Pb}/^{204}\text{Pb}$  ratios for the  
212 reference material NBS 981 is 0.03% (2RSD). Furthermore, the USGS reference  
213 material BCR-2 (basalt) had analysed ratios of  $^{208}\text{Pb}/^{204}\text{Pb}=38.736\pm 17$ ,  
214  $^{207}\text{Pb}/^{204}\text{Pb}=15.628\pm 3$ , and  $^{206}\text{Pb}/^{204}\text{Pb}=18.756\pm 10$  (2SD,  $n=22$ ), which are consistent  
215 within error of 0.03% with the published results ( $^{208}\text{Pb}/^{204}\text{Pb}=38.725\pm 22$ ,  
216  $^{207}\text{Pb}/^{204}\text{Pb}=15.621\pm 4$ ,  $^{206}\text{Pb}/^{204}\text{Pb}=18.753\pm 8$ , Zhang and Hu 2020). The internal  
217 precision of  $^{20x}\text{Pb}/^{204}\text{Pb}$  ratio is 0.002‰-0.025‰, and the analytical accuracy is better  
218 than 0.03%.

219

## 220 **5. Results**

### 221 **5.1 Major elements**

222 The major element compositions of the volcanic rock samples from different

223 regions of the Sichuan Basin are listed in Table 2. The samples have all experienced  
224 some degree of hydrothermal alteration, and so the whole-rock raw data has been  
225 normalised on a volatile-free basis. Samples ST1-2 and ST1-5 have high LOI values of  
226 5.9 wt.% and 6.0 wt.% respectively and so their major element compositions were not  
227 used in this study.

228 The samples of the Sichuan Basin show large variations in SiO<sub>2</sub> (45.6-49.2 wt.%)  
229 and MgO (4.3-7.1 wt.%). The rocks have total alkalis (Na<sub>2</sub>O+K<sub>2</sub>O) that range from 3.0  
230 to 5.8 wt.% and have K<sub>2</sub>O/Na<sub>2</sub>O ratios of ~1.7. They have high TiO<sub>2</sub> contents of 3.7 to  
231 4.2 wt.% and Ti/Y ratios of 604 to 720, indicating that the basin basalts belong to the  
232 high-Ti series (Fig. 5a). The analysed samples mainly plot in the sub-alkaline field on  
233 the Ol'-Ne'-Q' diagram (Fig. 5b). The concentrations of the Al<sub>2</sub>O<sub>3</sub> and CaO are  
234 positively correlated with MgO, whereas K<sub>2</sub>O, TiO<sub>2</sub>, P<sub>2</sub>O<sub>5</sub>, Fe<sub>2</sub>O<sub>3</sub><sup>T</sup>, La and Nb are  
235 negatively correlated with MgO (Fig. 6). Compared with the outer zone of the ELIP,  
236 the inner zone has variable volcanic rock types, ranging from low-Ti series to high-Ti  
237 series (Fig. 5a).

238

## 239 **5.2 Trace elements**

240 The trace element contents of the basalts in the Sichuan Basin are listed in Table  
241 2. Chondrite-normalised REE patterns are enriched in the LREE ((La/Yb)<sub>N</sub> = 9.8-13.2)  
242 and depleted in the HREE ((Dy/Yb)<sub>N</sub> = 1.8-2.0), with only slight negative Eu anomalies  
243 (δEu = 0.83-0.95) (Fig. 7a). On primitive mantle-normalised trace element diagrams  
244 (Fig. 7b), the large ion lithophile elements (LILE) are quite variable, especially the large  
245 negative anomalies of Rb and K, as well as positive anomalies of Ba and Pb, which  
246 may result from sub-solidus hydrothermal alteration. However, alteration-resistant

247 immobile high field strength elements (HFSE, e.g., Nb, Ta, Zr, Hf, Th) of the samples  
248 are much more consistent, with slightly negative Zr anomalies and positive Th  
249 anomalies (Fig. 7b). The trace element compositions of the samples ST1-2 and ST1-5  
250 have not been affected considerably except for some mobile elements, therefore, they  
251 are still used in the following discussion. Overall, the Sichuan basalts have OIB (ocean  
252 island basalt)-like REE and trace element signatures, which are similar to compositions  
253 of the Emeishan high-Ti basalts from other regions.

254

### 255 **5.3 Sr-Nd-Pb isotopes**

256 The isotopic data of the basalts in the Sichuan Basin are presented in Table 3. The  
257 initial Sr-Nd-Pb isotopic compositions have been age-corrected to 258.5 Ma based on  
258 the age range of the Emeishan basalts in this paper. The initial Sr isotopic compositions  
259 of the high-Ti basalts in the Sichuan Basin range from 0.705230 to 0.706935 and the  
260  $\epsilon_{\text{Nd}}(t)$  values range from -0.38 to 1.17 (Fig. 8a). The Sichuan Basin basalts show a  
261 relatively wide range in  $^{208}\text{Pb}/^{204}\text{Pb}(t)$  ratios between 38.403 and 38.845, whereas  
262  $^{206}\text{Pb}/^{204}\text{Pb}(t)$  (18.097-18.388) and  $^{207}\text{Pb}/^{204}\text{Pb}(t)$  (15.578-15.606) compositions are  
263 more uniform (Fig. 8c, d). Compared with low-Ti basalts in the inner zone, the  
264 compositional range of high-Ti basalts in the ELIP is relatively constant with typical  
265 OIB-like Sr-Nd-Pb isotopic characteristics. The Sichuan Basin samples have slightly  
266 higher  $^{87}\text{Sr}/^{86}\text{Sr}(t)$  ratios than the high-Ti samples in other areas of the ELIP, and show  
267 the characteristics of the EMII end-member. However, in general, the basin samples  
268 overlap with the field of high-Ti basalts in the outer zone, which indicates the Sichuan  
269 Basin basalts belong to the outer zone of the ELIP.

270 These data plot above the LoNd (low Nd) array, close to OIB and EMII, in distinct

271 contrast to the DM (depleted mantle) and MORB (mid-ocean ridge basalt) (Fig. 8a, b).  
272 The samples lie above the North Hemisphere Reference Line (NHRL) and overlap with  
273 the field of OIB (Fig. 8c, d). In terms of  $^{206}\text{Pb}/^{204}\text{Pb}(t)$  vs.  $^{208}\text{Pb}/^{204}\text{Pb}(t)$ , the Sichuan  
274 Basin samples data have similar compositions to the high-Ti basalts in the ELIP and  
275 overlap with alkaline lavas from the Kerguelen Plateau (Fig. 8d) (Fan et al., 2008). The  
276 Kerguelen Plateau in the South Indian Ocean (which comprises a large amount of  
277 alkaline basalts, (Zhu et al., 2007)) is one of the largest LIPs in the world, which is  
278 related to the Kerguelen plume activity from the Early Cretaceous.

279

## 280 **6. Discussion**

### 281 **6.1 Crustal contamination and fractional crystallization**

282 As previously noted fluid-mobile elements (LILE) such as Rb, Ba, K, Pb and Sr  
283 show large variations and both positive and negative peaks, which are most likely to be  
284 caused by sub-solidus hydrothermal alteration, however, the REE, Th and HFSE (e.g.,  
285 Hf, Nb and Ta) are relatively alteration-resistant and so are essentially immobile.  
286 Therefore, in the following discussion, only immobile elements are used to assess the  
287 petrogenesis of these rocks.

288 It is necessary to evaluate the role of crustal contamination and fractional  
289 crystallization during magma ascent before we discuss potential mantle sources of  
290 volcanic rocks. Importantly, the proxies for crustal contamination, Th/Nb, La/Nb,  
291 Th/Ta and Nb/U ratios are not changed by partial melting or fractional crystallization  
292 in magma. Crustal contamination usually results in high Th/Nb (>5), La/Nb (>12) and  
293 Th/Ta ratios, and low Nb/U ratios (Neal et al., 2002; Pearce, 2008; Rudnick and Gao,  
294 2003). The basalts in the present study have low La/Nb (1.01-1.23), Th/Nb (0.15-0.22)

295 and Th/Ta (2.41-3.27), and high Nb/U (21.48-28.00). These characteristics reveal that  
296 they were derived from mantle source without significant continental crust  
297 contamination. In addition, there is no clear mixing trend between the Sichuan Basin  
298 samples and average continental crust on a Ce vs. Nb/Th diagram (Fig. 9a). The  
299 analysed samples are broadly similar to primitive mantle (PM) values, and are close to  
300 the field of Kerguelen alkaline OIB, as well as plotting far from the values of middle  
301 and upper continental crust (MC and UC) (Fig. 9b). Moreover, slightly positive Th  
302 anomalies, and slightly negative Nb and Ta anomalies (Fig. 7b) also confirm that the  
303 Sichuan Basin basalts have not been significantly contaminated by crustal materials,  
304 because continental crust is enriched in Th and strongly depleted in Nb and Ta.  
305 Furthermore,  $(^{87}\text{Sr}/^{86}\text{Sr})_i$  and  $\epsilon_{\text{Nd}}(t)$  do not correlate with increasing  $\text{SiO}_2$  (Fig. 9c, d),  
306 which also suggests little crustal contamination occurred. Therefore, the magmatic  
307 evolution of basalts in the Sichuan Basin is dominated by fractional crystallization or  
308 partial melting.

309 Basalts from Sichuan Basin have low MgO values (4.3-7.1 wt.%) and display good  
310 correlations between MgO and other major oxides ( $\text{Al}_2\text{O}_3$ ,  $\text{K}_2\text{O}$ ,  $\text{Fe}_2\text{O}_3^{\text{T}}$ ) as well as trace  
311 elements (La, Nb) (Fig. 6), which indicates the likely occurrence of fractional  
312 crystallization. The basalts in the Sichuan Basin have lower Ni, Cr and MgO than  
313 primitive magma (Hirajima et al., 1990) (Fig. 6), further suggesting that the magma  
314 experienced a **substantial** amount of fractional crystallization (e.g., olivine,  
315 clinopyroxene) during ascent.

316 The basalts are characterised by a positive correlation between MgO and CaO (Fig.  
317 6b), indicating that the magma underwent the fractional crystallization of clinopyroxene  
318 (Wei et al., 2013). A slight negative Eu anomaly (Fig. 7b) suggests the magma also  
319 experienced slight fractional crystallization of plagioclase. As illustrated in Fig. 10a,



320 the Sichuan Basin basalts exhibit a positive correlation between CaO/Al<sub>2</sub>O<sub>3</sub> ratios and  
321 Mg# values, similar to other Emeishan basalts. The calculated effects of fractional  
322 crystallization are shown in mineral vector diagrams in Figs. 10b and c. The data mostly  
323 plot near the clinopyroxene crystallization vector (Fig. 10b, c), further suggesting that  
324 clinopyroxene is the most significant mineral phase in the fractional crystallization.  
325 This is consistent with the petrographic features (Fig. 3), as there are more  
326 clinopyroxene phenocrysts than plagioclase in YT1-7 (Fig. 3b) and ZG2-5 (Fig. 3d).  
327 Moreover, the Sichuan basalts have enriched Fe and Ti, and MgO vs. Fe<sub>2</sub>O<sub>3</sub><sup>T</sup> and TiO<sub>2</sub>  
328 show negative correlations (Fig. 6d, e). These characteristics may be induced by the  
329 early fractional crystallization of Ti and Fe-poor silicate minerals, which indicates little  
330 crystallization of titanomagnetite in low oxygen fugacity conditions (Li et al., 2017;  
331 Zhang et al., 2011). Furthermore, low oxygen fugacity may also have promoted the  
332 fractional crystallization of clinopyroxene and plagioclase in the Sichuan Basin basalts  
333 (Fig. 3) (Li et al., 2017).

334

## 335 **6.2 Magma Source and Petrogenesis**

336 The Sichuan Basin basalts have high TiO<sub>2</sub> contents (>3.5 wt.%), relative  
337 enrichment of alkalis (3.1-5.9 wt.%), LILE and HFSE, and significant REE  
338 fractionation with (La/Yb)<sub>N</sub> ratios ranging from 9.8 to 13.2. The trace element and Sr-  
339 Nd-Pb isotope signatures are OIB-like with ε<sub>Nd</sub>(t) values ranging from -0.38 to 1.17,  
340 (Fig. 7, 8). However, the origin of the Emeishan basalts with these characteristics is still  
341 controversial, and has been variously ascribed to the melting of either a mantle plume  
342 (Cheng et al., 2019; Liang et al., 2021; Wang et al., 2007; Xiao et al., 2004; Zhang et  
343 al., 2019) or lithospheric mantle (Lai et al., 2012; Xu et al., 2007). Alternatively, some  
344 authors propose that these basalts result from the interaction of mantle plume melts with

345 the lithospheric mantle (Cheng et al., 2019; Fan et al., 2008; He et al., 2010; Xu et al.,  
346 2007).

347 Like the high-Ti basalts in other regions of the ELIP, REEs, trace elements (except  
348 some LILEs) and incompatible element ratios of the Sichuan Basin high-Ti basalts are  
349 very similar to OIB and Kerguelen alkaline OIB-like basalts (Fig. 7, 11). Furthermore,  
350 the Sichuan Basin samples have OIB-like initial Sr-Nd-Pb isotopic characteristics,  
351 broadly fall in the field of OIB and Kerguelen basalts (Fig. 8). These geochemical  
352 signatures suggest the high-Ti basalts from the Sichuan Basin might have originated  
353 from a plume source, compositionally similar to other regions in the ELIP (e.g., Cheng  
354 et al., 2019; He et al., 2010; Liu et al., 2017; Song et al., 2008). It is proposed that the  
355 high-Ti basaltic magma from the Sichuan Basin is probably the product of partial  
356 melting of the head of the mantle plume, because the outer zone is further from the  
357 plume centre, and lower temperatures would have resulted in less lithospheric melting  
358 (Cheng et al., 2019).

359 In terms of incompatible trace element ratios, the Sichuan Basin basalts show  
360 broadly constant  $(La/Yb)_N$  ratios as  $\epsilon_{Nd}(t)$  values increase (Fig. 12a), and La/Yb ratios  
361 have a negative correlation with Yb compositions (Fig. 12b). These characteristics  
362 reveal that the Emeishan high-Ti basalts did not originate from partial melting of a  
363 homogeneous plume source. The samples from the Sichuan Basin define a linear array  
364 on Th/La vs. Nb/U (Fig. 12c) and  $^{206}Pb/^{204}Pb$  vs.  $\epsilon_{Nd}(t)$  (Fig. 12d) plots similar to other  
365 Emeishan high-Ti basalts, which would support this inference. In addition, it is  
366 generally argued that metasomatic melts derived from the primitive mantle have La/Nb  
367 ratios of  $\sim 0.53$ , whereas those from MORB source have values of  $\sim 1.02$  (McKenzie  
368 and O’Nions, 1995). The Sichuan Basin basalts have high La/Nb ratios of 1.01-1.23,  
369 with OIB-like Sr-Nd isotopes signatures significantly different from MORB (Fig. 8a),

370 indicating that they were likely derived from OIB-like enriched mantle source that was  
371 previously metasomatized. Moreover, the Sichuan Basin high-Ti samples plot around  
372 the field of OIB (Fig. 8c, d) and have an EMII-type signature (Fig. 8a, b) in terms of  
373 Sr-Nd-Pb isotope space. These features indicate the mantle plume may have been  
374 metasomatized by enriched materials before the eruption of the Late Permian basalts  
375 (Xu et al., 2021).

376 It is still unclear whether such enriched components originate from the  
377 asthenosphere, SCLM, crust, or recycled materials. The asthenosphere is ruled out since  
378 the trace elements and Sr-Nd-Pb isotopes of the Emeishan high-Ti basalts have OIB-  
379 like rather than MORB-like characteristics (Fig. 8) (Liu et al., 2017; Song et al., 2001;  
380 Wang et al., 2007; Xiao et al., 2004). Like the Emeishan high-Ti basalts in other regions,  
381 the basalts in the Sichuan Basin have relatively high Ti/Yb ratios, distant from OIB-  
382 SCLM and OIB-crust mixing lines. They are also significantly different from the  
383 Sangxiu Formation basalts which have a contribution from both continental lithospheric  
384 mantle materials and the Kerguelen mantle plume (Fig. 11b) (Zhu et al., 2007).  
385 Furthermore, the Sichuan Basin samples have high Ce, unlike continental lithosphere  
386 (Fig. 9a), **which indicates minimal involvement of SCLM**. As shown in Section 6.1, the  
387 samples were not significantly contaminated by crust. Therefore, the enriched  
388 components are unlikely to be related to either SCLM or crust.

389 It has been argued that the enriched signature in the OIB-like source is related to  
390 ancient recycled oceanic crust (Sobolev et al., 2000, 2007) or subducted terrigenous  
391 sediments (Eisele et al., 2002; Hofmann, 1997; Weaver, 1991). The Sichuan Basin  
392 basalts display  $(\text{Ta/La})_N$  ratios of 0.8-1.1, with an average of 0.94. Ta is depleted  
393 relative to La, and Th/Yb and Nb/Yb ratios are high (Fig. 11a), suggesting the  
394 involvement of crustal components during ascent or the contribution of subduction

395 component. The Sichuan Basin basalts have not experienced crustal contamination, so  
396 it is more likely that the Emeishan mantle plume has undergone metasomatism,  
397 accompanied by mixing of enriched components during subduction. Many studies on  
398 volcanic and sedimentary rocks in southwestern China and the Ailaoshan Region  
399 propose that the Ailaoshan Ocean crust (Paleotethyan slab) subducted eastward into the  
400 upper mantle beneath the western South China Block during the Permian-Middle  
401 Triassic (Hou et al., 2017; Qin et al., 2011; Wang et al., 2013; Xu et al., 2019, 2021;  
402 Yang et al., 2012; Yang and He, 2012; Zhong et al., 2013).

403       Based on a study of the Late Permian and Early Triassic A-type granites in the  
404 Yuanyang area of Yunnan, South China, Xu et al. (2021) proposed a geodynamic model  
405 of the interaction between the Emeishan mantle plume and the subducted Paleotethyan  
406 oceanic crust. According to the model, the Ailaoshan Ocean subducted eastward  
407 beneath the western South China Block, and the adjacent Emeishan mantle plume  
408 rapidly entrained the recycled lithospheric fragments (Xu et al., 2021). This model  
409 provides a mechanism for the metasomatism of the Emeishan mantle plume, and further  
410 explains why the composition of the Emeishan mantle plume is heterogeneous. In  
411 addition, many authors have proposed that the Emeishan mantle plume is likely to be  
412 intrinsically related to recycled ancient oceanic materials (Ren et al., 2017; Zhu et al.,  
413 2018). Zhu et al. (2018) proposed that the amount of recycled materials may be 10~20%  
414 in the Emeishan plume, which is broadly consistent with the view of Ren et al. (2017).  
415 In summary, we propose that the high-Ti basalts in the outer zone were derived from  
416 an OIB-like Emeishan mantle plume, which was modified by enriched materials  
417 derived from a subducted slab before the Late Permian.

418       The high-Ti basalts in the Sichuan Basin, which are located in the outer zone of  
419 the ELIP, are a similar age to the Emeishan basalts. Reconstruction of the thermal

420 history of the Sichuan Basin with a high paleogeothermal gradient of 23.0-42.6 °C/km  
421 in 259 Ma, indicates that the Sichuan Basin suffered an intensive thermal event related  
422 to the Emeishan mantle plume (Zhu et al., 2010, 2016). The basalts in Guangxi and  
423 Guizhou provinces that are relevant to the ELIP imply an extension of magmatism at  
424 the periphery (the outer zone) of the plume (Fan et al., 2008; Lai et al., 2012; Liu et al.,  
425 2017). This evidence indicates that the Sichuan Basin high-Ti basalts are related to the  
426 Emeishan mantle plume.

427 Rare-earth element ratios of the Sichuan Basin basalts (Fig. 13a) suggest they were  
428 derived from a mantle source containing garnet. The Emeishan high-Ti basalts lie  
429 between the melting curves for garnet and spinel lherzolites, indicating that they are  
430 derived from the spinel-garnet transition zone (Fig. 13b). In contrast, the low-Ti basalts  
431 in the inner zones have lower La/Sm, Sm/Yb and Dy/Yb ratios, revealing a higher  
432 degree of mantle melting at a shallower melting depth (Wang et al., 2007; Xiao et al.,  
433 2004). The low-Ti basalts also plot closer to SCLM end members than high-Ti basalts  
434 (Fig. 11b) We therefore argue that low-Ti magma might be generated from, or contain,  
435 a greater proportion of material from the SCLM (Fan et al., 2008; Xiao et al., 2004).

436

### 437 **6.3 Spatial and temporal distribution of the Emeishan basalts and tectonic** 438 **significance**

439 Chronological data give precise constraints on the duration of the ELIP eruption  
440 as 260~257 Ma (Table 1) (e.g., Fan et al., 2008; Lai et al., 2012; Li et al., 2016a; Li et  
441 al., 2016b; Zhou et al., 2006; Zi et al., 2010). Magnetostratigraphic studies of the  
442 Emeishan basalts indicate that a substantial number of basalts were formed during a  
443 period of normal polarity, with the main eruption lasting ~1-2 Ma (Zheng et al., 2010).

444 It has been proposed that the major eruption phase lasted less than 1 Ma (Xu et al., 2017;  
445 Zhu et al., 2018). Therefore, it is difficult to give the exact eruptive ages of high-Ti and  
446 low-Ti basalts, although most low-Ti basalts are stratigraphically below high-Ti basalts  
447 in most field profiles (Fig.14).

448 As summarised in Fig. 14, both high-Ti and low-Ti series are exposed in the inner  
449 zone (e.g. Binchuan, Ertan, and Miyi areas), with high-Ti basalts overlying low-Ti  
450 basalts, whereas only high-Ti basalts erupted in the outer zone, i.e., a greater distance  
451 from the centre of the mantle plume (Table 4) (Fan et al., 2008; He et al., 2010; Song  
452 et al., 2001, 2008; Xiao et al., 2004; Xu et al., 2001, 2007; Zhang et al., 2006). Overall,  
453 the Permian basalts are distributed from northeast (the Sichuan Basin) to southwest (the  
454 centre of the mantle plume) in the ELIP, and the thickness of basalts gradually decreases  
455 from the inner zone to the outer zone (Fig. 14). This distribution trend not only is  
456 consistent with the hotspot track of the Emeishan mantle plume (Fig. 1b) (Liu et al.,  
457 2021b), but also overlaps the seismic anomaly trends and residual gravity anomaly  
458 (Deng et al., 2014; Liu et al., 2021b; Xie et al., 2013).

459 Our petrogenetic model is shown in Fig. 15 and builds on previous models (e.g.,  
460 Feng et al., 2022; Liu et al., 2021b; Liu et al., 2022; Xiao et al., 2004; He et al., 2010).  
461 Based on our new data, we further consider the petrology, geochemistry, and  
462 distribution characteristics of the Sichuan Basin basalts in the outer zone of the ELIP,  
463 and consider the influence of subduction of the paleo-oceanic crust (Hou et al., 2017;  
464 Xu et al., 2019, 2021), the movement of the South China block (Liu et al., 2021b; Liu  
465 et al., 2022), and the successive eruptions of the late Permian low-Ti and high-Ti basalts  
466 (He et al., 2010; Xiao et al., 2004; Xu et al., 2001).

467 Paleomagnetic studies suggest that the Yangtze Craton moved northward between  
468 300 and ~260 Ma and experienced an overall ~27° clockwise rotation from Permian to

469 **present** (Huang et al., 2018; Liu et al., 2021b). The Western Yangtze block experienced  
470 Ailaoshan slab eastward subduction from the early-Guadalupian (~269 Ma) (Xu et al.,  
471 2021), and the adjacent Emeishan mantle plume was modified by the recycled  
472 lithospheric fragments (Fig. 15a) (e.g. Hou et al., 2017; Qin et al., 2011; Wang et al.,  
473 2013; Xu et al., 2019, 2021). Paleotethyan subduction resulted in an extensional  
474 tectonic setting in the Sichuan Basin during Middle-Late Permian (Xu et al., 2021; Liu  
475 et al., 2022). Before the eruption of the Emeishan basalts, mantle upflow reached the  
476 lithosphere (Liu et al., 2021b), resulting in plume-lithosphere interactions, and crustal  
477 uplift. The magnitude of uplift is greater than 1000 m at its core (the inner zone) (He et  
478 al., 2003), and the uplift range of the Sichuan Basin in the outer zone is relatively low.  
479 The upper part of the Maokou Formation was exposed at the surface, resulting in  
480 different degrees of weathering, denudation, and a paleo-karst landscape (Hu et al.,  
481 2012; Xiao et al., 2014; Zhang et al., 2020b). This resulted in variable degrees of uplift  
482 in the Sichuan Basin. As the South China block drifted northward, major eruptions  
483 including low-Ti and high-Ti series occurred throughout the ELIP during the end-  
484 Guadalupian (260~257 Ma) (Fig. 15b, c) (Liu et al., 2021b, Feng et al., 2022).

485 We propose that from 260 to ~257 Ma, the temperature of the lithosphere mantle  
486 in the inner zone rose dramatically due to underplating of the mantle plume, causing  
487 partial melting of lithosphere mantle and forming the low-Ti basalts (Fig. 15b). As the  
488 lithospheric mantle gradually became refractory, OIB-like high-Ti basalts derived from  
489 the plume became the predominant magma type that erupted over the low-Ti basalts  
490 (Fig. 14, 15d). In contrast, at the periphery of the plume, the lithospheric mantle was  
491 cooler due to the distance from the centre of the mantle plume. As a result, the  
492 temperature would have been insufficient to generate extensive melting of the  
493 lithospheric mantle (Xu et al., 2001; Xiao et al., 2004; He et al. al., 2010). Therefore,

494 only the mantle plume melted in the outer zone, forming high-Ti basalts (Fig. 15c). As  
495 discussed in Section 6.2, the geochemical evidence also indicates that the source of the  
496 high-Ti basalts did not involve melts from SCLM.

497 The coexistence of high-Ti and low-Ti magma in the inner zone of the Emeishan  
498 mantle plume could be attributed to plume-lithosphere interaction. Geochemical  
499 modeling suggests that the Emeishan high-Ti basalts are formed at a higher melting  
500 pressure than the low-Ti basalts (Liu et al., 2017; Zhang et al., 2019). Continuous  
501 polybaric melting of the mantle source might account for compositional variations of  
502 the rock types in the inner zone. Furthermore, Dy/Yb and La/Yb ratios of the high-Ti  
503 basalts in the outer zone are lower than those in the inner zone, indicating a shallower  
504 source and higher melting degree of mantle peridotite for the high-Ti basalts in the outer  
505 zone (Tian et al., 2021). It is proposed that melting generally happens beneath thin  
506 lithosphere rather than thickened lithosphere, i.e., lid-effect, and the extent of melting  
507 beneath the thin lithosphere is likely very low (no more than ~5%) (Fram and Leshner,  
508 1993; Niu et al., 2021). The lithosphere in the outer zone is thicker than that in the inner  
509 zone in the ELIP (Tian et al., 2021). The magmatic activity in the outer zone is more  
510 limited than that in the inner zone, which is consistent with the “lid effect” model.

511 Therefore, the high-Ti basalts from the Sichuan Basin are the result of partial  
512 melting of the plume in the outer zone of the ELIP. In contrast, relatively few low-Ti  
513 basalts derived from the lithosphere mantle have been discovered in the outer zone,  
514 because it is more distant from the centre of the mantle plume and so has a cooler  
515 lithosphere.

516

517 **7. Conclusions**



518 Based on petrography and geochemistry of the basalts in the Sichuan Basin, and  
519 combined with published data from the inner and outer zones of the Emeishan mantle  
520 plume, it is concluded that.

521 (1) In the outer zone of the ELIP, the volcanic rocks from the Sichuan Basin are  
522 part of the Emeishan flood basalts. Based on chronological data, the main duration of  
523 the basalt in outer zone eruption is 260~257 Ma.

524 (2) Unlike the inner zone, the volcanic rocks in Sichuan Basin of the outer zone  
525 are predominantly high-Ti sub-alkaline basalts. The Sichuan Basin basalts with OIB-  
526 like geochemical signatures originated from the Emeishan mantle plume, which was  
527 modified by enriched materials derived from a subducted slab before the Late Permian.  
528 The samples have compositions consistent with low degrees of partial mantle melting  
529 and fractional crystallization dominated by clinopyroxene during magma evolution.

530 (3) During the early-Guadalupian (~269 Ma), Western Yangtze Block experienced  
531 Ailaoshan slab (Paleotethys Ocean) eastward subduction, and the adjacent Emeishan  
532 mantle plume was modified by the recycled lithospheric fragments. During the end-  
533 Guadalupian (260~257 Ma), the Emeishan mantle plume underplated the lithosphere  
534 mantle in the Yangtze Continent.

535 (4) In the inner zone, the lithosphere mantle and the mantle plume melted  
536 successively, forming low-Ti basalts and overlying high-Ti basalts respectively.  
537 However, in the outer zone, only high-Ti basalts derived from the mantle plume were  
538 able to form.

539

#### 540 **Acknowledgements**

541 We are grateful to two anonymous reviewers, handle editor Liang Qiu and chief

542 editor Meifu Zhou for their constructive comments and suggestions. We thank  
543 Hongfang Chen for help with major and trace elements and Sr-Nd-Pb isotopic  
544 composition analyses at the Wuhan Sample Solution Analytical Technology Co., Ltd.,  
545 Wuhan, China. This study was supported by Marine S&T Fund of Shandong Province  
546 for Pilot National Laboratory for Marine Science and Technology (Qingdao)  
547 (2021QNLMO20001-1), National Natural Science Foundation of China Project  
548 (42272225; 42072169) and Shandong Provincial Natural Science Foundation, China  
549 (ZR2021MD083).

550

## 551 **References**

- 552 Aldanmaz, E., Pearce, J.A., Thirlwall, M.F., Mitchell, J.G., 2000. Petrogenetic  
553 evolution of late Cenozoic, post-collision volcanism in western Anatolia, Turkey.  
554 *J. Volcanol. Geotherm. Res.* 102(1-2), 67-95.
- 555 Barling, J., Goldstein, S.L., 1990. Extreme isotopic variations in Heard Island lavas and  
556 the nature of mantle reservoirs. *Nature* 348, 59-62.
- 557 Carlson, R.W., 1995. Isotopic inferences on the chemical structure of the mantle. *J.*  
558 *Geodyn.* 20, 365-386.
- 559 Chen, F., Satir, M., Ji, J., Zhong, D., 2002. Nd-Sr-Pb isotopes of Tengchong Cenozoic  
560 volcanic rocks from western Yunnan, China: evidence for an enriched-mantle  
561 source. *J. Asian Earth Sci.* 21, 39-45.
- 562 Chen, J.F., Jahn, B.M., 1998. Crustal evolution of southeastern China: Nd and Sr  
563 isotopic evidence. *Tectonophysics* 284, 101-133.
- 564 Chen, Y., Xu, Y.G., Xu, T., Si, S.K., Liang, X.F., Tian, X.B., Deng, Y.F., Chen, L., Wang,  
565 P., Xu, Y.H., Lan, H.Q., Xiao, F.H., Li, W., Zhang, X., Yuan, X.H., Badal, J., Teng,  
566 J.W., 2015. Magmatic underplating and crustal growth in the Emeishan Large

567 Igneous Province, SW China, revealed by a passive seismic experiment. *Earth*  
568 *Planet. Sci. Lett.* 432, 103-114.

569 Cheng, W.B., Dong, S.Y., Jin, C.H., Zhao, B., Zhang, Y., Wang, C., 2019.  
570 Characteristics of elemental geochemistry and petrogenesis discussion of the  
571 Emeishan basalts in Muchuan area, Sichuan province. *J. Mineral. Petrol.* 39(4),  
572 49-60. In Chinese with English abstract.

573 Chung, S.L., Jahn, B.M., Wu, G.Y., Lo, C.H., Cong, S.L., 1998. The Emeishan flood  
574 basalt in SW China: A mantle plume initiation model and its connection with  
575 continental breakup and mass extinction at the Permian-Triassic Boundary. *Mantle*  
576 *Dynamics and Plate Interactions in East Asia.* American Geophysical Union (AGU)  
577 798(12), 47-58.

578 Deng, Y., Zhang, Z., Mooney, W., Badal, J., Fan, W., Zhong, Q., 2014. Mantle origin of  
579 the Emeishan large igneous province (South China) from the analysis of residual  
580 gravity anomalies. *Lithos* 204, 4-13.

581 Deniel, C., 1998. Geochemical and isotopic (Sr, Nd, Pb) evidence for plume-lithosphere  
582 interactions in the genesis of Grande Comore magmas (Indian Ocean). *Chem. Geol.*  
583 144, 281-303.

584 Dong, S.Y., Zhang, Z.C., 2009. Geochemical Behavior of Yttrium in Fe-Ti Oxides - An  
585 Example Inferred from the Emeishan Large Igneous Province. *Geol. Rev.* 55(3),  
586 355-360. In Chinese with English abstract.

587 Eisele, J., Sharma, M., Galer, S.J.G., Blichert-Toft, J., Devey, C.W., Hofmann, A.W.,  
588 2002. The role of sediment recycling in EM-1 inferred from Os, Pb, Hf, Nd, Sr  
589 isotope and trace element systematics of the Pitcairn hotspot. *Earth Planet. Sci.*  
590 *Lett.* 196, 197-212.

591 Fan, W.M., Zhang, C.H., Wang, Y.J., Guo, F., Peng, T.P., 2008. Geochronology and

592 geochemistry of Permian basalts in western Guangxi Province, Southwest China:  
593 evidence for plume–lithosphere interaction. *Lithos* 102 (1-2), 218-236.

594 Feigenson, M.D., Patino, L.C., Carr, M.J., 1996. Constraints on partial melting imposed  
595 by rare earth element variations in Mauna Kea basalts. *J. Geophys. Res.* 101(B5),  
596 11815-11829.

597 Feng, Q.Q., Qiu, N.S., Fu, X.D., Li, W.Z., Liu, X., Ji, R.Y., 2022. Maturity evolution of  
598 Permian source rocks in the Sichuan Basin, southwestern China: The role of the  
599 Emeishan mantle plume. *J. Asian Earth Sci.* 229, 105180.

600 Fram, M.S., Leshner, C.E., 1993. Geochemical constraints on mantle melting during  
601 creation of the North Atlantic basin. *Nature* 363(6431), 712-715.

602 Gao, S., Ling, W., Qiu, Y., Lian, Z., Hartmann, G., Simon, K., 1999. Contrasting  
603 geochemical and Sm-Nd isotopic compositions of Archean metasediments from  
604 the Kongling high-grade terrain of the Yangtze craton: evidence for cratonic  
605 evolution and redistribution of REE during crustal anatexis. *Geochim. Cosmochim.*  
606 *Acta* 63(13-14), 2071-2088.

607 Hamelin, B., Allègre, C.J., 1985. Large scale regional units in the depleted upper mantle  
608 revealed by an isotopic study of the south-west India ridge. *Nature* 315, 196-198.

609 Hart, S.R., 1984. The Dupal anomaly: a large-scale isotopic anomaly in the southern  
610 hemisphere. *Nature* 309, 753-756.

611 Hao, Y.L., Zhang, Z.C., Wang, F.S., Mahoney, J.J., 2004. Petrogenesis of high-Ti and  
612 low-Ti basalts from the Emeishan large igneous province. *Geol. Rev.* 50(6), 587-  
613 592. In Chinese with English abstract.

614 Hawkesworth, C.J., Rogers, N.W., van Calsteren, P.W.C., Menzies, M.A., 1984. Mantle  
615 enrichment processes. *Nature* 311 (27), 331-335.

616 He, B., Xu, Y.G., Chung, S.L., Xiao, L., Wang, Y.M., 2003. Sedimentary evidence for

617 a rapid, kilometer-scale crustal doming prior to the eruption of the Emeishan flood  
618 basalts, *Earth Planet. Sci. Lett.* 213, 391-405.

619 He, B., Xu, Y.G., Huang, X.L., Luo, Z.Y., Shi, Y.R., Yang, Q.J., Yu, S.Y., 2007. Age  
620 and duration of the Emeishan flood volcanism, SW China: Geochemistry and  
621 SHRIMP zircon U–Pb dating of silicic ignimbrites, post-volcanic Xuanwei  
622 Formation and clay tuff at the Chaotian section. *Earth Planet. Sci. Lett.* 255, 306-  
623 323.

624 He, Q., Xiao, L., Balta, B., Gao, R., Chen, J.Y., 2010. Variety and complexity of the  
625 Late-Permian Emeishan basalts: Reappraisal of plume-lithosphere interaction  
626 processes. *Lithos* 119, 91-107.

627 Hirajima, T., Ishiwatari, A., Gong, B., Zhang, R.Y., Nozaka, A.T., 1990. Coesite from  
628 Mengzhong eclogite at Dhonghai county, northeastern Jiangsu province, China.  
629 *Mineral. Mag.* 54(377), 579-583.

630 Hofmann, A.W., 1997. Mantle geochemistry: The message from oceanic volcanism.  
631 *Nature* 385, 219-229.

632 Hofmann, A.W., Jochum, K.P., Seufert, M., White, W.M., 1986. Nb and Pb in oceanic  
633 basalts: new constraints on mantle evolution. *Earth Planet. Sci. Lett.* 79, 33-45.

634 Hou, T., Zhang, Z.C., Kusky, T., Du, Y.S., Liu, J.L., Zhao, Z.D., 2011. A reappraisal of  
635 the high-Ti and low-Ti classification of basalts and petrogenetic linkage between  
636 basalts and mafic-ultramafic intrusions in the Emeishan Large Igneous Province,  
637 SW China. *Ore Geol. Rev.* 41, 133-143.

638 Hou, Y.L., Zhong, Y.T., Xu, Y.G., He, B., 2017. The provenance of late Permian karstic  
639 bauxite deposits in SW China, constrained by the geochemistry of interbedded  
640 clastic rocks, and U-Pb-Hf-O isotopes of detrital zircons. *Lithos* 278-281, 240-254.

641 Hu, M.Y., Hu, Z.G., Wei, G.Q., Yang, W., Liu, M.C., 2012. Sequence lithofacies

642 paleogeography and reservoir prediction of the Maokou Formation in Sichuan  
643 Basin. *Petrol. Explor. Dev.* 39(1), 45-55. In Chinese with English abstract.

644 Huang, B., Yan, Y., Piper, J.D.A., Zhang, D., Yi, Z., Yu, S., Zhou, T., 2018.  
645 Paleomagnetic constraints on the paleogeography of the East Asian blocks during  
646 Late Paleozoic and Early Mesozoic times. *Earth-Sci. Rev.* 186, 8-36.

647 Huang, H., Huyskens, M.H., Yin, Q.Z., Cawood, P.A., Hou, M.C., Yang, J.H., Xiong,  
648 F.H., Du, Y.S., Yang, C.C., 2022. Eruptive tempo of Emeishan large igneous  
649 province, southwestern China and northern Vietnam: Relations to biotic crises and  
650 paleoclimate changes around the Guadalupian-Lopingian boundary. *Geology* doi:  
651 <https://doi.org/10.1130/G50183.1>.

652 Kamenetsky, V.S., Chung, S.L., Kamenetsky, M., Kuzmin, D.V., 2012. Picrites from  
653 the Emeishan Large Igneous Province, SW China: a Compositional Continuum in  
654 Primitive Magmas and their Respective Mantle Sources. *J. Petrol.* 53(10), 2095-  
655 2113.

656 LaFlèche, M.R., Camiré, G., Jenner, G.A., 1998. Geochemistry of post-Acadian,  
657 Carboniferous continental intraplate basalts from the Maritimes basin, Magdalen  
658 islands, Québec, Canada. *Chem. Geol.* 148, 115-136.

659 Lai, S.C., Qin, J.F., Li, Y.F., Li, S.Z., Santosh, M., 2012. Permian high-Ti/Y basalts  
660 from the eastern part of the Emeishan Large Igneous Province, Southwestern  
661 China: Petrogenesis and tectonic implications. *J. Asian Earth Sci.* 47, 216-230.

662 Lassiter J.C., Depaolo, D.J., 1997. Plume/lithosphere interaction in the generation of  
663 continental and oceanic flood basalts: Chemical and isotopic constraints. Large  
664 igneous provinces: Continental, oceanic, and planetary flood volcanism.  
665 *Geophysical Monograph* 100, 335-355.

666 Li, C., Ripley, E.M., Tao, Y., Hu, R.Z., 2016b. The significance of PGE variations with

667 Sr-Nd isotopes and lithophile elements in the Emeishan flood basalt province from  
668 SW China to northern Vietnam. *Lithos* 248-251, 1-11.

669 Li, C.F., Li, X.H., Li, Q.L., Guo, J.H., Yang, Y.H., 2012. Rapid and precise  
670 determination of Sr and Nd isotopic ratios in geological samples from the same  
671 filament loading by thermal ionization mass spectrometry employing a single-step  
672 separation scheme. *Anal. Chim. Acta* 727(10), 54-60.

673 Li, H.B., Zhang, Z.C., Ernst, R., Lu, L.S., Santosh, M., Zhang, D.Y., Cheng, Z.G., 2015.  
674 Giant radiating mafic dyke swarm of the Emeishan Large Igneous Province,  
675 Identifying the mantle plume centre. *Terra Nova* 27(4), 247-257.

676 Li, H.B., Zhang, Z.C., Santosh, M., Lü, L.S., Han, L., Liu, W., 2017a. Late Permian  
677 basalts in the Yanghe area, eastern Sichuan Province, SW China, Implications for  
678 the geodynamics of the Emeishan flood basalt province and Permian global mass  
679 extinction. *J. Asian Earth Sci.* 134, 293-308.

680 Li, H.B., Zhang, Z.C., Santosh, M., Lü, L.S., Han, L., Liu, W., Cheng, Z.G., 2016a.  
681 Late Permian basalts in the northwestern margin of the Emeishan Large Igneous  
682 Province, Implications for the origin of the Songpan-Ganzi terrane. *Lithos* 256-  
683 257, 75-87.

684 Li, J., Zhong, H., Zhu, W.G., Bai, Z.J., Hu, W.J., 2017c. Elemental and Sr–Nd isotopic  
685 geochemistry of Permian Emeishan flood basalts in Zhaotong, Yunnan Province,  
686 SW China. *Int. J. Earth Sci.* 106, 617-630.

687 Li, J., Tang, S.H., Zhu, X.K., Pan, C.X., 2017b. Production and Certification of the  
688 Reference Material GSB 04-3258-2015 as a  $^{143}\text{Nd}/^{144}\text{Nd}$  Isotope Ratio Reference.  
689 *Geostand. Geoanal. Res.* 41, 255-262.

690 Li, J., Xu, J.F., Suzuki, K., He, B., Xu, Y.G., Ren, Z.Y., 2010. Os, Nd and Sr isotope  
691 and trace element geochemistry of the Muli picrites: Insights into the mantle

692 source of the Emeishan Large Igneous Province. *Lithos* 119(1-2), 108-122.

693 Liang, Y.X., Li, H., Zhang, D.D., Yang, K., Zhou, D.W., Zheng, T.Y., Dong, Y.K., Zhai,  
694 L.G., 2021. Geochemical characteristics and genetic analysis of Huayingshan  
695 Emeishan basalt in Sichuan Basin. *Chin. J. Geol.* 56(1), 288-302. In Chinese with  
696 English abstract.

697 Liao, B.L., Zhang, Z.C., Kou, C.H., Li, H.B., 2012. Geochemistry of the Shuicheng  
698 Permian sodium trachybasalts in Guizhou Province and constraints on the mantle  
699 sources. *Acta Petrol. Sin.* 28(4), 1238-1250. In Chinese with English abstract.

700 Liu, R., Luo, B., Li, Y., Qiu, N.S., Wang, W., Zhang, Y., He, Q.L., Pei, S.Q., 2021a.  
701 Relationship between Permian volcanic rocks distribution and karst  
702 paleogeomorphology of Maokou Formation and its significance for petroleum  
703 exploration in western Sichuan Basin, SW China. *Petrol. Explor. Dev.* 48(3), 575-  
704 585. In Chinese with English abstract.

705 Liu, X.J., Liang, Q.D., Li, Z.L., Castillo, P.R., Shi Y., Xu, J.F., Huang, X.L., Liao, S.A.,  
706 Huang, W.L., Wu, W.N., 2017. Origin of Permian extremely high-Ti/Y mafic lavas  
707 and dykes from Western Guangxi, SW China: Implications for the Emeishan  
708 mantle plume magmatism. *J. Asian Earth Sci.* 141, 97-111.

709 Liu, X.Y., Qiu, N.S., Søger, N., Fu, X.D., Liu, R., 2022. Geochemistry of Late Permian  
710 basalts from boreholes in the Sichuan Basin, SW China: Implications for an  
711 extension of the Emeishan large igneous province. *Chem. Geol.* 588, 120636.

712 Liu, Y.D., Li, L., van Wijk, J., Li, A.B., Fu, Y. V., 2021b. Surface-wave tomography of  
713 the Emeishan large igneous province (China): Magma storage system, hidden  
714 hotspot track, and its impact on the Capitanian mass extinction. *Geology* 49(9),  
715 1032-1037.

716 Liu, Y.S., Zong, K.Q., Kelemen, P.B., Gao, S., 2008. Geochemistry and magmatic



717 history of eclogites and ultramafic rocks from the Chinese continental scientific  
718 drill hole: subduction and ultrahigh-pressure metamorphism of lower crustal  
719 cumulates. *Chem. Geol.* 247, 133-153.

720 Ma, C.Q., Ehlers, C., Xu, C.H., 2000. The roots of the Dabieshan ultrahigh-pressure  
721 metamorphic terrain: constraints from geochemistry and Nd-Sr isotope  
722 systematics. *Precambrian Res.* 102, 279-301.

723 McDonough, W.F., 1990. Constraints on the composition of the continental lithosphere  
724 mantle. *Earth Planet. Sci. Lett.* 101, 1-18.

725 McKenzie, D., O’Nions, R.K., 1991. Partial melt distributions from inversion of rare  
726 earth element concentrations. *J. Petrol.* 32, 1021-1091.

727 McKenzie, D., O’Nions, R.K., 1995. The Source Regions of Ocean Island Basalts. *J.*  
728 *Petrol.* 36(1), 133-159.

729 Neal, G.R., Mahoney, J.J., Chazey III, W.J., 2002. Mantle sources and the highly  
730 variable role of the continental lithosphere in basalt petrogenesis of the Kerguelen  
731 Plateau and the broken ridge LIP: results from ODP Leg 183. *J. Petrol.* 43, 1177-  
732 1205.

733 Niu, Y.L., 2021. Lithosphere thickness controls the extent of mantle melting, depth of  
734 melt extraction and basalt compositions in all tectonic settings on Earth-A review  
735 and new perspectives. *Earth-Sci. Rev.* 217, 103614.

736 Norman, M.D., 1998. Melting and metasomatism in the continental lithosphere: laser  
737 ablation ICPMS analysis of minerals in spinel lherzolites from eastern Australia.  
738 *Contrib. Mineral. Petrol.* 130(3-4), 240-255.

739 Palacz, Z.A., Saunders, A.D., 1986. Coupled trace element and isotope enrichment in  
740 the Cook–Austral– Samoa islands, southwest Pacific. *Earth Planet. Sci. Lett.* 79,  
741 270-280.

742 Pearce, J.A., 2008. Geochemical fingerprinting of oceanic basalts with applications to  
743 ophiolite classification and the search for Archean oceanic crust. *Lithos* 100(1–4),  
744 14-48.

745 Qin, X. F., Wang, Z. Q., Zhang, Y. L., Pan, L. Z., Hu, G. A., Zhou, F. S., 2011.  
746 Geochronology and geochemistry of early Mesozoic acid volcanic rocks from  
747 Southwest Guangxi: Constraints on tectonic evolution of the southwestern  
748 segment of Qinzhou- Hangzhou joint belt. *Acta Petrol. Sin.* 27(3), 794-808.

749 Ren, Z.Y., Wu, Y.D., Zhang, L., Nichols, A.R.L., Hong, L.B., Zhang, Y.H., Zhang, Y.,  
750 Liu, J.Q., Xu, Y.G., 2017. Primary magmas and mantle sources of Emeishan  
751 basalts constrained from major element, trace element and Pb isotope  
752 compositions of olivine-hosted melt inclusions. *Geochim. Cosmochim. Acta*  
753 208(2), 63-85.

754 Rudnick, R.L., Gao, S., 2003. Composition of the Continental Crust. *Treatise Geochem.*  
755 3, 1-64.

756 Rudnick, R.L., Gao, S., Ling, W.L., Liu, Y.S., McDonough, W.F., 2004. Petrology and  
757 geochemistry of spinel peridotite xenoliths from Hannuoba and Qixia, North  
758 China Craton. *Lithos* 77, 609-637.

759 Shellnutt, J. G., 2014. The Emeishan large igneous province: a synthesis. *Geosci. Front.*  
760 5(3), 369-394.

761 Shellnutt, J.G., Denyszyn, S.W., Mundil, R., 2012. Precise age determination of mafic  
762 and felsic intrusive rocks from the Permian Emeishan large igneous province (SW  
763 China). *Gondwana Res.* 22, 118-126.

764 Sobolev, A.V., Hofmann, A.W., Kuzmin, D.V., Yaxley, G.M., Arndt, N.T., Chung, S.L.,  
765 Danyushevsky, L.V., Elliott, T., Frey, F.A., Garcia, M.O., 2007. The amount of  
766 recycled crust in sources of mantle-derived melts. *Science* 316, 412-417.

767 Sobolev, A.V., Hofmann, A.W., Nikogosian, I.K., 2000. Recycled oceanic crust  
768 observed in “ghost plagioclase” within the source of Mauna Loa lavas. *Nature* 404,  
769 986-990.

770 Song, X.Y., Qi, H.W., Robinson, P.T., Zhou, M.F., Cao, Z.M., Chen, L.M., 2008.  
771 Melting of the subcontinental lithosphere mantle by the Emeishan mantle plume:  
772 evidence from the basal alkaline basalts in Dongchuan, Yunnan, Southwestern  
773 China. *Lithos* 100, 93-111.

774 Song, X.Y., Zhou, M.F., Hou, Z.Q., Cao, Z.M., Wang, Y.L., Li, Y.G., 2001.  
775 Geochemical constraints on the mantle source of the Upper Permian Emeishan  
776 continental flood basalts, southwestern China. *Int. Geol. Rev.* 43, 213-225.

777 Stanley, C.R., Russel, J.K., 1989. Petrologic hypothesis testing with Pearce element  
778 ration diagrams derivation of diagram axes. *Contrib. Mineral. Petrol.* 103, 78-89.

779 Sun, S.S., McDonough, W.F., 1989. Chemical and isotopic systematics of oceanic  
780 basalt: Implications for mantle composition and processes. *Geo. Soc. London*  
781 *Special Pub.* 42, 313-345.

782 Tao, Y., Ma, Y., Miao, L., Zhu, F., 2009. SHRIMP U-Pb zircon age of the Jinbaoshan  
783 ultramafic intrusion, Yunnan Province, SW China. *Chin. Sci. Bull.* 54, 168-172.

784 Thirlwall, M.F., Upton, B.G.J., Jenkins, C., 1994. Interaction between continental  
785 lithosphere and the Iceland plume—Sr-Nd-Pb isotope geochemistry of Tertiary  
786 basalts, NE Greenland. *J. Petrol.* 35(3), 839-879.

787 Thompson, G.M., Ali, J.R., Song, X.Y., Jolley, D.W., 2001. Emeishan basalts, SW  
788 China: Reappraisal of the formation’s type area stratigraphy and a discussion of its  
789 significance as a large igneous province. *J. Geol. Soc.* 158(4), 593-599.

790 Tian, J.C., Lin, X.B., Guo, W., Zhang, X., Huang, P.H., 2017. Geological significance  
791 of oil and gas in the Permian basalt eruption event in Sichuan Basin, China. *J.*

792 Chengdu University Technology (Sci. Technology Edition) 44(1), 14-20. In  
793 Chinese with English abstract.

794 Tian, Y.L., Li, Y., Meng, F.C., Zhao, L.K., Wu, Z.P., Du, Q., 2021. A study of the  
795 petrogenesis and spatial difference of the Emeishan large igneous province: Based  
796 on geochemical analysis and simulation of the high-Ti basalts in the whole region.  
797 *Acta Petrol. Mineral.* 40(4), 687-703. In Chinese with English abstract.

798 Wang, C.Y., Zhou, M.F., 2006. Genesis of the Permian Baimazhai magmatic Ni-Cu-  
799 (PGE) sulfide deposit, Yunnan, SW China. *Miner. Deposita* 41, 771-783.

800 Wang, C.Y., Zhou, M.F., Qi, L., 2007. Permian flood basalts and mafic intrusions in the  
801 Jinping (SW China)-Song Da (northern Vietnam) district: Mantle sources, crustal  
802 contamination and sulfide segregation. *Chem. Geol.* 243, 317-343.

803 Wang, Z. L., Xu, D.R., WU, C.J., Fu, W.W., Wang, L., Wu, J., 2013. Discovery of the  
804 late Paleozoic ocean island basalts (OIB) in Hainan Island and their geodynamic  
805 implications. *Acta Petrol. Sin.* 29(3), 875-886.

806 Weaver, B.L., 1991. The origin of ocean island basalt end-member compositions: trace  
807 element and isotopic constraints. *Earth Planet. Sci. Lett.* 104, 381-397.

808 Wei, X., Xu, Y.G., 2013. Petrogenesis of the mafic dykes from Bachu and implications  
809 for the magma evolution of the Tarim large igneous province, SW China. *Acta*  
810 *Petrol. Sin.* 29(10), 3323-3335.

811 Weis, D., Kieffer, B., Maerschalk, C., Pretorius, W., Barling, J., 2005. High-precision  
812 Pb-Sr-Nd-Hf isotopic characterization of USGS BHVO-1 and BHVO-2 reference  
813 materials. *Geochem. Geophys. Geosyst.* 6(2), 1-10.

814 Xiao, D., Tan, X.C., Shan, S.J., Chen, Y.Q., Xia, J.W., Yang, J., Zhou, T., Cheng, Y.,  
815 2014. The restoration of palaeokarst geomorphology of middle Permian Maokou  
816 Formation and its petroleum geological significance in southern Sichuan Basin.

817 Acta Geol. Sin. 88(10), 1992-2002. In Chinese with English abstract.

818 Xiao, L., Xu, Y.G., Chung, S.L., He, B., Mei, H.J., 2003. Chemostratigraphic  
819 correlation of Upper Permian lavas from Yunnan province, China: extent of the  
820 Emeishan large igneous province. *Int. Geol. Rev.* 45, 753-766.

821 Xiao, L., Xu, Y.G., Mei, H.J., Zheng, Y.F., He, B., Pirajno, F., 2004. Distinct mantle  
822 sources of low-Ti and high-Ti basalts from the Eastern Emeishan Large Igneous  
823 Province, SW China: implications for plume-lithosphere interaction. *Earth Planet.*  
824 *Sci. Lett.* 228(3-4), 525-546.

825 Xie, J., Ritzwoller, M.H., Shen, W., Yang, Y., Zheng, Y., Zhou, L., 2013. Crustal radial  
826 anisotropy across eastern Tibet and the western Yangtze craton. *J. Geophys. Res.*  
827 *- Sol. Ea.* 118(8), 4226-4252.

828 Xu, J., Xia, X.P., Lai, C.K., Zhou, M., Ma, P., 2019. First identification of Late Permian  
829 Nb- enriched basalts in Ailaoshan region (SW Yunnan, China): Contribution from  
830 Emeishan plume to subduction of eastern Paleotethys. *Geophys. Res. Lett.* 46,  
831 2511-2523.

832 Xu, J., Xia, X.P., Wang, Q., Spencer, C.J., He, B., Lai, C.K., 2021. Low- $\delta^{18}\text{O}$  A-type  
833 granites in SW China: Evidence for the interaction between the subducted  
834 Paleotethyan slab and the Emeishan mantle plume. *Geol Soc. Am. Bull.*  
835 <https://doi.org/10.1130/B35929.1>.

836 Xu, J.F., Suzuki K., Xu Y.G., Mei H.J., Li J., 2007. Os, Pb, and Nd isotope geochemistry  
837 of the Permian Emeishan continental flood basalts: Insights into the source of a  
838 large igneous province. *Geochim. Cosmochim. Acta* 71, 2104-2119.

839 Xu, R., Liu, Y., Lambart, S., 2020. Melting of a hydrous peridotite mantle source under  
840 the Emeishan large igneous province. *Earth-Sci. Rev.* 207, 103253.

841 Xu, Y.G., Chung, S.L., Jahn, B.M., Wu, G.Y., 2001. Petrologic and geochemical

842 constraints on the petrogenesis of Permian-Triassic Emeishan flood basalts in  
843 southern China. *Lithos* 58, 145-168.

844 Xu, Y.G., He, B., Chung, S.L., Menzies, M.A., Frey, F.A., 2014. Geologic, geochemical  
845 and geophysical consequences of plume involvement in the Emeishan flood-basalt  
846 province. *Geology* 32, 917-920.

847 Xu, Y.G., He, B., Luo, Z.Y., Liu, H.Q., 2013. Study on mantle plume and Large igneous  
848 provinces in China: An overview and perspectives. *Bull. Mineral. Petrol.*  
849 *Geochem.* 32(1), 25-39. In Chinese with English abstract.

850 Xu, Y.G., Luo, Z.Y., Huang, X.L., He, B., Xiao, L., Xie, L.W., Shi, Y.R., 2008. Zircon  
851 U-Pb and Hf isotope constraints on crustal melting associated with the Emeishan  
852 mantle plume. *Geochim. Cosmochim. Acta* 72(13), 3084-3104.

853 Xu, Y.G., Zhong, Y.T., Wei, X., Chen, J., Liu, H.Q., Xie, W., Luo, Z.Y., Li, H.Y., He,  
854 B., Huang, X.L., Wang, Y., Chen, Y., 2017. Permian Mantle Plumes and Earth's  
855 Surface System Evolution. *Bull. Mineral. Petrol. Geochem.* 36(3), 359-373+358.  
856 In Chinese with English abstract.

857 Yan, D.P., Qiu, L., Wells, M.L., Zhou, M.F., Meng, X., Lu, S., Zhang, S., Wang, Y., Li,  
858 S.B., 2018a. Structural and Geochronological constraints on the early Mesozoic  
859 North Longmen Shan Thrust Belt: Foreland fold- thrust propagation of the SW  
860 Qinling Orogenic Belt, Northeastern Tibetan plateau. *Tectonics* 37(12), 4595-4624.

861 Yan, D.P., Zhou, Y., Qiu, L., Wells, M.L., Mu, H., Xu, C.G., 2018b. The Longmenshan  
862 tectonic complex and adjacent tectonic units in the eastern margin of the Tibetan  
863 Plateau: a review. *J. Asian Earth Sci.* 164, 33-57.

864 Yang, J., Cawood, P. A., Du, Y., Huang, H., Hu, L., 2012. Detrital record of Indosinian  
865 mountain building in SW China: Provenance of the middle Triassic turbidites in  
866 the Youjiang Basin. *Tectonophysics* 574- 575, 105-117.

867 Yang, Z., He, B., 2012. Geochronology of detrital zircons from the middle Triassic  
868 sedimentary rocks in the Nanpanjiang Basin: Provenance and its geological  
869 significance. *Geotectonica et Metallogenia* 36(4), 581-596. In Chinese with  
870 English abstract.

871 Zhai, M.G., Yang, R.Y., 1986. Early Precambrian gneiss basement in the Panxi area,  
872 Southwest China. *Acta Petrol. Sin.* 2(3), 22-37. In Chinese with English abstract.

873 Zhang, J., Cao, X.M., Wang, J.L., Zhang, Z.C., 2011. Petrology of the Permian  
874 Langmao Basaltic Porphyry, Luquan County, Yunnan Province: Implications for  
875 the Petrogenesis of High-Ti Basalts. *Geoscience* 25(4), 692-702. In Chinese with  
876 English abstract.

877 Zhang, L., Ren, Z.Y., Handler, M.R., Wu, Y.D., Xu, Y.G., 2019. The origins of high-Ti  
878 and low-Ti magmas in large igneous provinces, insights from melt inclusion trace  
879 elements and Sr-Pb isotopes in the Emeishan large Igneous Province. *Lithos* 344-  
880 345, 122-133.

881 Zhang, L., Ren, Z.Y., Zhang, L., Wu, Y.D., Qian, S.P., Xia, X.P., Xu, Y.G., 2021. Nature  
882 of the mantle plume under the Emeishan large igneous province: Constraints from  
883 olivine-hosted melt inclusions of the Lijiang picrites. *J. Geophys. Res. Sol. Ea.*  
884 126, e2020JB021022.

885 Zhang, W., Hu Z.C., 2020. Estimation of isotopic reference values for pure materials  
886 and geological reference materials. *At. Spectrosc.* 41(3), 93-102.

887 Zhang, W., Hu, Z.C., Liu, Y.S., 2020a. Iso-Compass: new freeware software for isotopic  
888 data reduction of LA-MC-ICP-MS. *J. Anal. At. Spectrom.* 35, 1087-1096.

889 Zhang, Y., Chen, S.L., Zhang, X.L., Zhang, X.H., Xie, C., Chen, C., Yang, Y.R., Gao,  
890 Y.L., 2020b. Restoration of paleokarst geomorphology of Lower Permian Maokou  
891 Formation and its petroleum exploration implication in Sichuan Basin. *Lithologic*

892 Reservoirs 32(3), 44-55. In Chinese with English abstract.

893 Zhang, Y.X. 1988. Panxi rift. Beijing: Geological Press.

894 Zhang, Z.C., Mahoney, J.J., Mao, J.W., Wang, F.S., 2006. Geochemistry of picritic and  
895 associated basalt flows of the western Emeishan flood basalt province, China. *J.*  
896 *Petrol.* 47, 1997-2019.

897 Zhang, Z.C., Wang, F.S., 2003. Sr, Nd and Pb Isotopic Characteristics of Emeishan  
898 Basalt Province and Discussion on Their Source Region. *Earth Sci.- J. China*  
899 *University of Geosciences* 28(4), 431-439. In Chinese with English abstract.

900 Zhang, Z.C., Wang, F.S., Fan, W.M., Deng, H.L., Xu, Y.G., Xu, J.F., Wang, Y.J., 2001.  
901 A Discussion on Some Problems Concerning the Study of the Emeishan Basalts.  
902 *Acta Petrol. Mineral.* 20(3), 239-246. In Chinese with English abstract.

903 Zhang, Z.C., Zhi, X.C., Chen, L., Saunders, A.D., Reichow, M.K., 2008. Re-Os isotopic  
904 compositions of picrites from the Emeishan flood basalt province, China. *Earth*  
905 *Planet. Sci. Lett.* 276, 30-39.

906 Zheng, L.D., Yang, Z.Y., Tong, Y.B., Yuan, W., 2010. Magnetostratigraphic constraints  
907 on two-stage eruptions of the Emeishan continental flood basalts. *Geochem.*  
908 *Geophys. Geosy.* 11(12), 1-19.

909 Zhong, H., Zhu, W.G., 2006. Geochronology of layered mafic intrusions from the Pan-  
910 Xi area in the Emeishan large igneous province, SW China. *Miner. Deposita* 41,  
911 599-606.

912 Zhong, Y.T., He, B., Mundil, R., Xu, Y.G., 2014. CA-TIMS zircon U-Pb dating of felsic  
913 ignimbrite from the Binchuan section: implications for the termination age of  
914 Emeishan large igneous province. *Lithos* 204, 14-19.

915 Zhong, Y.T., He, B., Xu, Y.G., 2013. Mineralogy and geochemistry of claystones from  
916 the Guadalupian– Lopingian boundary at Penglaitan, South China: Insights into



917 the pre- Lopingian geological events. *J. Asian Earth Sci.* 62, 438-462.

918 Zhou, M.F., Chen, W.T., Wang, C.Y., Prevec, S.A., Liu, P.P., Howarth, G.H., 2013. Two  
919 stages of immiscible liquid separation in the formation of Panzhihua-type Fe-Ti-  
920 V oxide deposits, SW China. *Geosci. Front.* 4, 481-502.

921 Zhou, M.F., Malpas, J.G., Song, X.Y., Robinson, P.T., Sun, M., Kennedy, A., Leshner,  
922 M., Keays, R.R., 2002. A temporal link between the Emeishan large igneous  
923 province (SW China) and the end-Guadalupian mass extinction. *Earth Planet. Sci.*  
924 *Lett.* 196(3-4), 113-122.

925 Zhou, M.F., Wang, Z.C., Zhao, W.W., Qi, L., Zhao, Z., Zhou, J.X., Huang, Z.L., Chen,  
926 W.T., 2022. A reconnaissance study of potentially important scandium deposits  
927 associated with carbonatite and alkaline igneous complexes of the Permian  
928 Emeishan Large Igneous Province, SW China. *J. Asian Earth Sci.* 236, 105309.

929 Zhou, M.F., Zhao, J.H., Qi, L., Su, W.C., Hu, R.Z., 2006. Zircon U-Pb geochronology  
930 and elemental and Sr-Nd isotope geochemistry of Permian mafic rocks in the  
931 Funing area, SW China. *Contrib. Mineral. Petrol.* 151, 1-19.

932 Zhu, C.Q., Hu, S.B., Qiu, N.S., Rao, S., Yuan, Y.S., 2016. The thermal history of the  
933 Sichuan Basin, SW China: evidence from the deep boreholes. *Sci. China, Ser. D:*  
934 *Earth Sci.* 59, 70-82.

935 Zhu, C.Q., Xu, M., Yuan, Y.S., Zhao, Y.Q., Shan, J.N., He, Z.G., Tian, Y.T., Hu, S.B.,  
936 2010. Palaeogeothermal response and record of the effusing of Emeishan basalts  
937 in the Sichuan basin. *Chin. Sci. B* 55, 949-956.

938 Zhu, D.C., Mo, X.X., Wang, L.Q., Zhao, Z.D., Liao, Z.L., 2008. Hotspot-ridge  
939 interaction of the evolution of Neo-Tethys: insights from the Late Jurassic-Early  
940 Cretaceous magmatism in southern Tibet. *Acta Petrol. Sin.* 24(2), 225-237.

941 Zhu, D.C., Pan, G.T., Mo, X.X., Liao, Z.L., Jiang, X.S., Wang, L.Q., Zhao, Z.D., 2007.

942 Petrogenesis of volcanic rocks in the sangxiu formation, central segment of  
943 Tethyan Himalaya: a probable example of plume-lithosphere interaction. *J. Asian*  
944 *Earth Sci.* 29(2-3), 320-335.

945 Zhu, J., 2019. A study of mantle plume dynamics and its environmental effect in the  
946 Emeishan large igneous province. Beijing: China University of Geosciences  
947 (Beijing). In Chinese with English abstract.

948 Zhu, J., Zhang, Z.C., Reichow, M.K., Li, H.B., Cai, W.C., Pan, R.H., 2018. Weak  
949 vertical surface movement caused by the ascent of the Emeishan mantle anomaly.  
950 *J. Geophys. Res. Sol. Ea.* 123(2), 1018-1034.

951 Zi, J.W., Fan, W.M., Wang, Y.J., Cawood, P.A., Peng, T.P., Sun, L.H., Xu, Z.Q., 2010.  
952 U-Pb geochronology and geochemistry of the Dashibao Basalts in the Songpan-  
953 Ganzi Terrane, SW China, with implications for the age of Emeishan volcanism.  
954 *Am. J. Sci.* 310(9), 1054-1080.

955 **Fig. 1.** Simplified geological map showing the inner, intermediate and outer zones of  
956 the ELIP and sampling locations (modified after He et al., 2003; Zi et al., 2010).

957 The inner, intermediate, and outer zones in the ELIP area were defined by He et al.,  
958 2003. The hotspot track was obtained from Liu et al., 2021b. The ELIP eruption centre  
959 was obtained from He et al., 2010.

960 CAO = Central Asia Orogen; TM = Tarim Block; AHO = Alpine–Himalaya Orogen;  
961 QKO = Qinling-Qilian-Kunlun Orogen; NCC = North China Craton; YC = Yangtze  
962 Craton; CC = Cathaysia Craton.

963

964 **Fig. 2.** Schematic map of southwestern China showing the distribution of volcanic rocks  
965 in the Late Permian (a), and geological map of the Sichuan Basin showing the  
966 distribution of the Late Permian volcanic rocks (b) (modified after Liu et al., 2021a).

967

968 **Fig. 3.** Representative photos of field geology and petrographic features of the volcanic  
969 rocks from the drill cores and outcrops in and around the Sichuan Basin.

970 a. ST1-2, stomata almond basalt; b. YT1-7, massive basalt (cross-polarised light); c.  
971 ZG2-5, massive basalt; d. ZG2-5, massive basalt (cross-polarised light); e.  
972 Longmendong section; f. Longmendong basalt outcrop; g. Longchi basalt outcrop; h.  
973 Xinlin basalt outcrop.

974 Pl-plagioclase, Cpx-clinopyroxene.

975

976 **Fig. 4.** The connecting well section of boreholes ZG2-YT1-TF2-ZJ2-ST1 in the  
977 Sichuan Basin (based on logging data from Southwest Oil and Gas Field Company,

978 PetroChina).

979 The location of the connecting well section is shown in Fig. 2

980

981 **Fig. 5.**  $\text{TiO}_2$  vs.  $\text{Ti/Y}$  (a), and  $\text{O}'\text{-Ne}'\text{-Q}'$  (b) classification diagrams for the basalts in  
982 Sichuan Basin (LT and HT data from the inner zone in the ELIP were obtained from  
983 Song et al., 2001; Xiao et al., 2004; Xu et al., 2001; Zhang et al., 2006; data of HT from  
984 the outer zone were obtained from Fan et al., 2008; Lai et al., 2012; Li et al., 2016b;  
985 Wang et al., 2007; Xu et al., 2007).

986 (a) LT-low Ti series, HT-high low series. (b). A-Alkaline, S-Sub-alkaline.

987

988 **Fig. 6.** Selected elements plotted vs. MgO for the basalts from the Sichuan Basin

989

990 **Fig. 7.** Chondrite-normalised REE (a), and primitive mantle-normalised trace element  
991 (b) for the basalts in the Sichuan Basin (data for chondrite, primitive mantle and OIB  
992 are from Sun and McDonough, 1989; sources of geochemical data from other regions  
993 in the ELIP as for Fig. 5).

994

995 **Fig. 8.** Plots of  $^{87}\text{Sr}/^{86}\text{Sr}(t)$  vs.  $\epsilon_{\text{Nd}}(t)$  (a),  $^{206}\text{Pb}/^{204}\text{Pb}(t)$  vs.  $^{87}\text{Sr}/^{86}\text{Sr}(t)$  (b),  $^{206}\text{Pb}/^{204}\text{Pb}(t)$   
996 vs.  $^{207}\text{Pb}/^{204}\text{Pb}(t)$  (c), and  $^{206}\text{Pb}/^{204}\text{Pb}(t)$  vs.  $^{208}\text{Pb}/^{204}\text{Pb}(t)$  (d) for the basalts in the  
997 Sichuan Basin (Sources of geochemical data from other regions in the ELIP as for Fig.  
998 5. The fields of DM, MORB, Atlantic-Pacific MORB, Indian Ocean MORB, FOZO  
999 (focal zone), OIB, Dupal OIB, BSE (bulk silicate earth), HIMU (mantle with high U/Pb  
1000 ratios), EMI and EMII (enriched mantle), Kerguelen are from Barling and Goldstein,  
1001 1990; Deniel, 1998; Hamelin and Allègre, 1985; Hart, 1984; Hawkesworth et al., 1984;

1002 and Weaver, 1991. The LoNd (low Nd) array and NHRL (Northern Hemisphere  
1003 Reference Line) are from Hart, 1984. The Yangtze Block crustal compositions are from  
1004 Chen and Jahn, 1998; Gao et al., 1999; Ma et al., 2000 and Zhang et al., 2008.)

1005

1006 **Fig. 9.** Plots of Ce vs. Nb/Th (a),  $(Th/Ta)_P$  vs.  $(La/Nb)_P$  (b),  $SiO_2$  vs.  $^{87}Sr/^{86}Sr(t)$  (c), and  
1007  $SiO_2$  vs.  $\epsilon_{Nd}(t)$  (d) for the basalts in the Sichuan Basin (The fields of PM, N-MORB and  
1008 E-MORB are from Sun and McDonough, 1989; SCLM are from McDonough, 1990;  
1009 UC (upper crust), MC (middle crust) and LC (lower crust) are from Rudnick and Gao,  
1010 2003; Kerguelen alkaline basalts are from [http://georoc.mpch-](http://georoc.mpch-mainz.gwdg.de/georoc/Entry.html)  
1011 [mainz.gwdg.de/georoc/Entry.html](http://georoc.mpch-mainz.gwdg.de/georoc/Entry.html).)

1012

1013 **Fig. 10.** Plots of Mg# vs.  $CaO/Al_2O_3$  (a),  $Eu_N/Eu^*$  vs. Th+U (b), and  $Eu_N/Eu^*$  vs.  $\sum REE$   
1014 (c) for the basalts in the Sichuan Basin (sources of geochemical data from other regions  
1015 in the ELIP as for Fig. 5; the sample 20LMD05 is assumed as the initial melt of  
1016 fractional crystallization, mineral fractionation vectors are calculated using Rayleigh  
1017 fractionation law, and partition coefficients are from McKenzie and O'Nions, 1991).  
1018 Pl-plagioclase, Cpx-clinopyroxene and Opx-orthopyroxene.

1019

1020 **Fig. 11.** Diagrams of Nb/Yb vs. Th/Yb (a), and Ti/Yb vs. Nb/Th (b) for the basalts in  
1021 the Sichuan Basin (sources of geochemical data from other regions in the ELIP as for  
1022 Fig. 5. (a) MORB-OIB array, subduction component adding models are from Pearce,  
1023 2008. The arrow in the Figure represents the trend of adding subduction component. (b)  
1024 SCLM are from McDonough, 1990; UC, MC and LC are from Rudnick et al., 2003;  
1025 Hawaiian OIB mean was obtained from Feigenson et al., 1996; Kerguelen alkaline

1026 basalts are from <http://georoc.mpch-mainz.gwdg.de/georoc/Entry.html>; Sangxiu  
1027 Formation basalts were obtained from Zhu et al., 2007).

1028

1029 **Fig. 12.** Plots of  $\epsilon_{Nd}(t)$  vs.  $(La/Yb)_N$  (a), Yb vs. La/Yb (b), Th/La vs. Nb/U (c), and  
1030  $^{206}Pb/^{204}Pb$  vs.  $\epsilon_{Nd}(t)$  (d) for the basalts in the Sichuan Basin (sources of geochemical  
1031 data from other regions in the ELIP as for Fig. 5).

1032

1033 **Fig. 13.** Diagrams of  $(La/Sm)_N$  vs.  $(Tb/Yb)_N$  (a), and Sm/Yb vs. La/Sm (b) for the  
1034 basalts in the Sichuan Basin (sources of geochemical data from other regions in the  
1035 ELIP as for Fig. 5; (b) batch melting trends for garnet and spinel lherzolite were  
1036 obtained from Lassiter and Depaolo, 1997).

1037

1038 **Fig. 14.** Stratigraphic variation of the representative lava successions in the ELIP  
1039 (modified after Xiao et al., 2004; Xu et al., 2001, 2014).

1040

1041 **Fig. 15.** Evolution model of EILP during the Middle Permian. (The framework for the  
1042 plumbing system of ELIP associated with the Emeishan mantle plume was modified  
1043 from Feng et al. (2022) and Liu et al. (2021b). The boundaries of the inner-intermediate-  
1044 outer zones in the ELIP was defined by He et al. (2003) and Xiao et al. (2004). LQF,  
1045 HYF and QYF represent the Longquanshan fault, Huayingshan fault and Longquanshan  
1046 fault, respectively. LT and HT represent low-Ti basalts and high-Ti basalts, respectively.  
1047 The NE (northeastward) arrows show the direction of movement of the South China  
1048 Block (Liu et al., 2021b).)

1049 a. During the early-Guadalupian (~269 Ma), Western Yangtze Block experienced  
1050 Ailaoshan slab (Paleotethys Ocean) eastward subduction, and the adjacent Emeishan  
1051 mantle plume was modified by the recycled lithospheric fragments. b. In the first stage  
1052 of end-Guadalupian (260~257 Ma), lithosphere mantle melted and formed the low-Ti  
1053 basalts (LT) in the inner zone. c. In the second stage of end-Guadalupian (260~257 Ma),  
1054 the mantle plume melted and formed the high-Ti basalts (HT) in the inner-intermediate-  
1055 outer zones, with high-Ti basalts overlying low-Ti basalts in the inner zone.

**Table 1** Zircon U-Pb dating results of the Emeishan large igneous province

|                 | Locality                   | Rock type          | Analytical method     | Age/Ma              | Reference               |                      |                    |
|-----------------|----------------------------|--------------------|-----------------------|---------------------|-------------------------|----------------------|--------------------|
|                 | Dali-Jiangwei              | acid volcanic rock | ID-TIMS zircon U-Pb   | 258.9±0.5           | Xu et al. (2013)        |                      |                    |
|                 | Midu-Jinbaoshan            | wehrlite           | Shrimp zircon U-Pb    | 260.6±3.5           | Tao et al. (2009)       |                      |                    |
|                 |                            | hornblendite       | Shrimp zircon U-Pb    | 260.7±5.6           |                         |                      |                    |
|                 | Binchuan                   | acid tuff          | ID-TIMS zircon U-Pb   | 259.1±0.5           | Zhong et al. (2014)     |                      |                    |
|                 |                            | basalt             | Shrimp zircon U-Pb    | 256.2±1.4           | Li et al. (2016a)       |                      |                    |
|                 | Panxi-Daheishan            | syenite            | ID-TIMS zircon U-Pb   | 259.1±0.5           | Shellnutt et al. (2012) |                      |                    |
|                 | Panxi-Baima                | granite            | ID-TIMS zircon U-Pb   | 259.2±0.4           |                         |                      |                    |
|                 | Panxi-Huangcao             | syenite            | ID-TIMS zircon U-Pb   | 258.9±0.7           |                         |                      |                    |
| Inner Zone      | Panxi-Cida                 | granite            | ID-TIMS zircon U-Pb   | 258.4±0.6           | Xu et al. (2008)        |                      |                    |
|                 | Panxi-Maomaogou            | syenite            | Shrimp zircon U-Pb    | 261.6 ± 4.4         |                         |                      |                    |
|                 | Panxi-Miyi                 | syenite            | Shrimp zircon U-Pb    | 259.8 ± 3.5         |                         |                      |                    |
|                 | Panxi-Salian               | diorite            | Shrimp zircon U-Pb    | 260.4 ± 3.6         |                         |                      |                    |
|                 | Panxi-Taihe                | granite            | Shrimp zircon U-Pb    | 261.4 ± 2.3         |                         |                      |                    |
|                 | Panxi-Hongge               | gabbro             | Shrimp zircon U-Pb    | 259.3±1.3           |                         | Zhong and Zhu (2006) |                    |
|                 |                            | gabbro             | Shrimp zircon U-Pb    | 259.3 ± 1.3         |                         |                      |                    |
|                 |                            | Panxi-Binggu       | gabbro                | Shrimp zircon U-Pb  |                         | 260.7 ± 0.8          |                    |
|                 |                            | Xinjie             | gabbro                | Shrimp zircon U-Pb  |                         | 259±3                | Zhou et al. (2002) |
|                 | Intermediate Zone          | Guizhou-Weining    | boundary clay rock    | ID-TIMS zircon U-Pb |                         | 258.1±0.6            | Xu et al. (2013)   |
| Panxian-Zhudong |                            | ignimbrite         | ID-TIMS zircon U-Pb   | 258.3±1.4           | Zhu (2019)              |                      |                    |
| Xingyi-Xiongwu  |                            | tuff               | ID-TIMS zircon U-Pb   | 258.5±0.9           |                         |                      |                    |
| Puan-Louxia     |                            | tuff               | ID-TIMS zircon U-Pb   | 258.1±1.1           |                         |                      |                    |
|                 |                            | Baimazhai          | pyroxenite            | Shrimp zircon U-Pb  | 258.5±3.5               | Wang et al. (2006)   |                    |
| Outer Zone      | Tubagou                    | basalt             | Shrimp zircon U-Pb    | 257.3±2.0           | Li et al. (2016b)       |                      |                    |
|                 | Baise-Yangxu               | basalt             | Shrimp zircon U-Pb    | 259.1 ± 4.0         | Fan et al. (2008)       |                      |                    |
|                 | Bama-Minan                 | basalt             | Shrimp zircon U-Pb    | 259.6±5.9           |                         |                      |                    |
|                 | Nayong-Xilin-Tianyang Area | basalt             | LA-ICP-MS zircon U-Pb | 257.0±9.0           | Lai et al. (2012)       |                      |                    |



|                        |                       |                          |           |                     |
|------------------------|-----------------------|--------------------------|-----------|---------------------|
| Guangyuan-<br>Chaotian | boundary clay<br>rock | ID-TIMS<br>zircon U-Pb   | 258.6±1.4 | Xu et al. (2013)    |
|                        |                       |                          | 259.2±0.3 | Zhong et al. (2014) |
| Funing                 | diabase               | Shrimp zircon<br>U-Pb    | 260±3     | Zhou et al. (2006)  |
|                        | diorite               | Shrimp zircon<br>U-Pb    | 258±3     |                     |
| Mianhuadi              | metagabbro            | MC-ICP-MS<br>zircon U-Pb | 259.6±0.8 | Zhou et al. (2013)  |

1058 **Table 2** Major elements (wt.%) and trace elements ( $\times 10^{-6}$ ) contents for the analysed volcanic rocks in the Sichuan Basin

| Samples                                     | ST1<br>-2 | ST1<br>-5 | YT1<br>-1 | YT1<br>-3 | YT1<br>-4 | YT1<br>-5 | YT1<br>-6 | YT1<br>-7 | ZG2<br>-4 | ZG2<br>-5 | ZG2<br>-7   | ZG2<br>-8 | 20L<br>MD0<br>4 | 20L<br>MD0<br>5 | 20LC<br>04 | 20LC<br>06 | 20XL<br>01 | 20XL<br>02 | 20XL02<br>(replicate) |
|---|-----------|-----------|-----------|-----------|-----------|-----------|-----------|-----------|-----------|-----------|-------------|-----------|-----------------|-----------------|------------|------------|------------|------------|-----------------------|
| Locality                                    | ST1 Well  |           | YT1 Well  |           |           |           | ZG2 Well  |           |           |           | Longmendong |           | Longchi         |                 | Xinlin     |            |            |            |                       |
| SiO <sub>2</sub>                            | 49.64     | 48.78     | 48.62     | 47.55     | 46.69     | 47.67     | 48.67     | 48.96     | 46.59     | 47.64     | 48.74       | 45.59     | 45.99           | 48.99           | 45.94      | 49.08      | 49.21      | 48.12      | 48.32                 |
| TiO <sub>2</sub>                            | 4.01      | 3.87      | 4.06      | 3.91      | 4.17      | 4.19      | 3.83      | 3.71      | 4.01      | 3.98      | 4.05        | 4.14      | 3.69            | 3.73            | 4.08       | 3.69       | 4.24       | 3.82       | 3.84                  |
| Al <sub>2</sub> O <sub>3</sub>              | 13.75     | 13.66     | 13.69     | 13.66     | 13.64     | 13.82     | 14.99     | 14.96     | 13.07     | 12.98     | 13.30       | 13.70     | 13.44           | 13.90           | 13.91      | 13.88      | 13.57      | 13.08      | 13.06                 |
| Fe <sub>2</sub> O <sub>3</sub> <sup>T</sup> | 12.92     | 13.82     | 13.86     | 15.65     | 16.91     | 16.10     | 13.41     | 13.60     | 18.43     | 17.46     | 14.02       | 16.27     | 15.44           | 12.75           | 15.75      | 12.40      | 14.32      | 14.16      | 14.23                 |
| MnO   | 0.21      | 0.17      | 0.18      | 0.16      | 0.17      | 0.17      | 0.16      | 0.16      | 0.20      | 0.19      | 0.20        | 0.19      | 0.21            | 0.16            | 0.17       | 0.17       | 0.18       | 0.17       | 0.17                  |
| MgO   | 3.43      | 3.68      | 4.92      | 4.81      | 4.38      | 4.47      | 4.99      | 5.08      | 4.69      | 4.33      | 4.69        | 4.89      | 7.12            | 5.28            | 5.24       | 5.41       | 4.65       | 5.06       | 5.10                  |
| CaO   | 4.88      | 4.27      | 6.53      | 8.26      | 6.03      | 7.39      | 7.22      | 7.21      | 6.99      | 7.87      | 7.01        | 7.40      | 6.79            | 9.09            | 7.20       | 6.75       | 9.15       | 8.08       | 8.13                  |
| Na <sub>2</sub> O                           | 4.38      | 3.91      | 3.82      | 2.29      | 3.44      | 2.39      | 2.78      | 2.75      | 4.32      | 2.14      | 2.38        | 2.34      | 2.81            | 1.97            | 2.47       | 3.52       | 2.05       | 2.78       | 2.76                  |
| K <sub>2</sub> O                            | 0.22      | 0.56      | 1.96      | 1.73      | 2.36      | 1.98      | 1.92      | 1.93      | 0.85      | 1.94      | 2.21        | 2.03      | 1.51            | 1.42            | 1.17       | 2.15       | 0.99       | 1.83       | 1.85                  |
| P <sub>2</sub> O <sub>5</sub>               | 0.45      | 0.45      | 0.40      | 0.40      | 0.42      | 0.42      | 0.40      | 0.43      | 0.44      | 0.43      | 0.43        | 0.43      | 0.37            | 0.39            | 0.43       | 0.39       | 0.45       | 0.40       | 0.40                  |
| LOI   | 5.87      | 6.04      | 1.89      | 1.70      | 1.33      | 1.12      | 1.15      | 1.21      | 0.54      | 0.77      | 2.59        | 2.68      | 2.89            | 2.03            | 3.03       | 1.99       | 1.38       | 2.25       | 2.24                  |
| Total                                       | 99.76     | 99.20     | 99.94     | 100.1     | 99.56     | 99.70     | 99.51     | 99.99     | 100.1     | 99.71     | 99.61       | 99.66     | 100.2           | 99.71           | 99.37      | 99.41      | 100.1      | 99.75      | 100.12                |
| Mg#   | 34.45     | 34.49     | 41.29     | 37.85     | 33.92     | 35.47     | 42.42     | 42.53     | 33.53     | 32.93     | 39.85       | 37.33     | 47.74           | 45.09           | 39.72      | 46.36      | 39.15      | 41.42      | 39.12                 |
| La  | 45.2      | 45.1      | 47.9      | 46.8      | 47.1      | 49.4      | 45.2      | 45.8      | 49.5      | 48.7      | 44.2        | 44.8      | 37.4            | 47.2            | 43.3       | 44.3       | 48.4       | 42.0       | 41.9                  |
| Ce  | 96.3      | 95.6      | 98.3      | 97.5      | 99.4      | 103       | 93.6      | 95.6      | 99.1      | 101       | 95.0        | 97.6      | 85.9            | 104             | 98.0       | 101        | 106        | 94.9       | 93.4                  |
| Pr  | 12.4      | 12.2      | 12.8      | 12.7      | 12.9      | 13.0      | 11.8      | 12.4      | 12.9      | 13.4      | 12.8        | 12.8      | 11.3            | 13.2            | 12.8       | 13.1       | 13.8       | 12.5       | 12.3                  |
| Nd  | 52.6      | 51.9      | 52.1      | 52.0      | 52.9      | 52.7      | 49.5      | 50.4      | 51.4      | 56.0      | 52.8        | 54.0      | 48.7            | 54.3            | 53.4       | 53.7       | 56.8       | 52.8       | 51.5                  |
| Sm  | 11.7      | 11.0      | 11.0      | 10.6      | 10.6      | 10.6      | 9.41      | 9.91      | 9.99      | 11.6      | 10.6        | 11.4      | 10.8            | 11.5            | 11.4       | 11.6       | 12.0       | 11.3       | 10.7                  |
| Eu  | 3.00      | 2.82      | 2.97      | 3.06      | 3.01      | 2.98      | 2.87      | 2.95      | 2.94      | 3.01      | 2.96        | 3.04      | 2.84            | 3.08            | 3.06       | 3.02       | 3.30       | 3.11       | 3.03                  |
| Gd  | 9.72      | 9.91      | 9.55      | 9.83      | 9.58      | 9.51      | 9.05      | 9.25      | 9.67      | 10.3      | 9.80        | 10.3      | 9.48            | 10.0            | 9.69       | 9.69       | 10.4       | 9.64       | 9.46                  |
| Tb  | 1.36      | 1.31      | 1.26      | 1.28      | 1.26      | 1.27      | 1.13      | 1.22      | 1.29      | 1.33      | 1.33        | 1.39      | 1.32            | 1.41            | 1.35       | 1.41       | 1.43       | 1.34       | 1.31                  |
| Dy  | 8.07      | 7.36      | 7.47      | 7.50      | 7.80      | 7.51      | 6.90      | 7.02      | 7.90      | 8.13      | 7.83        | 8.02      | 7.28            | 7.65            | 7.47       | 7.79       | 7.91       | 7.64       | 7.38                  |
| Ho  | 1.45      | 1.26      | 1.29      | 1.26      | 1.30      | 1.35      | 1.16      | 1.15      | 1.37      | 1.35      | 1.29        | 1.39      | 1.31            | 1.40            | 1.33       | 1.44       | 1.42       | 1.35       | 1.28                  |

|    |      |      |      |      |      |      |      |      |      |      |      |      |      |      |      |      |      |      |      |
|----|------|------|------|------|------|------|------|------|------|------|------|------|------|------|------|------|------|------|------|
| Er | 3.61 | 3.36 | 3.45 | 3.41 | 3.42 | 3.38 | 3.12 | 3.08 | 3.51 | 3.59 | 3.51 | 3.61 | 3.36 | 3.61 | 3.49 | 3.70 | 3.55 | 3.47 | 3.44 |
| Tm | 0.47 | 0.46 | 0.44 | 0.45 | 0.46 | 0.46 | 0.41 | 0.44 | 0.50 | 0.49 | 0.50 | 0.51 | 0.45 | 0.47 | 0.46 | 0.48 | 0.47 | 0.47 | 0.45 |
| Yb | 2.93 | 2.73 | 2.73 | 2.70 | 2.77 | 2.69 | 2.48 | 2.53 | 2.93 | 2.75 | 2.86 | 2.98 | 2.74 | 2.91 | 2.80 | 2.97 | 2.84 | 2.81 | 2.73 |
| Lu | 0.38 | 0.36 | 0.36 | 0.37 | 0.37 | 0.35 | 0.35 | 0.36 | 0.40 | 0.40 | 0.39 | 0.41 | 0.39 | 0.40 | 0.40 | 0.42 | 0.40 | 0.39 | 0.38 |
| V  | 355  | 346  | 369  | 366  | 351  | 342  | 307  | 298  | 403  | 388  | 379  | 389  | 382  | 348  | 382  | 329  | 388  | 389  | 375  |
| Cr | 345  | 437  | 406  | 76.1 | 81.6 | 73.0 | 346  | 332  | 123  | 111  | 459  | 543  | 197  | 302  | 222  | 271  | 337  | 184  | 166  |
| Co | 48.4 | 45.6 | 47.5 | 45.8 | 46.1 | 45.3 | 49.9 | 50.6 | 43.3 | 46.7 | 49.9 | 57.8 | 48.1 | 41.4 | 48.7 | 40.1 | 46.6 | 44.9 | 43.6 |
| Ni | 226  | 265  | 257  | 139  | 158  | 131  | 247  | 246  | 302  | 257  | 255  | 293  | 136  | 172  | 132  | 163  | 195  | 120  | 107  |
| Cu | 254  | 284  | 284  | 249  | 304  | 266  | 259  | 267  | 364  | 541  | 193  | 412  | 257  | 241  | 234  | 64.4 | 247  | 332  | 326  |
| Zn | 128  | 124  | 141  | 133  | 134  | 131  | 116  | 118  | 150  | 123  | 140  | 146  | 136  | 120  | 145  | 120  | 142  | 136  | 132  |
| Ga | 25.8 | 23.1 | 26.2 | 25.8 | 25.2 | 25.7 | 25.4 | 25.5 | 24.5 | 25.7 | 25.4 | 26.5 | 27.9 | 25.5 | 27.3 | 23.5 | 26.0 | 26.6 | 25.7 |
| Rb | 3.82 | 13.3 | 43.4 | 38.5 | 52.1 | 45.7 | 53.5 | 53.1 | 22.6 | 65.1 | 70.6 | 68.9 | 58.5 | 38.8 | 46.9 | 70.3 | 23.1 | 59.7 | 58.6 |
| Sr | 882  | 870  | 830  | 580  | 1027 | 639  | 661  | 672  | 457  | 484  | 742  | 785  | 451  | 511  | 448  | 569  | 586  | 546  | 539  |
| Y  | 38.3 | 36.9 | 36.5 | 36.0 | 36.2 | 35.4 | 32.7 | 33.6 | 37.1 | 37.0 | 36.7 | 37.7 | 34.4 | 36.9 | 35.4 | 37.6 | 37.2 | 36.1 | 35.0 |
| Zr | 365  | 350  | 350  | 348  | 360  | 349  | 327  | 324  | 366  | 352  | 356  | 377  | 304  | 349  | 352  | 353  | 370  | 341  | 335  |
| Nb | 40.8 | 40.4 | 42.0 | 42.2 | 41.8 | 43.3 | 42.0 | 40.2 | 43.0 | 39.4 | 41.8 | 44.3 | 33.3 | 39.0 | 39.9 | 38.7 | 41.9 | 37.1 | 36.3 |
| Ba | 239  | 424  | 1306 | 405  | 1621 | 524  | 472  | 498  | 239  | 741  | 1065 | 1003 | 627  | 479  | 578  | 697  | 407  | 510  | 490  |
| Hf | 9.47 | 8.78 | 8.81 | 8.56 | 8.79 | 8.66 | 7.74 | 7.91 | 8.65 | 8.50 | 8.55 | 9.19 | 7.74 | 8.96 | 8.96 | 9.22 | 9.51 | 8.76 | 8.67 |
| Ta | 2.38 | 2.38 | 2.54 | 2.52 | 2.55 | 2.58 | 2.48 | 2.52 | 2.56 | 2.34 | 2.57 | 2.83 | 2.20 | 2.57 | 2.62 | 2.57 | 2.69 | 2.46 | 2.38 |
| Pb | 8.48 | 8.92 | 7.42 | 7.74 | 12.4 | 8.94 | 6.61 | 5.97 | 5.63 | 7.64 | 6.95 | 8.15 | 6.54 | 11.9 | 7.80 | 7.64 | 6.64 | 8.62 | 8.95 |
| Th | 7.12 | 6.90 | 6.84 | 6.77 | 7.03 | 6.97 | 6.70 | 6.63 | 6.58 | 6.61 | 6.57 | 6.81 | 7.21 | 8.12 | 6.49 | 8.35 | 6.97 | 6.47 | 6.25 |
| U  | 1.60 | 1.58 | 1.69 | 1.60 | 1.74 | 1.69 | 1.52 | 1.58 | 1.55 | 1.48 | 1.49 | 1.68 | 1.52 | 1.82 | 1.50 | 1.76 | 1.65 | 1.47 | 1.46 |

1059 LOI: weight loss on ignition to 1000 °C. Mg# =  $Mg^{2+}/(Mg^{2+}+Fe^{2+})$  in atomic ratio, assuming 15% of total iron oxide is ferric.

1060

**Table 3** Sr-Nd-Pb isotope ratios for the analysed volcanic rocks in the Sichuan Basin

| Sample                               | ST1-5    | YT1-1    | YT1-3    | YT1-6    | YT1-7    | ZG2-5    | ZG2-7    | ZG2-8    | 20LMD05     | 20LC06   | 20XL01   |
|--------------------------------------|----------|----------|----------|----------|----------|----------|----------|----------|-------------|----------|----------|
| Locality                             | ST1 Well | YT1 Well |          |          |          |          | ZG2 Well |          | Longmendong | Longchi  | Xinlin   |
| Rb( $\times 10^{-6}$ )               | 13.3     | 43.4     | 38.5     | 53.5     | 53.1     | 65.1     | 70.6     | 68.9     | 38.8        | 70.3     | 23.1     |
| Sr( $\times 10^{-6}$ )               | 870      | 830      | 580      | 661      | 672      | 484      | 742      | 785      | 511         | 569      | 586      |
| $^{87}\text{Rb}/^{86}\text{Sr}$      | 0.044372 | 0.151194 | 0.192215 | 0.234105 | 0.228342 | 0.389072 | 0.275352 | 0.254148 | 0.219834    | 0.357378 | 0.113896 |
| $^{87}\text{Sr}/^{86}\text{Sr}$      | 0.706884 | 0.707491 | 0.707355 | 0.706681 | 0.706694 | 0.706661 | 0.707085 | 0.707075 | 0.706865    | 0.707546 | 0.705942 |
| $^{26}\text{Al}$                     | 0.000008 | 0.000007 | 0.000001 | 0.000008 | 0.000008 | 0.000008 | 0.000006 | 0.000007 | 0.000007    | 0.000001 | 0.000009 |
| $^{87}\text{Sr}/^{86}\text{Sr}(t)$   | 0.706721 | 0.706935 | 0.706648 | 0.705820 | 0.705854 | 0.705230 | 0.706072 | 0.706140 | 0.706057    | 0.706232 | 0.705523 |
| Sm( $\times 10^{-6}$ )               | 11.0     | 11.0     | 10.6     | 9.41     | 9.91     | 11.6     | 10.6     | 11.4     | 11.5        | 11.6     | 12.0     |
| Nd( $\times 10^{-6}$ )               | 51.9     | 52.1     | 52.0     | 49.5     | 50.4     | 56.0     | 52.8     | 54.0     | 54.3        | 53.7     | 56.8     |
| $^{147}\text{Sm}/^{144}\text{Nd}$    | 0.128166 | 0.127908 | 0.123307 | 0.114987 | 0.118988 | 0.125756 | 0.121209 | 0.128019 | 0.128721    | 0.130854 | 0.127975 |
| $^{143}\text{Nd}/^{144}\text{Nd}$    | 0.512530 | 0.512533 | 0.512526 | 0.512528 | 0.512528 | 0.512567 | 0.512570 | 0.512573 | 0.512507    | 0.512507 | 0.512561 |
| $^{26}\text{Al}$                     | 0.000005 | 0.000008 | 0.000005 | 0.000006 | 0.000005 | 0.000004 | 0.000006 | 0.000013 | 0.000004    | 0.000004 | 0.000008 |
| $^{143}\text{Nd}/^{144}\text{Nd}(t)$ | 0.512313 | 0.512317 | 0.512317 | 0.512333 | 0.512327 | 0.512354 | 0.512365 | 0.512356 | 0.512289    | 0.512286 | 0.512344 |
| $\epsilon_{\text{Nd}}(t)$            | 0.16     | 0.22     | 0.24     | 0.55     | 0.42     | 0.96     | 1.17     | 1.00     | -0.31       | -0.38    | 0.77     |
| $T_{\text{DM}}(\text{Ma})$           | 1106     | 1098     | 1054     | 962      | 1002     | 1012     | 958      | 1028     | 1154        | 1184     | 1049     |
| $f_{\text{Sm}/\text{Nd}}$            | -0.35    | -0.35    | -0.37    | -0.42    | -0.40    | -0.36    | -0.38    | -0.35    | -0.35       | -0.33    | -0.35    |
| $^{206}\text{Pb}/^{204}\text{Pb}$    | 18.715   | 18.751   | 18.728   | 18.757   | 18.789   | 18.800   | 18.888   | 18.867   | 18.789      | 18.881   | 18.899   |
| $^{26}\text{Al}$                     | 0.001    | 0.001    | 0.001    | 0.001    | 0.001    | 0.001    | 0.001    | 0.001    | 0.000       | 0.001    | 0.000    |
| $^{207}\text{Pb}/^{204}\text{Pb}$    | 15.609   | 15.613   | 15.612   | 15.611   | 15.613   | 15.617   | 15.620   | 15.621   | 15.626      | 15.629   | 15.614   |
| $^{26}\text{Al}$                     | 0.001    | 0.001    | 0.001    | 0.001    | 0.001    | 0.001    | 0.001    | 0.001    | 0.000       | 0.001    | 0.000    |
| $^{208}\text{Pb}/^{204}\text{Pb}$    | 39.236   | 39.292   | 39.271   | 39.310   | 39.357   | 39.276   | 39.356   | 39.316   | 39.432      | 39.628   | 39.349   |
| $^{26}\text{Al}$                     | 0.002    | 0.002    | 0.002    | 0.002    | 0.002    | 0.002    | 0.001    | 0.002    | 0.001       | 0.002    | 0.001    |
| $^{206}\text{Pb}/^{204}\text{Pb}(t)$ | 18.251   | 18.154   | 18.185   | 18.156   | 18.097   | 18.293   | 18.323   | 18.325   | 18.388      | 18.272   | 18.245   |
| $^{207}\text{Pb}/^{204}\text{Pb}(t)$ | 15.585   | 15.582   | 15.584   | 15.580   | 15.578   | 15.592   | 15.591   | 15.593   | 15.606      | 15.598   | 15.581   |
| $^{208}\text{Pb}/^{204}\text{Pb}(t)$ | 38.572   | 38.500   | 38.520   | 38.440   | 38.403   | 38.533   | 38.542   | 38.597   | 38.845      | 38.685   | 38.446   |

1062

Notes:

1063

1.  $^{87}\text{Rb}/^{86}\text{Sr}$  and  $^{147}\text{Sm}/^{144}\text{Nd}$  ratios are calculated using Rb, Sr, Sm and Nd contents by ICP-MS and measured  $^{87}\text{Sr}/^{86}\text{Sr}$  and  $^{143}\text{Nd}/^{144}\text{Nd}$  ratios by MC-ICP-MS.

1064

2. In  $T_{\text{DM}}$  calculation, ratios of  $(^{143}\text{Nd}/^{144}\text{Nd})_{\text{DM}}$  and  $(^{147}\text{Sm}/^{144}\text{Nd})_{\text{DM}}$  took values of 0.51315 and 0.225, respectively.

1065

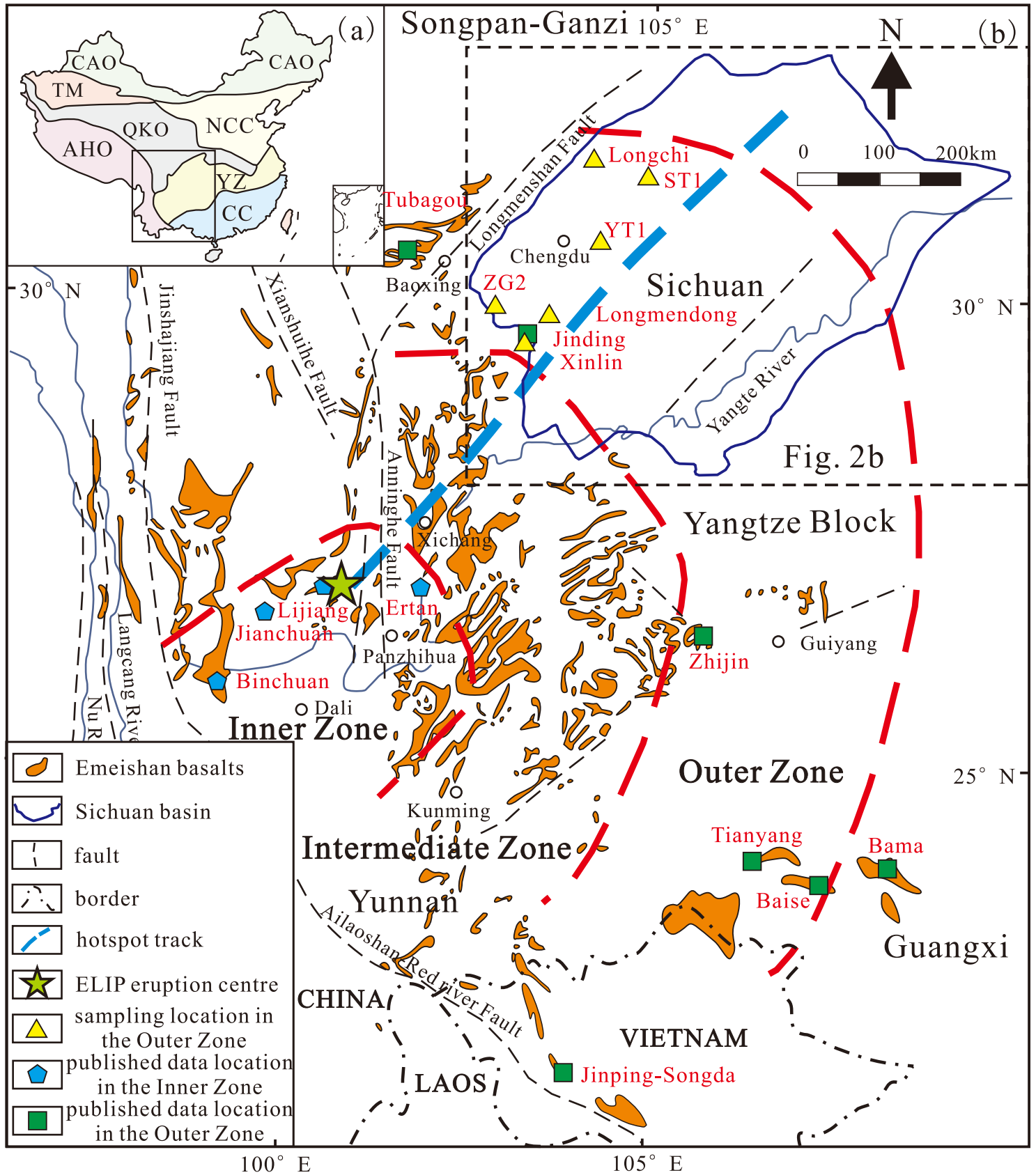
3. In  $\epsilon_{\text{Nd}}(t)$  calculations, ratios of  $(^{87}\text{Sr}/^{86}\text{Sr})_{\text{CHUR}}$ ,  $(^{87}\text{Rb}/^{86}\text{Sr})_{\text{CHUR}}$ ,  $(^{143}\text{Nd}/^{144}\text{Nd})_{\text{CHUR}}$  and  $(^{147}\text{Sm}/^{144}\text{Nd})_{\text{CHUR}}$  are 0.7045, 0.0847, 0.512638 and 0.1967, respectively,

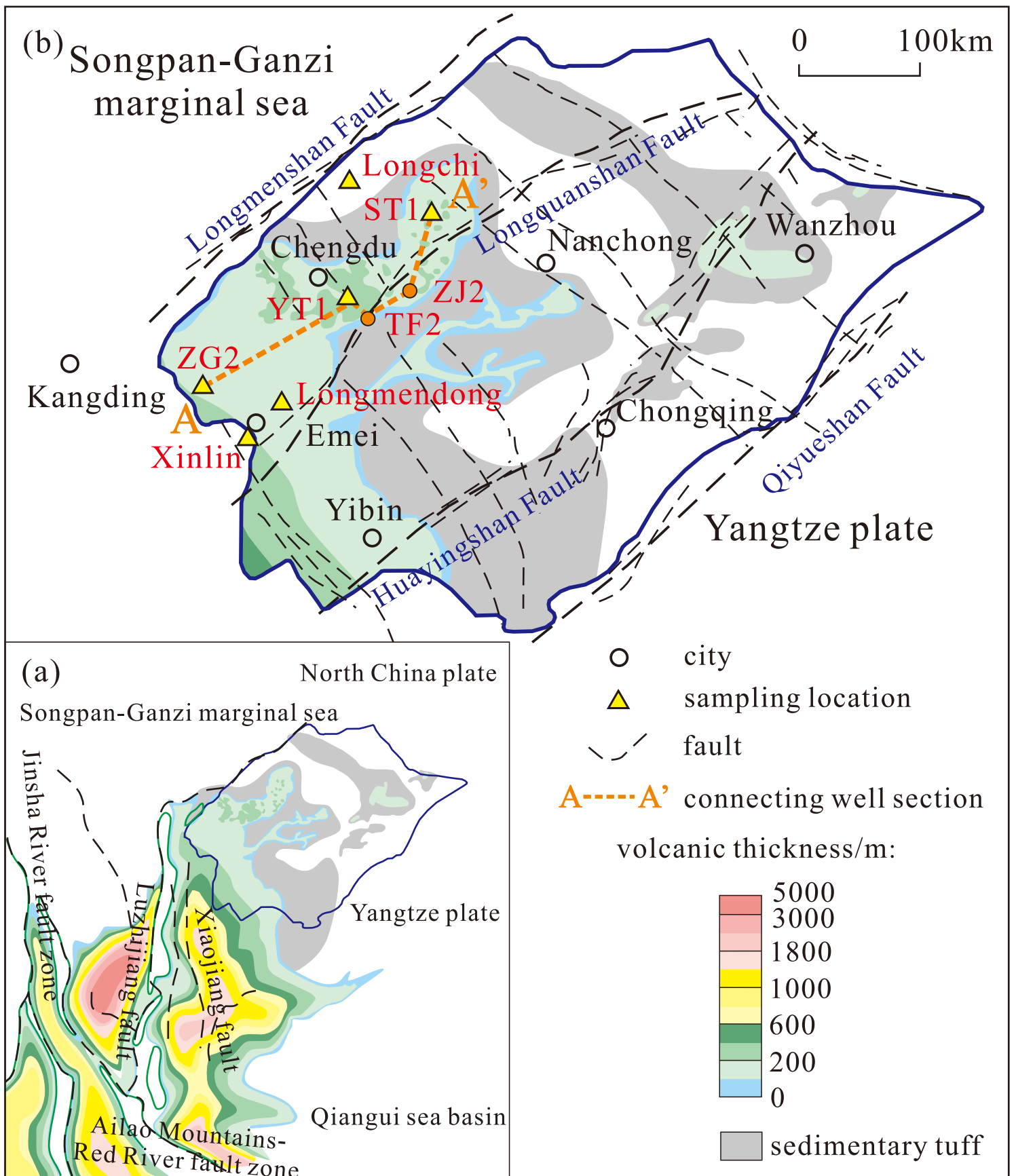
1066

while  $t = 258.5$  Ma.

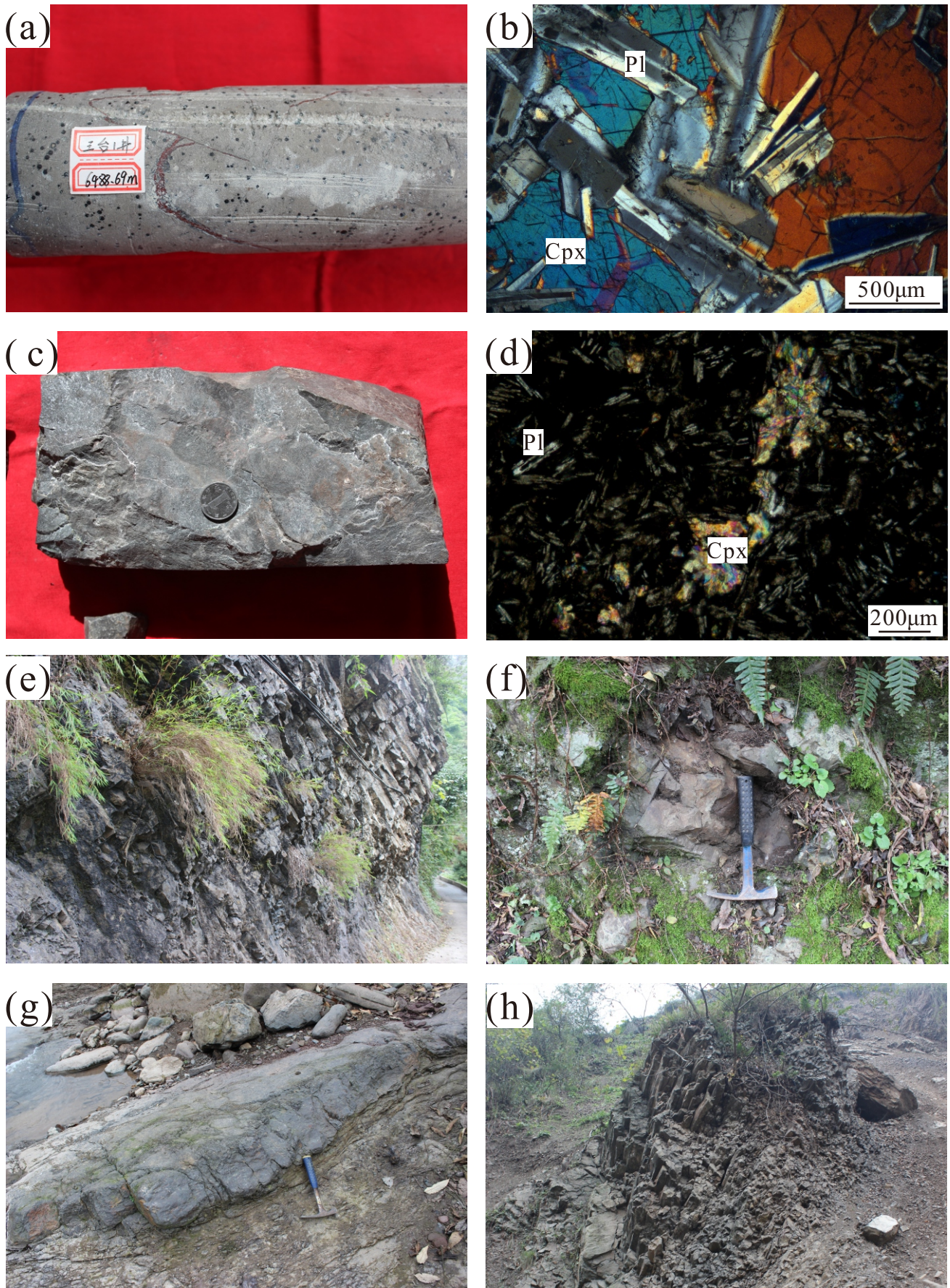
**Table 4** Distribution of the Emeishan basalts in the ELIP

| Zone              | Locality                        | Rock type                       | Reference   |
|-------------------|---------------------------------|---------------------------------|---|
| Inner zone        | Dali                            | High-Ti basalts, low Ti basalts | Hanski et al. (2010)  |
|                   | Lijiang                         | High-Ti basalts, low Ti basalts | Song et al. (2001), Zhang et al. (2006)                                       |
|                   | Binchuan                        | High-Ti basalts, low Ti basalts | Song et al. (2001), Xiao et al. (2004),<br>Xu et al. (2007), Xu et al. (2001) |
|                   | Ertan                           | High-Ti basalts, low Ti basalts | Song et al. (2001), Xu et al. (2001)  |
|                   | Jianchuan                       | High-Ti basalts, low Ti basalts | Song et al. (2001)  |
|                   | Pingchuan                       | Low Ti basalts                  | Xu et al. (2014)  |
|                   | Miyi                            | High-Ti basalts                 | Xu et al. (2014)  |
|                   | Kangsi                          | High-Ti basalts                 | He et al. (2010)  |
|                   | Wanmachang                      | High-Ti basalts                 | He et al. (2010)  |
|                   | Shuidiqiao                      | High-Ti basalts                 | He et al. (2010)  |
|                   | Longzhoushan                    | High-Ti basalts                 | Xu et al. (2007)  |
| Yongsheng         | High-Ti basalts, low Ti basalts | Hao et al. (2004)               |   |
| Intermediate zone | Dongchuan                       | High-Ti basalts                 | Song et al. (2008), Xu et al. (2001)  |
|                   | Qingyin                         | High-Ti basalts                 | Xu et al. (2014)  |
|                   | Qiaojia                         | High-Ti basalts                 | Xu et al. (2014)  |
|                   | Weining                         | High-Ti basalts                 | Xu et al. (2014)  |
|                   | Duge                            | High-Ti basalts                 | Xu et al. (2014)  |
|                   | Zhaotong                        | High-Ti basalts                 | Li et al. (2017c)   |
| Outer zone        | Zhijin                          | High-Ti basalts                 | Lai et al. (2012), Xu et al. (2007)   |
|                   | Jinding                         | High-Ti basalts                 | Xu et al. (2007)  |
|                   | Tubagou                         | High-Ti basalts                 | Li et al. (2016b)   |
|                   | Baise                           | High-Ti basalts                 | Fan et al. (2008)   |
|                   | Bama                            | High-Ti basalts                 | Fan et al. (2008), Lai et al. (2012), Liu<br>et al. (2017)                    |
|                   | Tianyang                        | High-Ti basalts                 | Fan et al. (2008), Liu et al. (2017)  |
|                   | Sichuan Basin                   | High-Ti basalts                 | This study  |

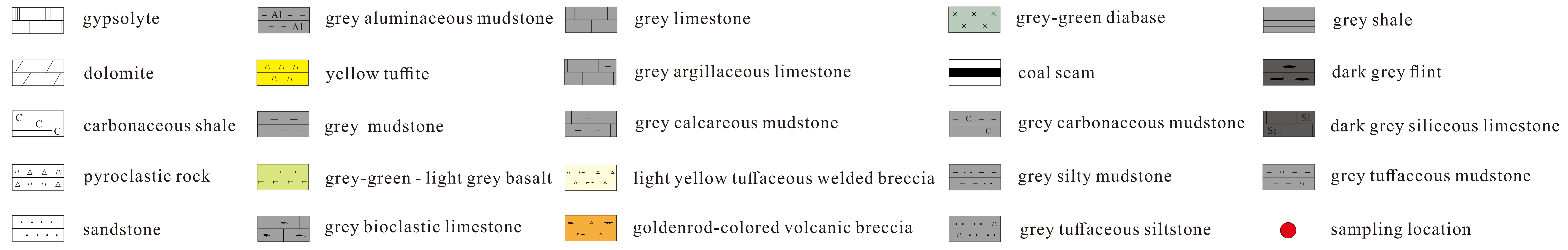
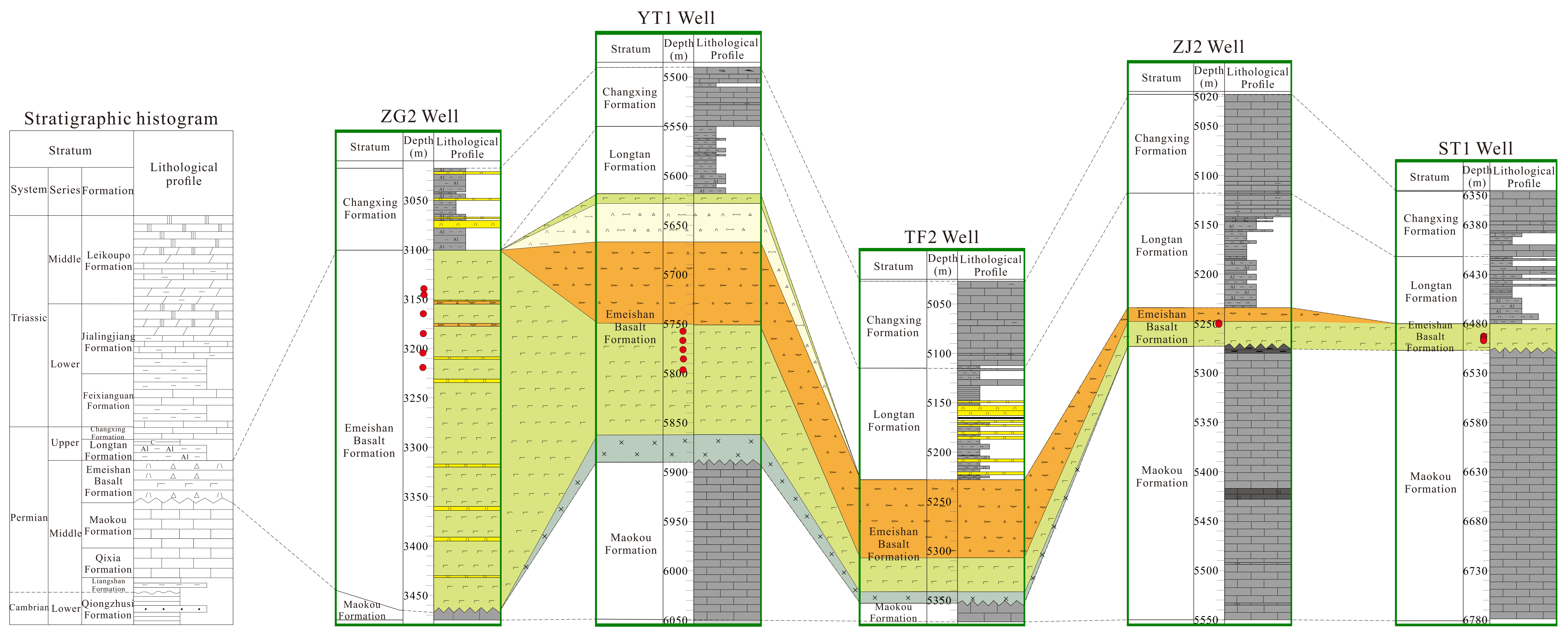


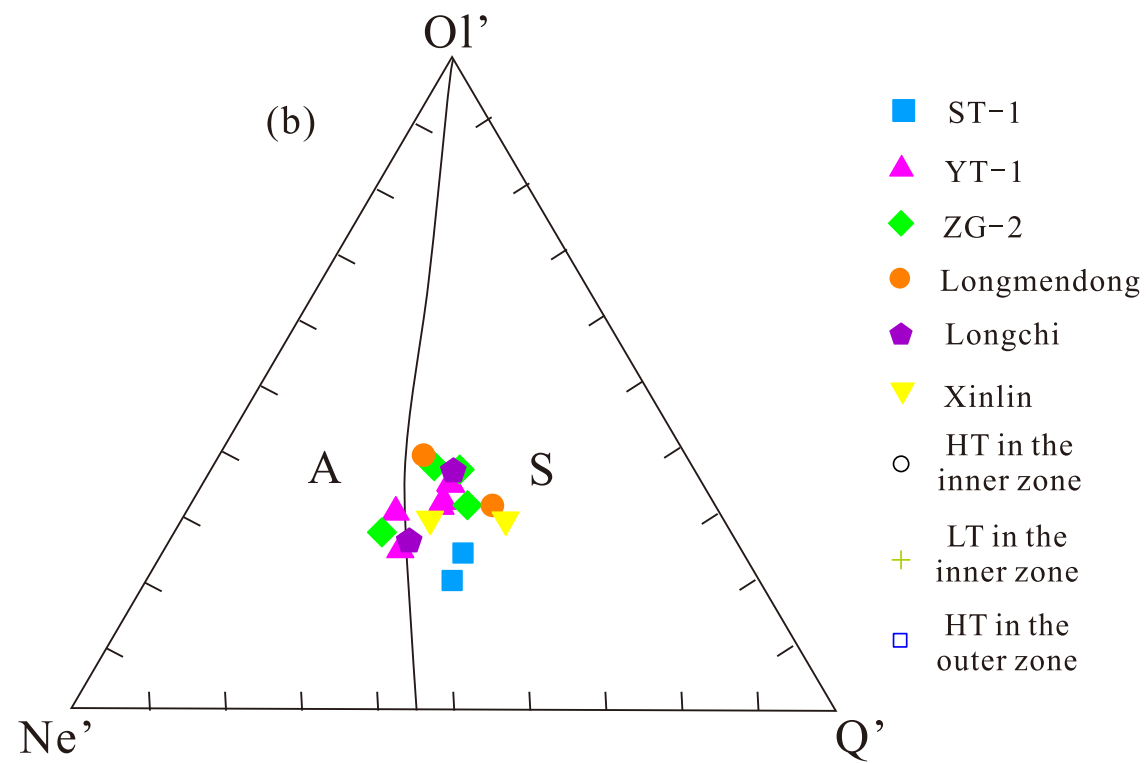
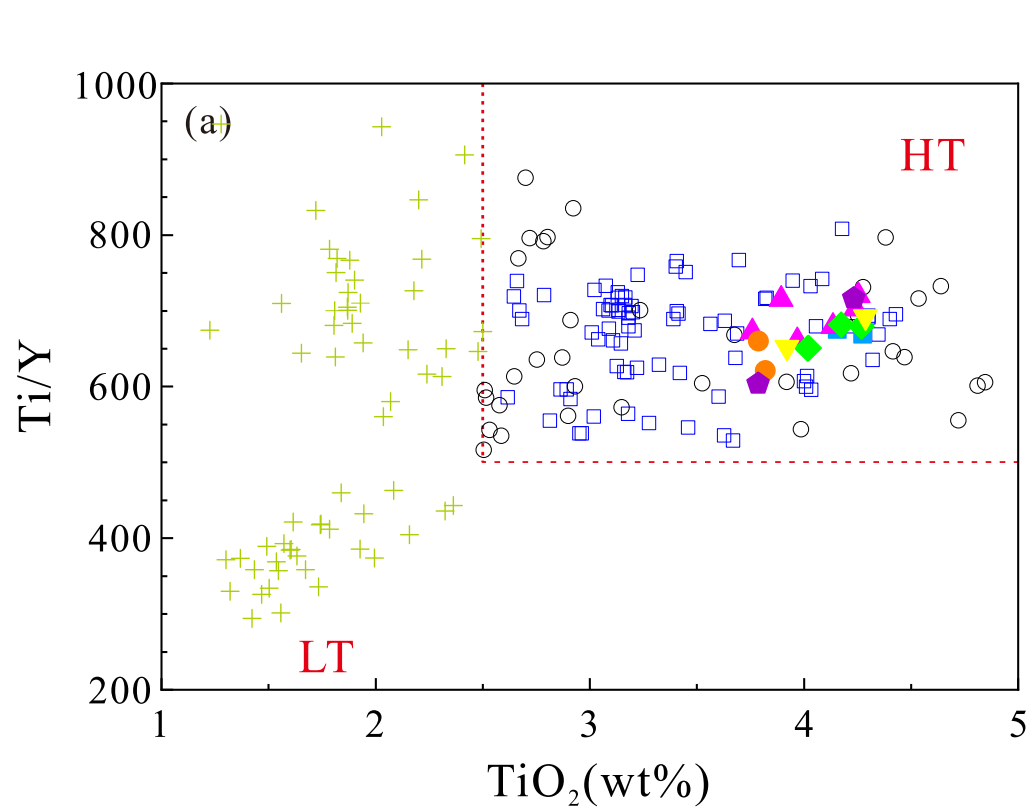


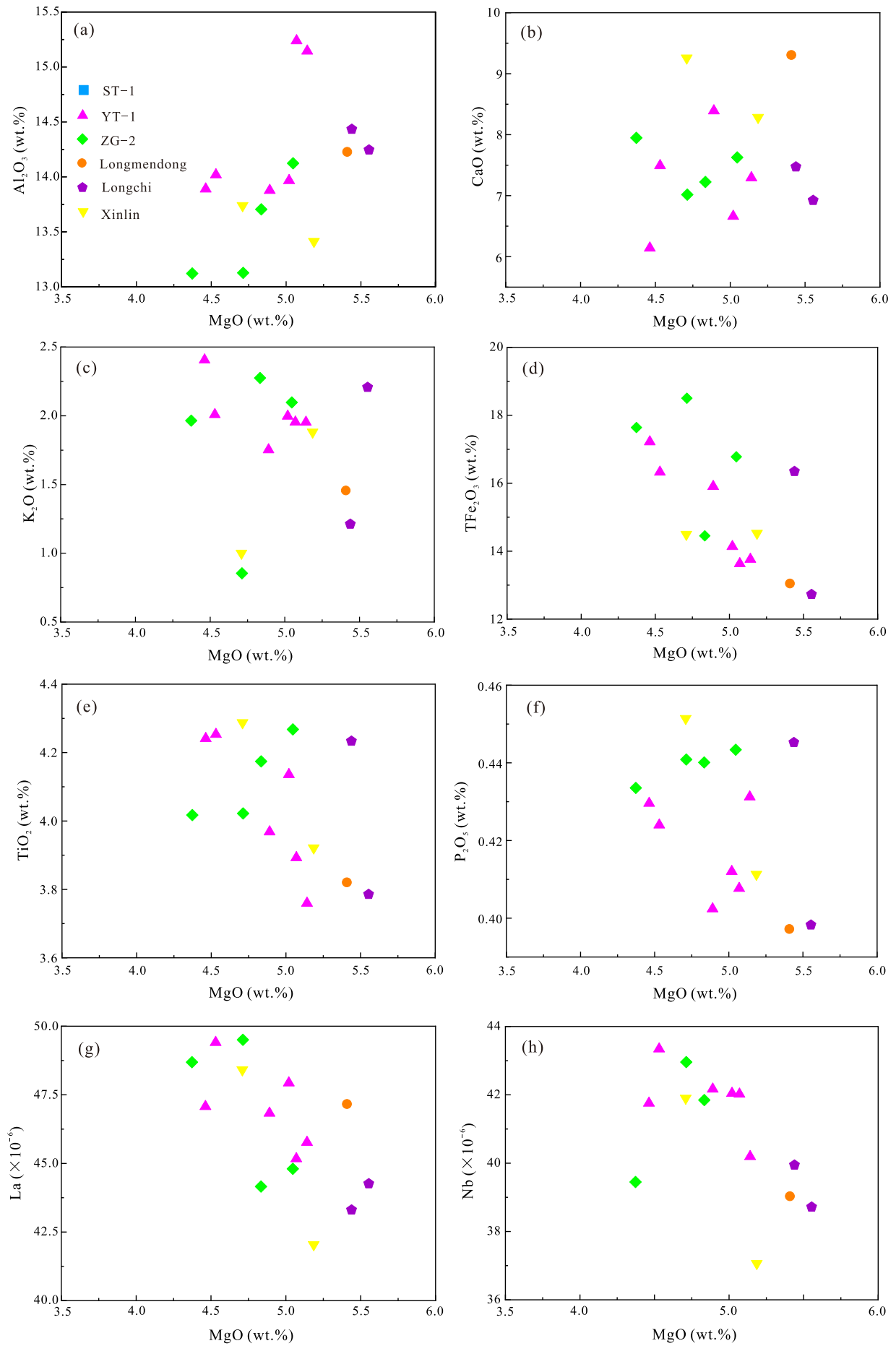


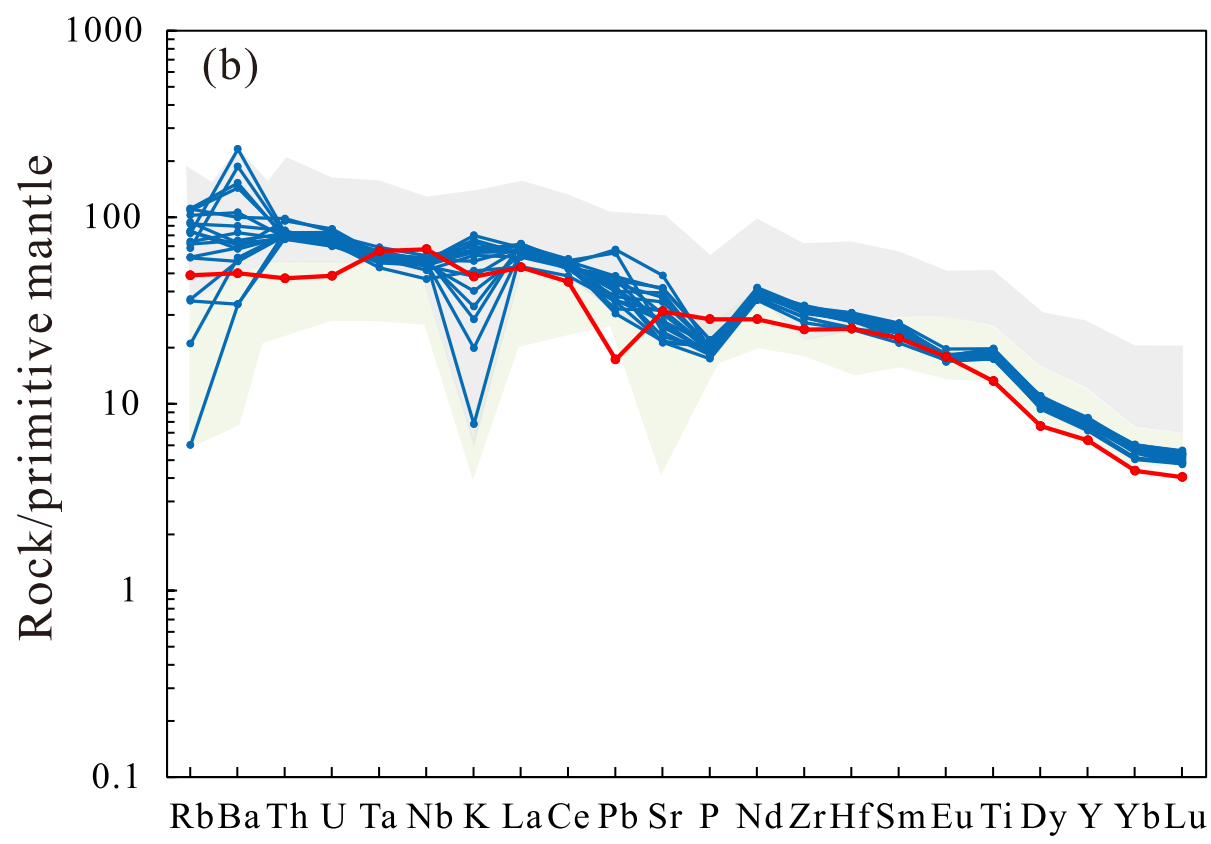
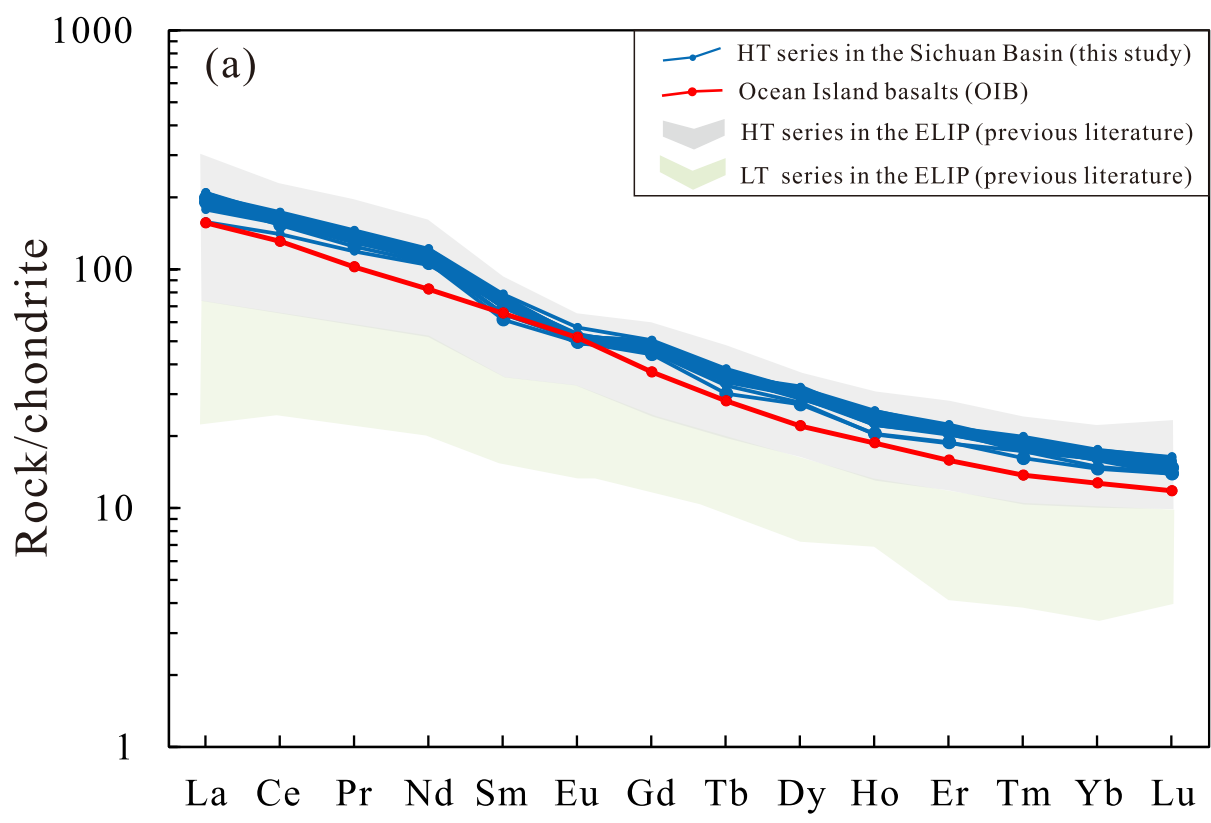


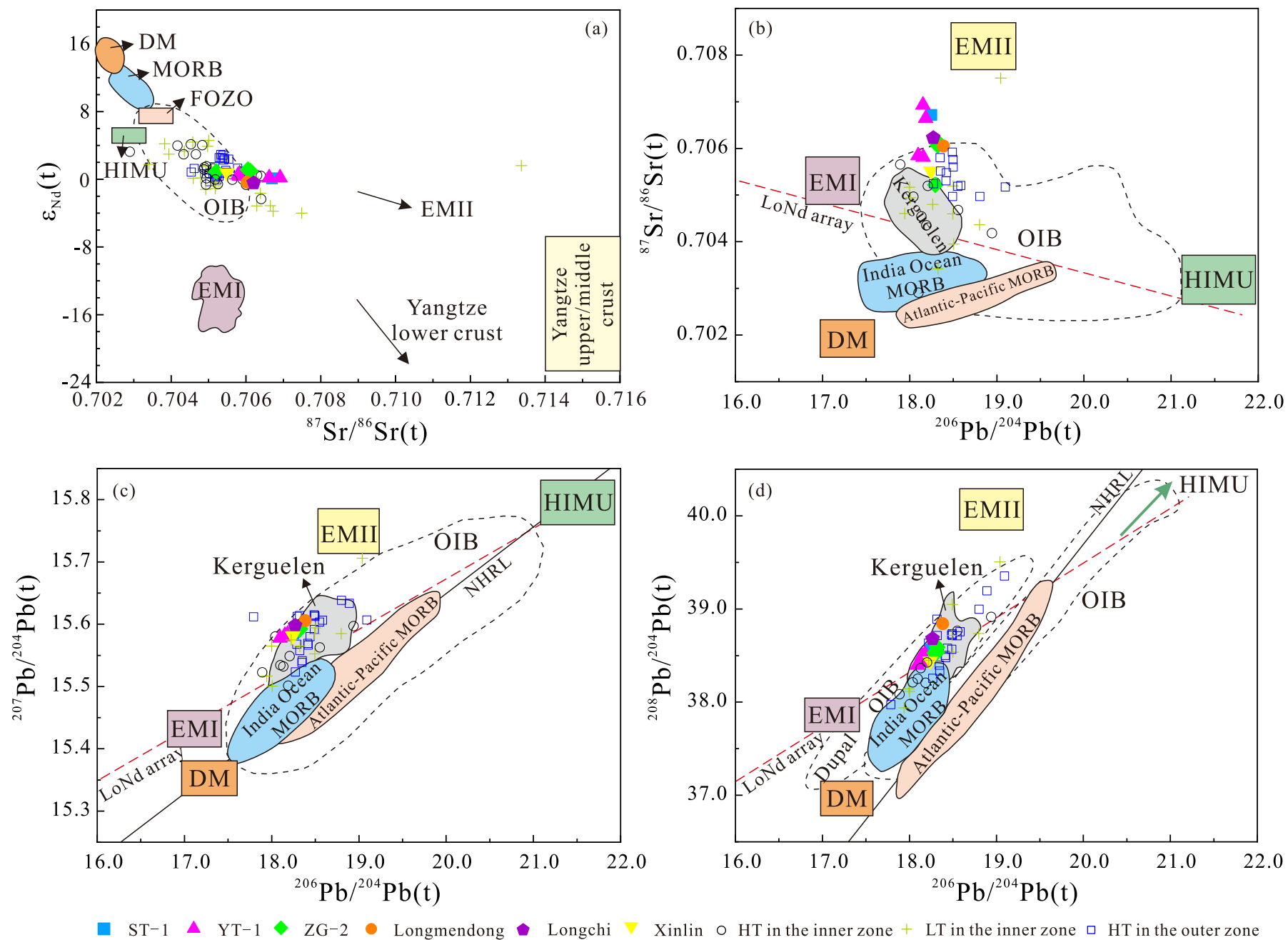


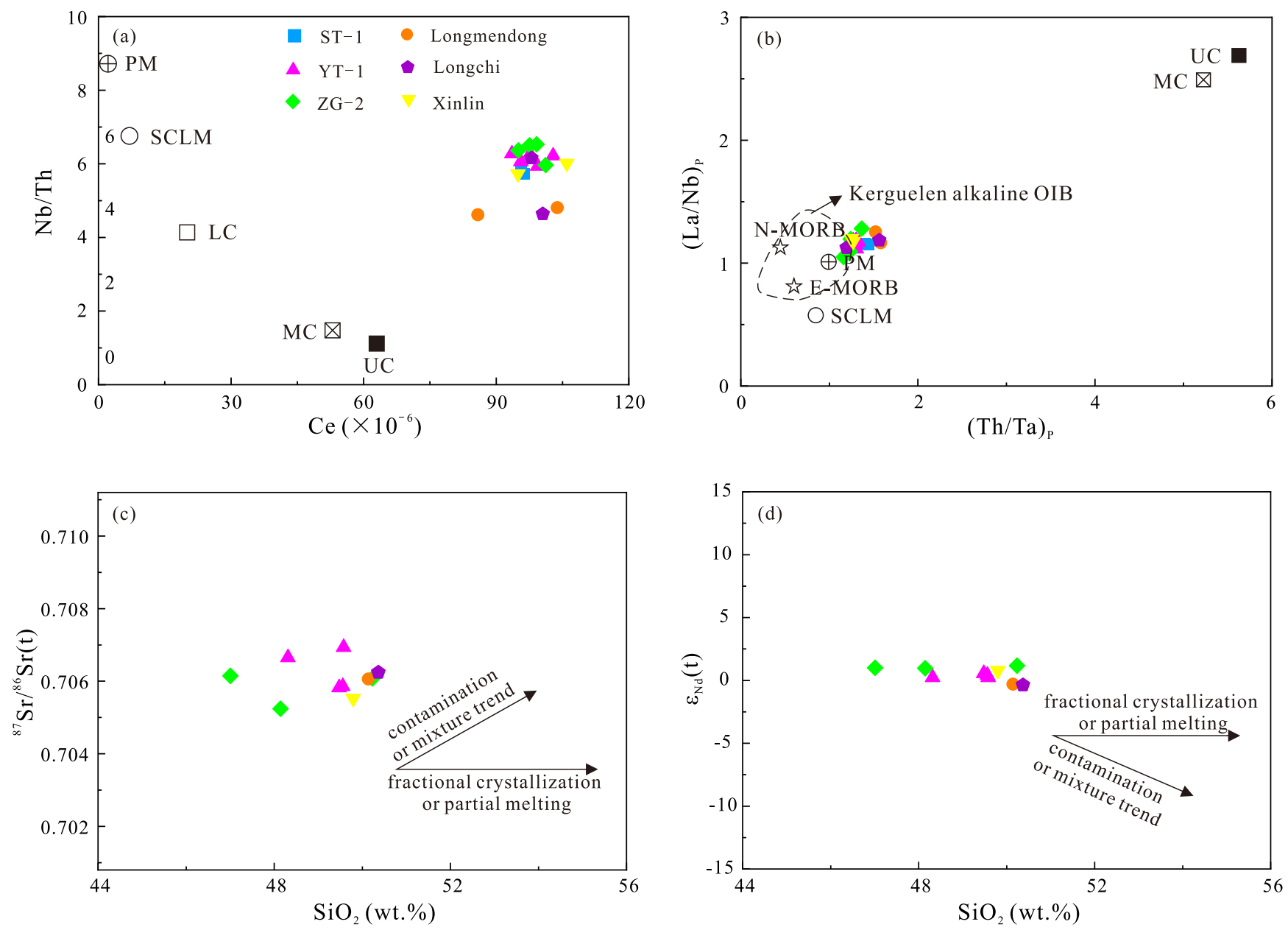


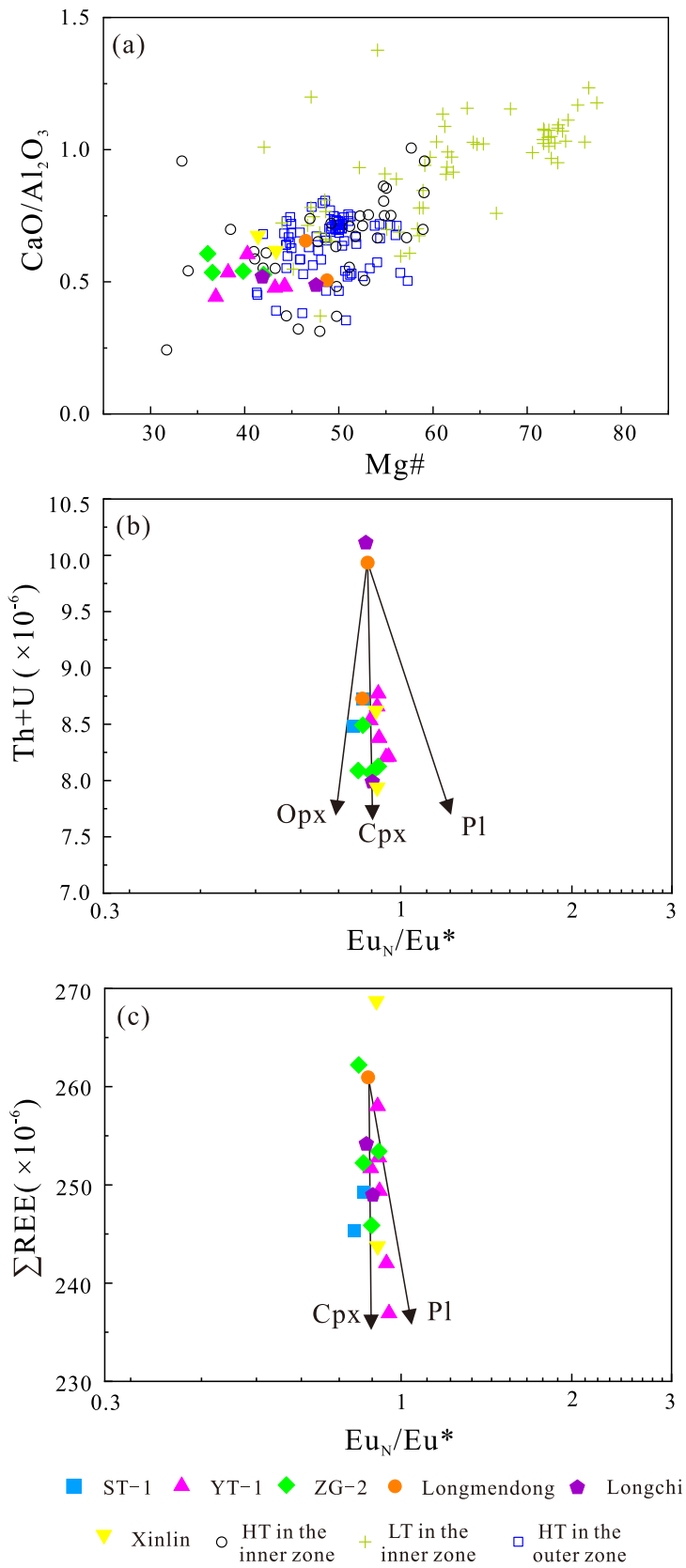




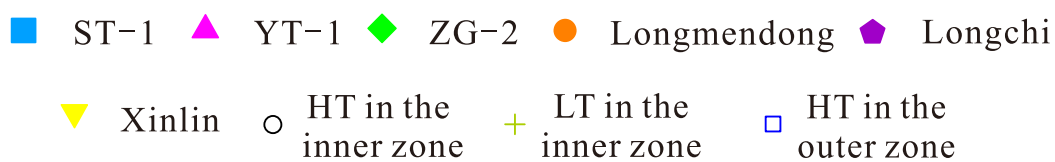
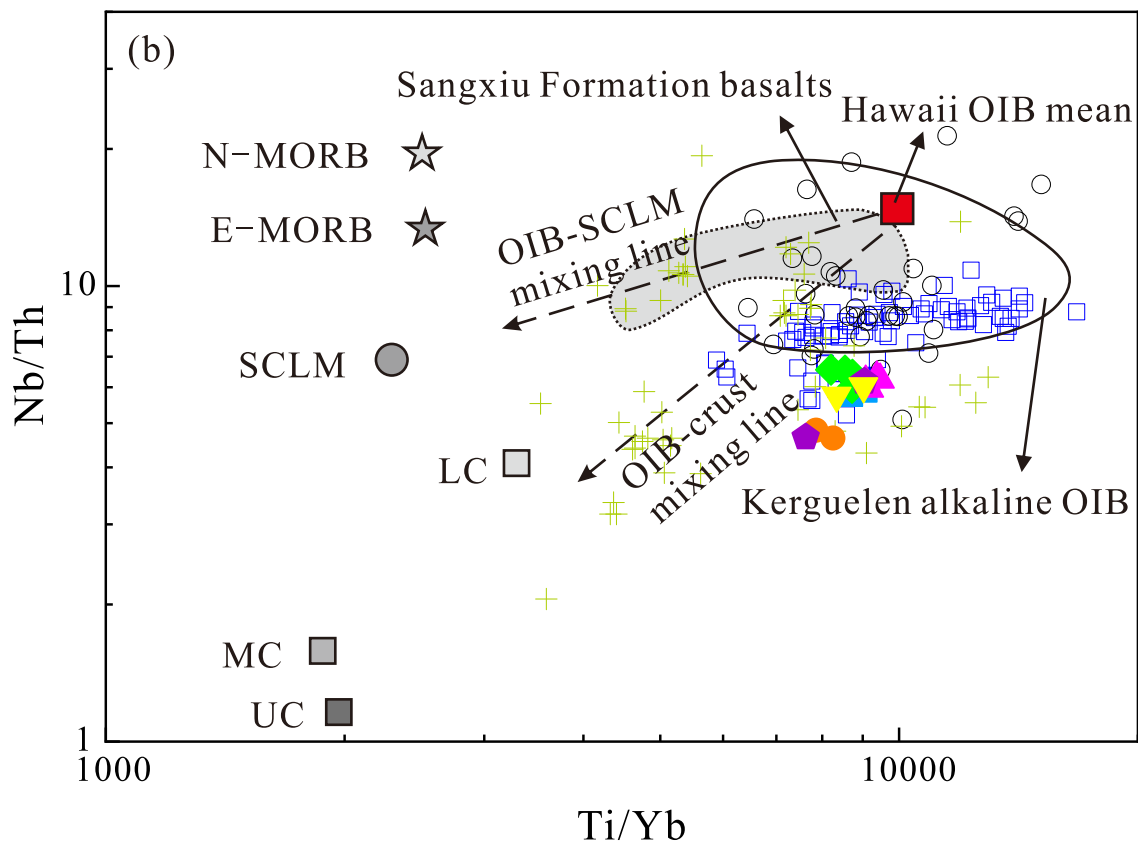
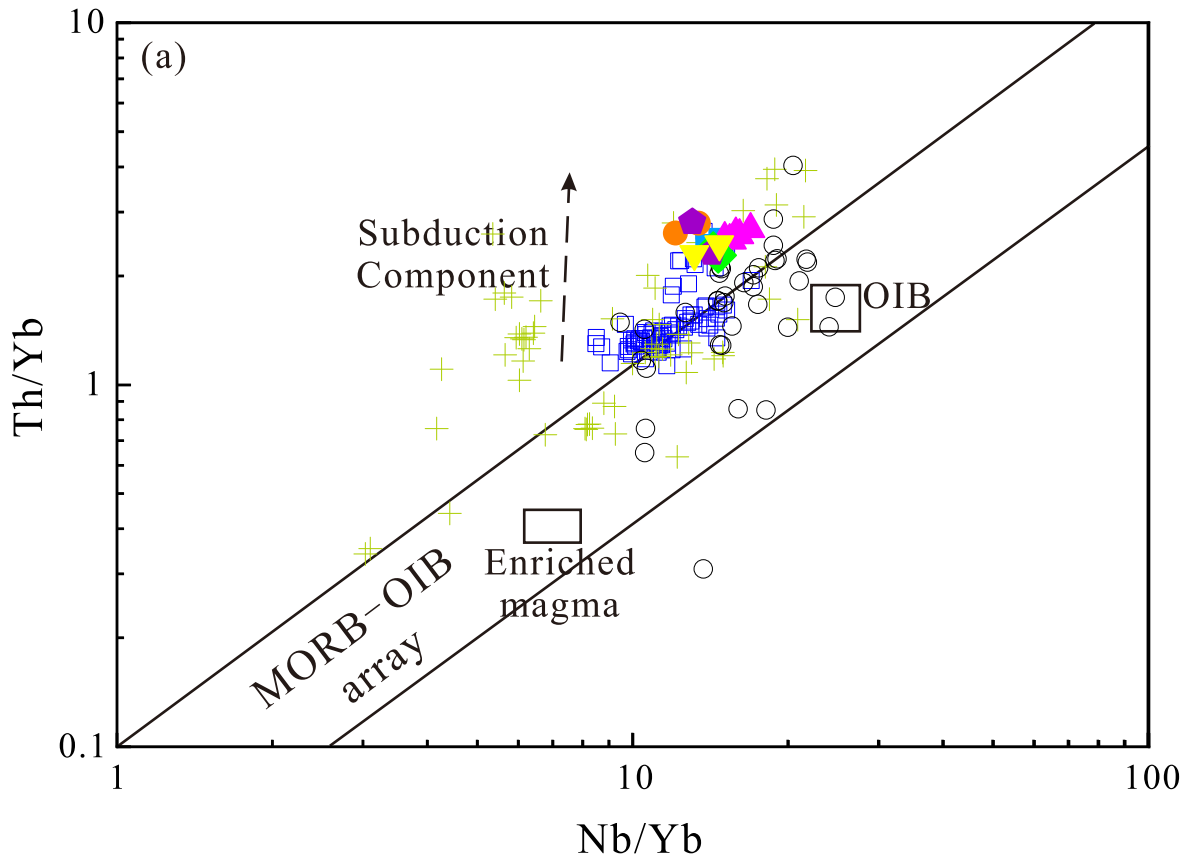




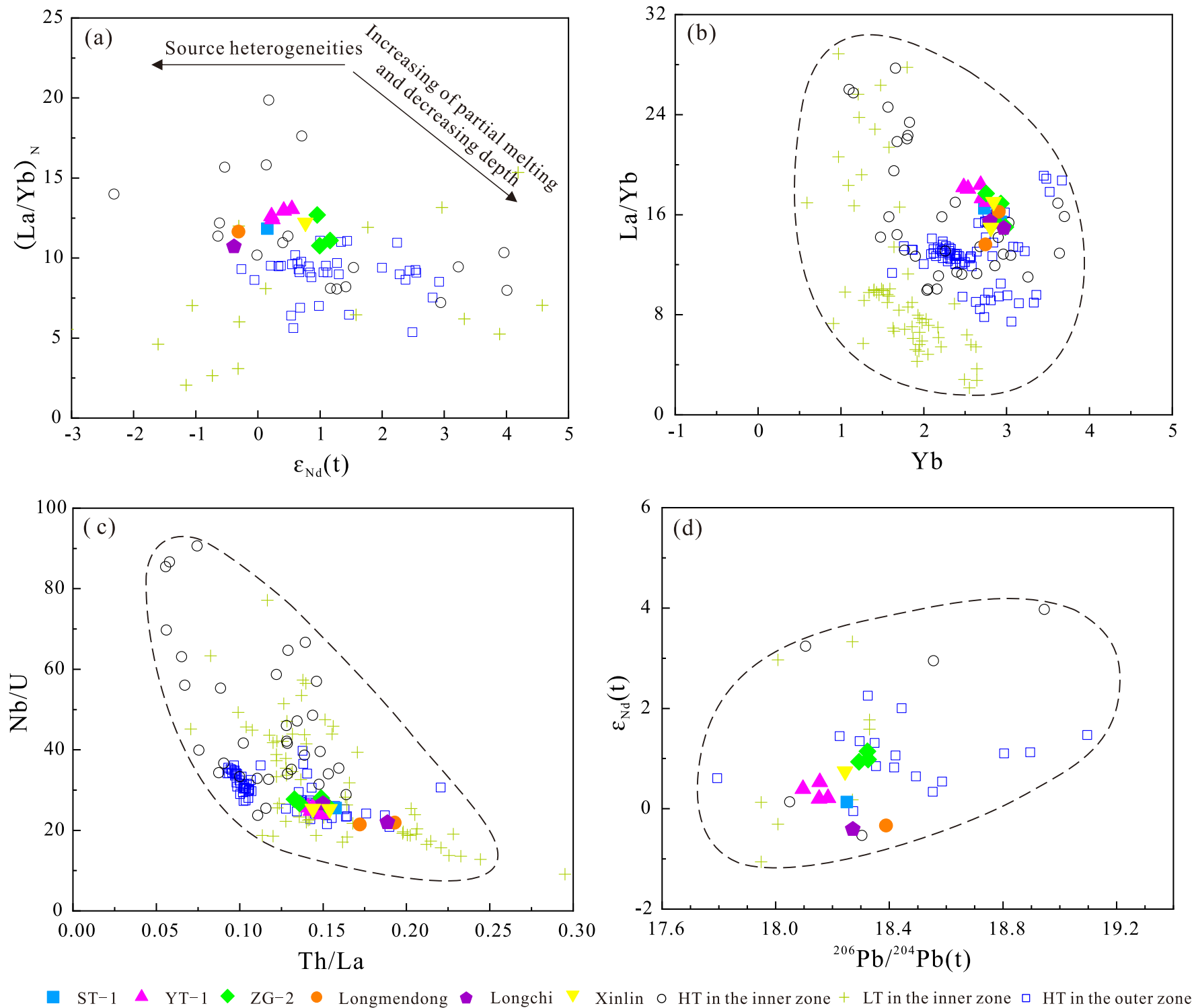


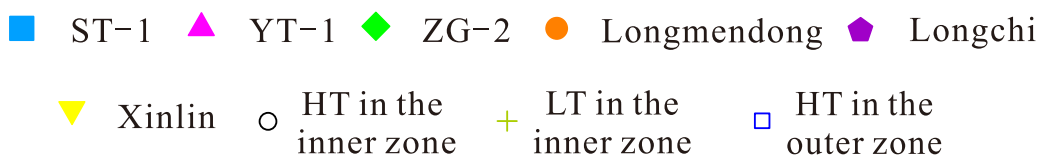
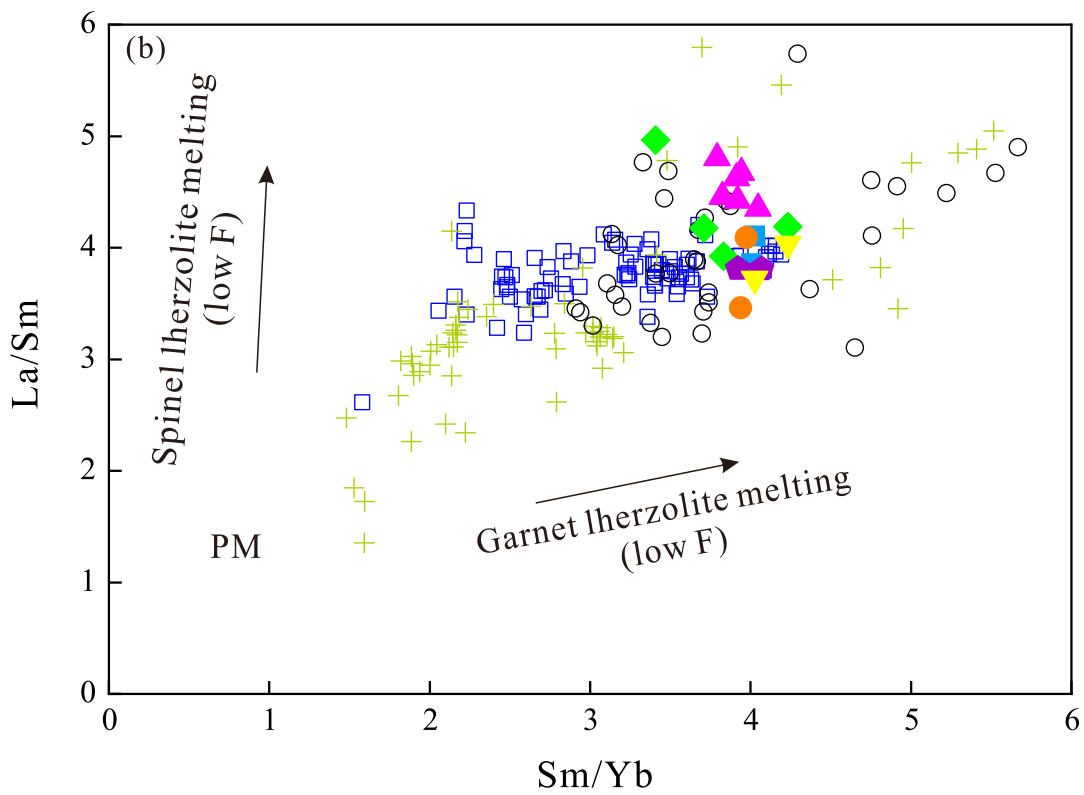
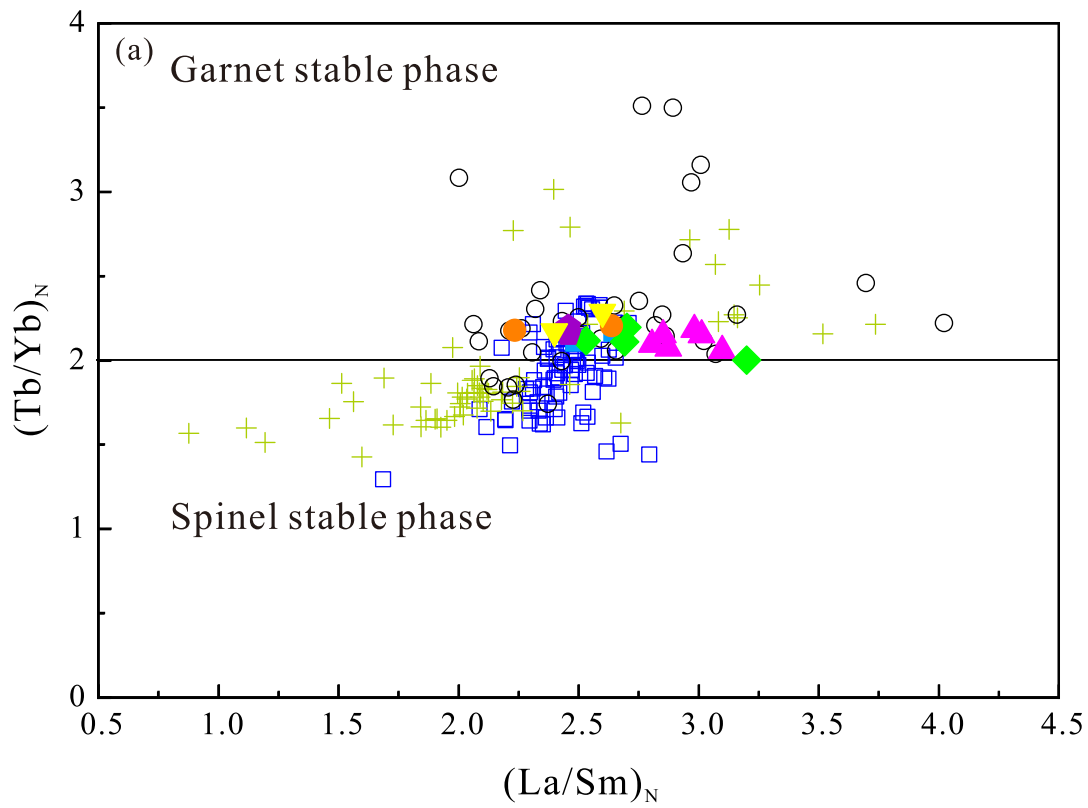


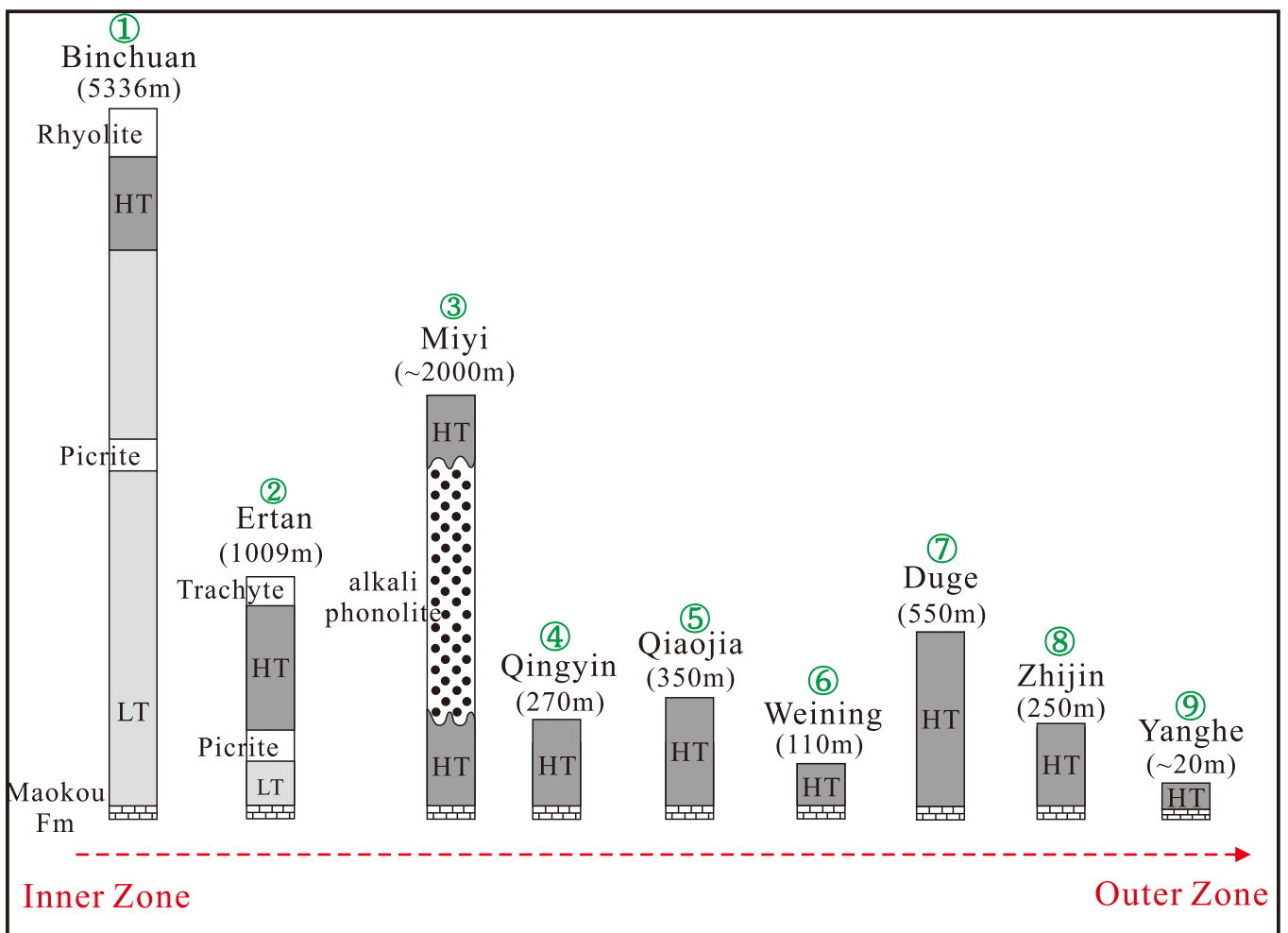
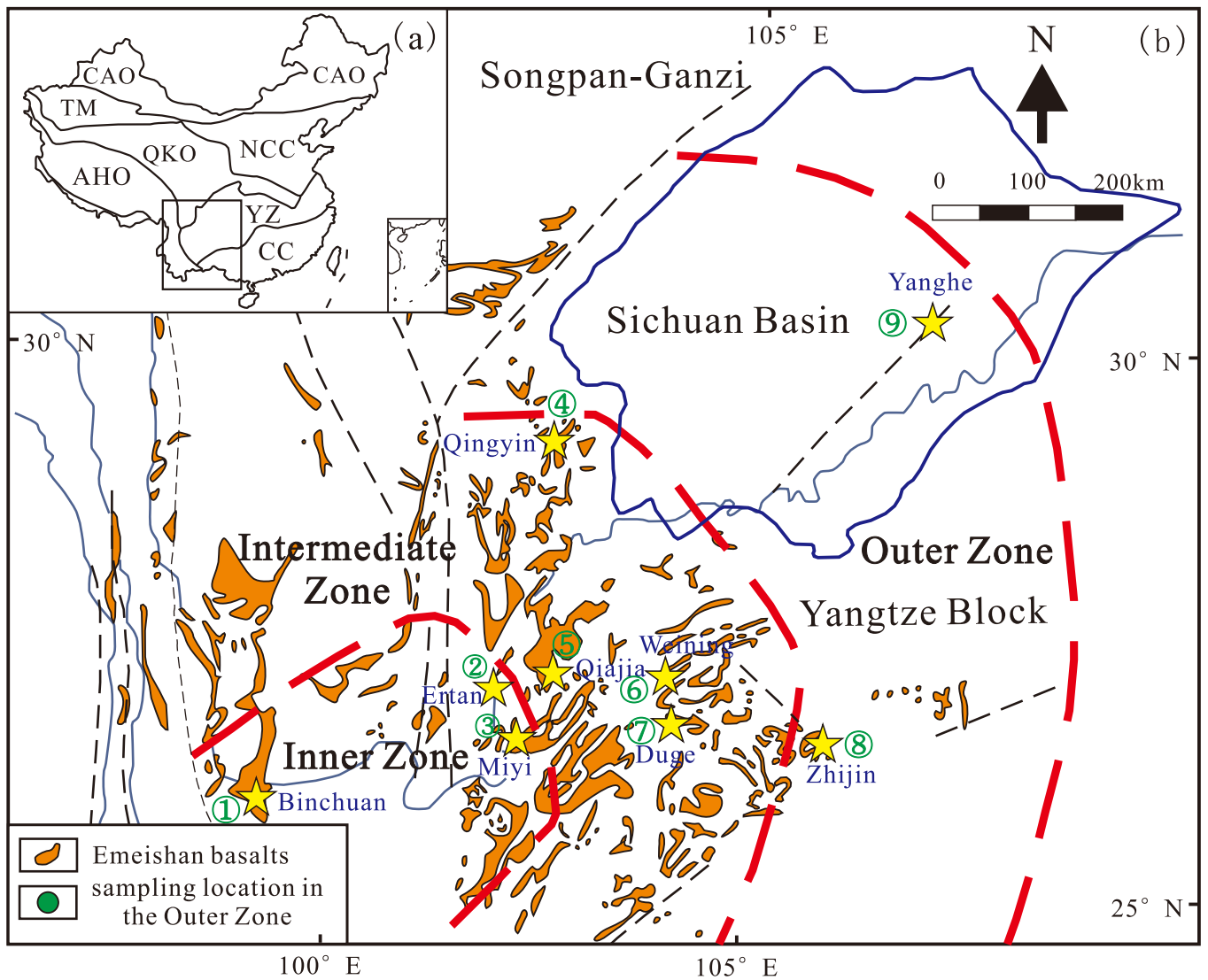




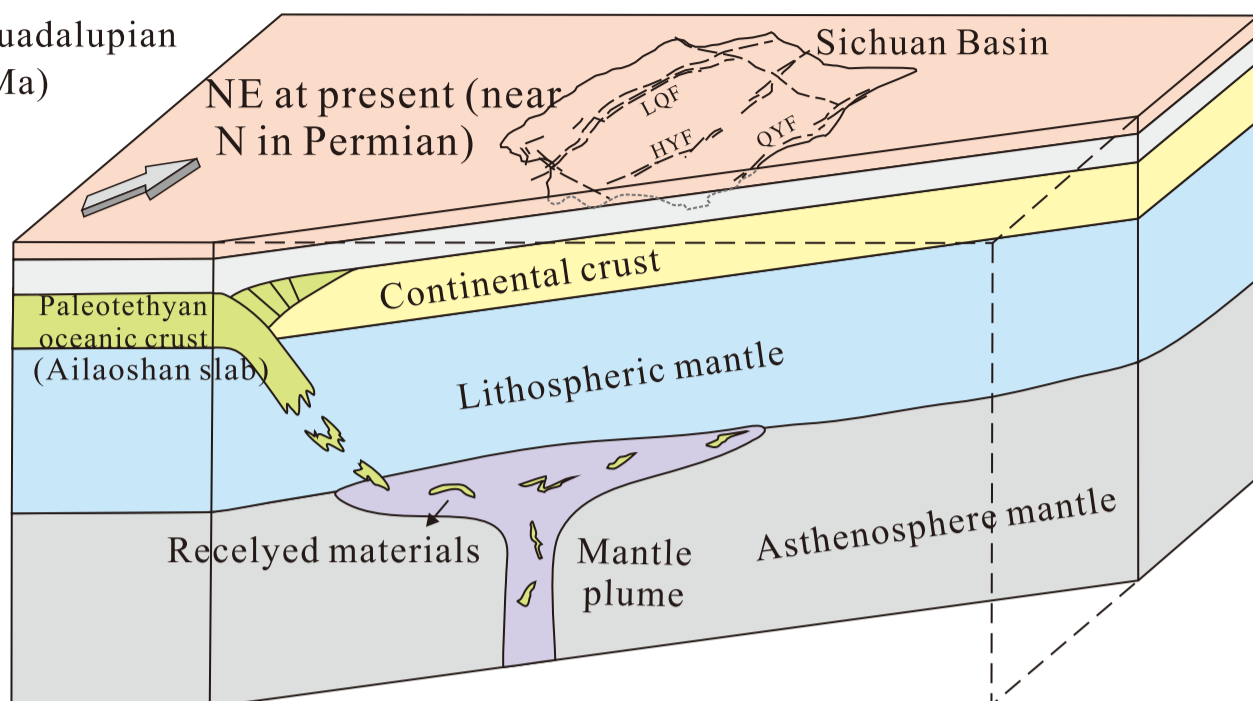




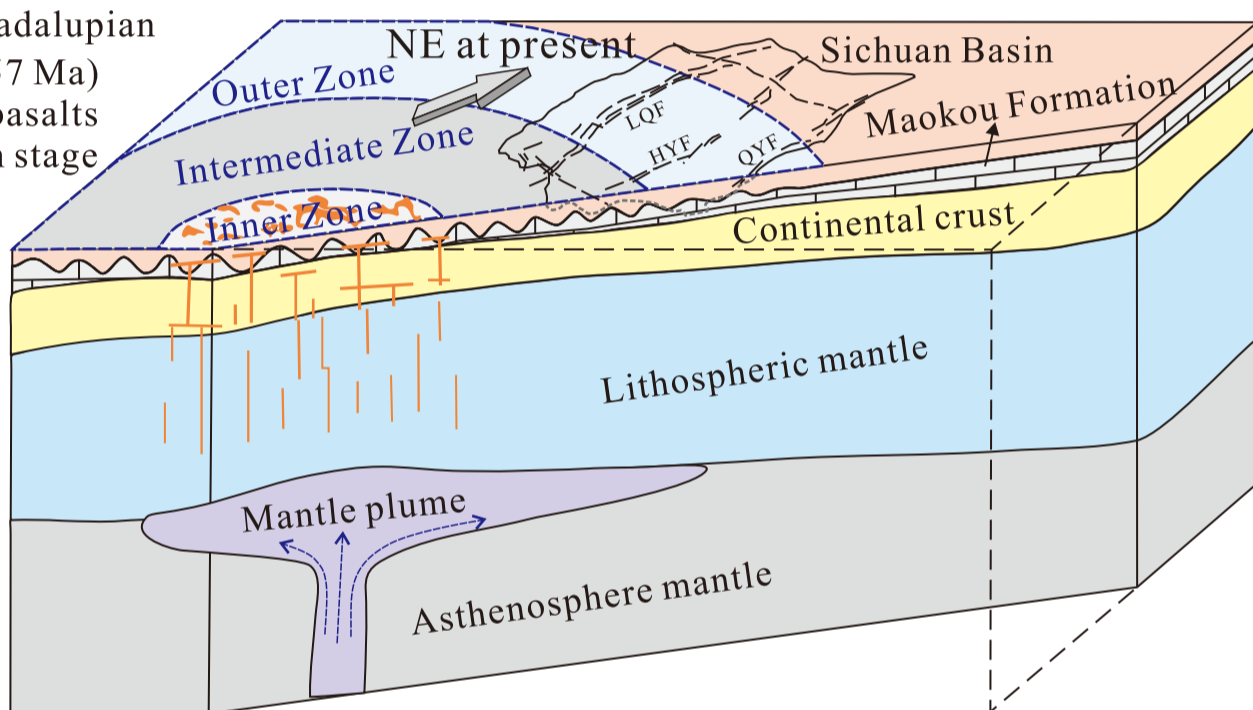




(a) Early-Guadalupian  
(~269 Ma)



(b) End-Guadalupian  
(260~257 Ma)  
low-Ti basalts eruption stage



(c) End-Guadalupian  
(260~257 Ma)  
high-Ti basalts eruption stage

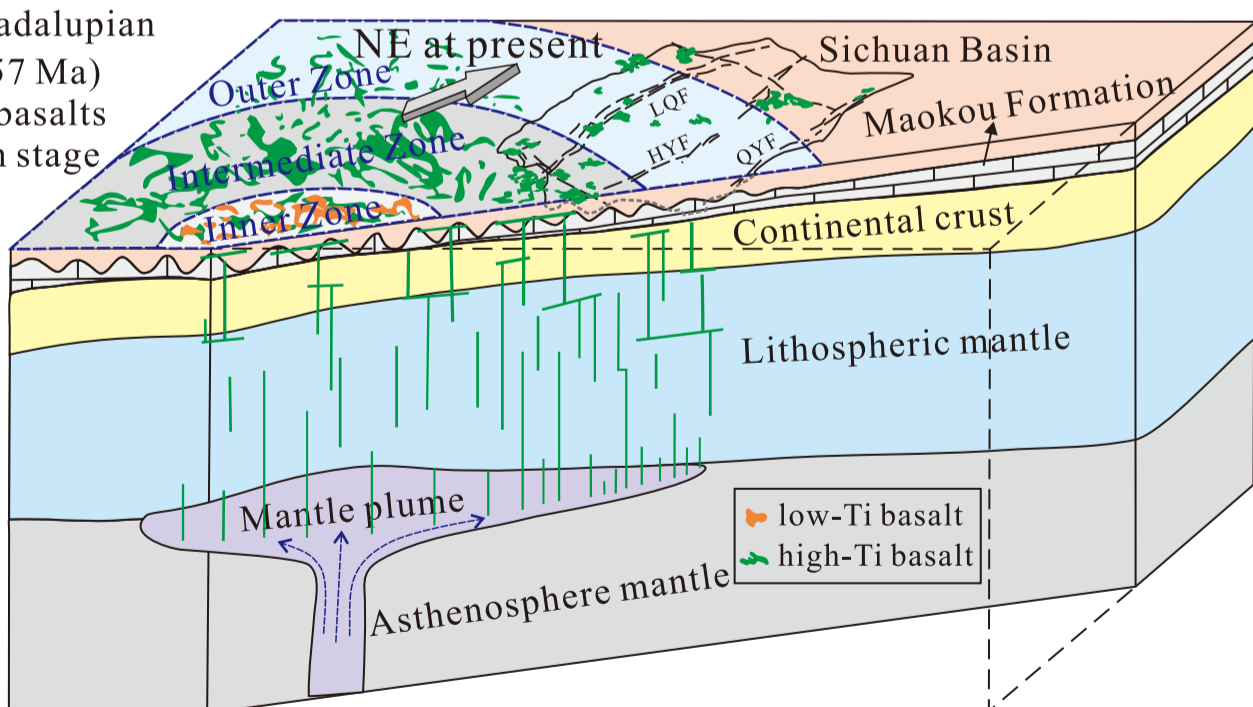


**Table 1** Zircon U-Pb dating results of the Emeishan large igneous province

| Locality                      | Rock type          | Analytical method     | Age/Ma             | Reference               |                   |
|-------------------------------|--------------------|-----------------------|--------------------|-------------------------|-------------------|
| Dali-Jiangwei                 | acid volcanic rock | ID-TIMS zircon U-Pb   | 258.9±0.5          | Xu et al. (2013)        |                   |
| Midu-Jinbaoshan               | wehrlite           | Shrimp zircon U-Pb    | 260.6±3.5          | Tao et al. (2009)       |                   |
|                               | hornblendite       | Shrimp zircon U-Pb    | 260.7±5.6          |                         |                   |
| Binchuan                      | acid tuff          | ID-TIMS zircon U-Pb   | 259.1±0.5          | Zhong et al. (2014)     |                   |
|                               | basalt             | Shrimp zircon U-Pb    | 256.2±1.4          | Li et al. (2016a)       |                   |
| Panxi-Daheishan               | syenite            | ID-TIMS zircon U-Pb   | 259.1±0.5          | Shellnutt et al. (2012) |                   |
| Panxi-Baima                   | granite            | ID-TIMS zircon U-Pb   | 259.2±0.4          |                         |                   |
| Panxi-Huangcao                | syenite            | ID-TIMS zircon U-Pb   | 258.9±0.7          |                         |                   |
| Panxi-Cida                    | granite            | ID-TIMS zircon U-Pb   | 258.4±0.6          |                         |                   |
| Inner Zone<br>Panxi-Maomaogou | syenite            | Shrimp zircon U-Pb    | 261.6 ± 4.4        |                         |                   |
|                               | syenite            | Shrimp zircon U-Pb    | 259.8 ± 3.5        |                         | Xu et al. (2008)  |
|                               | Panxi-Salian       | diorite               | Shrimp zircon U-Pb |                         |                   |
| Panxi-Taihe                   | granite            | Shrimp zircon U-Pb    | 261.4 ± 2.3        |                         |                   |
| Panxi-Hongge                  | gabbro             | Shrimp zircon U-Pb    | 259.3±1.3          | Zhong and Zhu (2006)    |                   |
|                               | gabbro             | Shrimp zircon U-Pb    | 259.3 ± 1.3        |                         |                   |
| Panxi-Binggu                  | gabbro             | Shrimp zircon U-Pb    | 260.7 ± 0.8        | Zhou et al. (2005)      |                   |
| Panxi-Panzhihua               | gabbro             | Shrimp zircon U-Pb    | 263±3              |                         |                   |
|                               | Picrate dyke       | LA-ICP-MS zircon U-Pb | 261.4±4.6          |                         | Hou et al. (2013) |
|                               | Ultramafic dyke    | Shrimp zircon U-Pb    | 262±3              | Guo et al. (2004)       |                   |
| Xinjie                        | gabbro             | Shrimp zircon U-Pb    | 259±3              | Zhou et al. (2002)      |                   |

|                      |                                |                          |                          |                    |                     |
|----------------------|--------------------------------|--------------------------|--------------------------|--------------------|---------------------|
|                      | Limahe                         | gabbro                   | Shrimp zircon<br>U-Pb    | 263±3              | Zhou et al. (2008)  |
|                      | Zhubu                          | diorite                  | Shrimp zircon<br>U-Pb    | 261 ± 2            |                     |
| Intermediate<br>Zone | Guizhou-<br>Weining            | boundary clay<br>rock    | ID-TIMS<br>zircon U-Pb   | 258.1±0.6          | Xu et al. (2013)    |
|                      | Panxian-<br>Zhudong            | ignimbrite               | ID-TIMS<br>zircon U-Pb   | 258.3±1.4          | Zhu (2019)          |
|                      | Xingyi-Xiongwu                 | tuff                     | ID-TIMS<br>zircon U-Pb   | 258.5±0.9          |                     |
|                      | Puan-Louxia                    | tuff                     | ID-TIMS<br>zircon U-Pb   | 258.1±1.1          |                     |
|                      | Baimazhai                      | pyroxenite               | Shrimp zircon<br>U-Pb    | 258.5±3.5          | Wang et al. (2006)  |
| Outer Zone           | Tubagou                        | basalt                   | Shrimp zircon<br>U-Pb    | 257.3±2.0          | Li et al. (2016b)   |
|                      | Baise-Yangxu                   | basalt                   | Shrimp zircon<br>U-Pb    | 259.1 ± 4.0        | Fan et al. (2008)   |
|                      |                                |                          |                          | 253.7±6.1          | Fan et al. (2004)   |
|                      | Bama-Minan                     | basalt                   | Shrimp zircon<br>U-Pb    | 259.6±5.9          | Fan et al. (2008)   |
|                      | Nayong-Xilin-<br>Tianyang Area | basalt                   | LA-ICP-MS<br>zircon U-Pb | 257.0±9.0          | Lai et al. (2012)   |
|                      | Guangyuan-<br>Chaotian         | boundary clay<br>rock    | ID-TIMS<br>zircon U-Pb   | 258.6±1.4          | Xu et al. (2013)    |
|                      |                                |                          |                          | 259.2±0.3          | Zhong et al. (2014) |
|                      | Funing                         | diabase                  | Shrimp zircon<br>U-Pb    | 260±3              | Zhou et al. (2006)  |
| diorite              |                                | Shrimp zircon<br>U-Pb    | 258±3                    |                    |                     |
| Mianhuadi            | metagabbro                     | MC-ICP-MS<br>zircon U-Pb | 259.6±0.8                | Zhou et al. (2013) |                     |

**Table 2** Major elements (wt.%) and trace elements ( $\times 10^{-6}$ ) contents for the analysed volcanic rocks in the Sichuan Basin

| Samples                                     | ST1<br>-2 | ST1<br>-5 | YT1<br>-1 | YT1<br>-3 | YT1<br>-4 | YT1<br>-5 | YT1<br>-6 | YT1<br>-7 | ZG2<br>-4 | ZG2<br>-5 | ZG2<br>-7   | ZG2<br>-8 | 20L<br>MD0<br>4 | 20L<br>MD0<br>5 | 20LC<br>04 | 20LC<br>06 | 20XL<br>01 | 20XL<br>02 | 20XL02<br>(replicate) |
|---|-----------|-----------|-----------|-----------|-----------|-----------|-----------|-----------|-----------|-----------|-------------|-----------|-----------------|-----------------|------------|------------|------------|------------|-----------------------|
| Locality                                    | ST1 Well  |           | YT1 Well  |           |           |           | ZG2 Well  |           |           |           | Longmendong |           | Longchi         |                 | Xinlin     |            |            |            |                       |
| SiO <sub>2</sub>                            | 49.64     | 48.78     | 48.62     | 47.55     | 46.69     | 47.67     | 48.67     | 48.96     | 46.59     | 47.64     | 48.74       | 45.59     | 45.99           | 48.99           | 45.94      | 49.08      | 49.21      | 48.12      | 48.32                 |
| TiO <sub>2</sub>                            | 4.01      | 3.87      | 4.06      | 3.91      | 4.17      | 4.19      | 3.83      | 3.71      | 4.01      | 3.98      | 4.05        | 4.14      | 3.69            | 3.73            | 4.08       | 3.69       | 4.24       | 3.82       | 3.84                  |
| Al <sub>2</sub> O <sub>3</sub>              | 13.75     | 13.66     | 13.69     | 13.66     | 13.64     | 13.82     | 14.99     | 14.96     | 13.07     | 12.98     | 13.30       | 13.70     | 13.44           | 13.90           | 13.91      | 13.88      | 13.57      | 13.08      | 13.06                 |
| Fe <sub>2</sub> O <sub>3</sub> <sup>T</sup> | 12.92     | 13.82     | 13.86     | 15.65     | 16.91     | 16.10     | 13.41     | 13.60     | 18.43     | 17.46     | 14.02       | 16.27     | 15.44           | 12.75           | 15.75      | 12.40      | 14.32      | 14.16      | 14.23                 |
| MnO   | 0.21      | 0.17      | 0.18      | 0.16      | 0.17      | 0.17      | 0.16      | 0.16      | 0.20      | 0.19      | 0.20        | 0.19      | 0.21            | 0.16            | 0.17       | 0.17       | 0.18       | 0.17       | 0.17                  |
| MgO   | 3.43      | 3.68      | 4.92      | 4.81      | 4.38      | 4.47      | 4.99      | 5.08      | 4.69      | 4.33      | 4.69        | 4.89      | 7.12            | 5.28            | 5.24       | 5.41       | 4.65       | 5.06       | 5.10                  |
| CaO   | 4.88      | 4.27      | 6.53      | 8.26      | 6.03      | 7.39      | 7.22      | 7.21      | 6.99      | 7.87      | 7.01        | 7.40      | 6.79            | 9.09            | 7.20       | 6.75       | 9.15       | 8.08       | 8.13                  |
| Na <sub>2</sub> O                           | 4.38      | 3.91      | 3.82      | 2.29      | 3.44      | 2.39      | 2.78      | 2.75      | 4.32      | 2.14      | 2.38        | 2.34      | 2.81            | 1.97            | 2.47       | 3.52       | 2.05       | 2.78       | 2.76                  |
| K <sub>2</sub> O                            | 0.22      | 0.56      | 1.96      | 1.73      | 2.36      | 1.98      | 1.92      | 1.93      | 0.85      | 1.94      | 2.21        | 2.03      | 1.51            | 1.42            | 1.17       | 2.15       | 0.99       | 1.83       | 1.85                  |
| P <sub>2</sub> O <sub>5</sub>               | 0.45      | 0.45      | 0.40      | 0.40      | 0.42      | 0.42      | 0.40      | 0.43      | 0.44      | 0.43      | 0.43        | 0.43      | 0.37            | 0.39            | 0.43       | 0.39       | 0.45       | 0.40       | 0.40                  |
| LOI   | 5.87      | 6.04      | 1.89      | 1.70      | 1.33      | 1.12      | 1.15      | 1.21      | 0.54      | 0.77      | 2.59        | 2.68      | 2.89            | 2.03            | 3.03       | 1.99       | 1.38       | 2.25       | 2.24                  |
| Total                                       | 99.76     | 99.20     | 99.94     | 100.1     | 99.56     | 99.70     | 99.51     | 99.99     | 100.1     | 99.71     | 99.61       | 99.66     | 100.2           | 99.71           | 99.37      | 99.41      | 100.1      | 99.75      | 100.12                |
| Mg#   | 34.45     | 34.49     | 41.29     | 37.85     | 33.92     | 35.47     | 42.42     | 42.53     | 33.53     | 32.93     | 39.85       | 37.33     | 47.74           | 45.09           | 39.72      | 46.36      | 39.15      | 41.42      | 39.12                 |
| La  | 45.2      | 45.1      | 47.9      | 46.8      | 47.1      | 49.4      | 45.2      | 45.8      | 49.5      | 48.7      | 44.2        | 44.8      | 37.4            | 47.2            | 43.3       | 44.3       | 48.4       | 42.0       | 41.9                  |
| Ce  | 96.3      | 95.6      | 98.3      | 97.5      | 99.4      | 103       | 93.6      | 95.6      | 99.1      | 101       | 95.0        | 97.6      | 85.9            | 104             | 98.0       | 101        | 106        | 94.9       | 93.4                  |
| Pr  | 12.4      | 12.2      | 12.8      | 12.7      | 12.9      | 13.0      | 11.8      | 12.4      | 12.9      | 13.4      | 12.8        | 12.8      | 11.3            | 13.2            | 12.8       | 13.1       | 13.8       | 12.5       | 12.3                  |
| Nd  | 52.6      | 51.9      | 52.1      | 52.0      | 52.9      | 52.7      | 49.5      | 50.4      | 51.4      | 56.0      | 52.8        | 54.0      | 48.7            | 54.3            | 53.4       | 53.7       | 56.8       | 52.8       | 51.5                  |
| Sm  | 11.7      | 11.0      | 11.0      | 10.6      | 10.6      | 10.6      | 9.41      | 9.91      | 9.99      | 11.6      | 10.6        | 11.4      | 10.8            | 11.5            | 11.4       | 11.6       | 12.0       | 11.3       | 10.7                  |
| Eu  | 3.00      | 2.82      | 2.97      | 3.06      | 3.01      | 2.98      | 2.87      | 2.95      | 2.94      | 3.01      | 2.96        | 3.04      | 2.84            | 3.08            | 3.06       | 3.02       | 3.30       | 3.11       | 3.03                  |
| Gd  | 9.72      | 9.91      | 9.55      | 9.83      | 9.58      | 9.51      | 9.05      | 9.25      | 9.67      | 10.3      | 9.80        | 10.3      | 9.48            | 10.0            | 9.69       | 9.69       | 10.4       | 9.64       | 9.46                  |
| Tb  | 1.36      | 1.31      | 1.26      | 1.28      | 1.26      | 1.27      | 1.13      | 1.22      | 1.29      | 1.33      | 1.33        | 1.39      | 1.32            | 1.41            | 1.35       | 1.41       | 1.43       | 1.34       | 1.31                  |
| Dy  | 8.07      | 7.36      | 7.47      | 7.50      | 7.80      | 7.51      | 6.90      | 7.02      | 7.90      | 8.13      | 7.83        | 8.02      | 7.28            | 7.65            | 7.47       | 7.79       | 7.91       | 7.64       | 7.38                  |
| Ho  | 1.45      | 1.26      | 1.29      | 1.26      | 1.30      | 1.35      | 1.16      | 1.15      | 1.37      | 1.35      | 1.29        | 1.39      | 1.31            | 1.40            | 1.33       | 1.44       | 1.42       | 1.35       | 1.28                  |

|    |      |      |      |      |      |      |      |      |      |      |      |      |      |      |      |      |      |      |      |
|----|------|------|------|------|------|------|------|------|------|------|------|------|------|------|------|------|------|------|------|
| Er | 3.61 | 3.36 | 3.45 | 3.41 | 3.42 | 3.38 | 3.12 | 3.08 | 3.51 | 3.59 | 3.51 | 3.61 | 3.36 | 3.61 | 3.49 | 3.70 | 3.55 | 3.47 | 3.44 |
| Tm | 0.47 | 0.46 | 0.44 | 0.45 | 0.46 | 0.46 | 0.41 | 0.44 | 0.50 | 0.49 | 0.50 | 0.51 | 0.45 | 0.47 | 0.46 | 0.48 | 0.47 | 0.47 | 0.45 |
| Yb | 2.93 | 2.73 | 2.73 | 2.70 | 2.77 | 2.69 | 2.48 | 2.53 | 2.93 | 2.75 | 2.86 | 2.98 | 2.74 | 2.91 | 2.80 | 2.97 | 2.84 | 2.81 | 2.73 |
| Lu | 0.38 | 0.36 | 0.36 | 0.37 | 0.37 | 0.35 | 0.35 | 0.36 | 0.40 | 0.40 | 0.39 | 0.41 | 0.39 | 0.40 | 0.40 | 0.42 | 0.40 | 0.39 | 0.38 |
| V  | 355  | 346  | 369  | 366  | 351  | 342  | 307  | 298  | 403  | 388  | 379  | 389  | 382  | 348  | 382  | 329  | 388  | 389  | 375  |
| Cr | 345  | 437  | 406  | 76.1 | 81.6 | 73.0 | 346  | 332  | 123  | 111  | 459  | 543  | 197  | 302  | 222  | 271  | 337  | 184  | 166  |
| Co | 48.4 | 45.6 | 47.5 | 45.8 | 46.1 | 45.3 | 49.9 | 50.6 | 43.3 | 46.7 | 49.9 | 57.8 | 48.1 | 41.4 | 48.7 | 40.1 | 46.6 | 44.9 | 43.6 |
| Ni | 226  | 265  | 257  | 139  | 158  | 131  | 247  | 246  | 302  | 257  | 255  | 293  | 136  | 172  | 132  | 163  | 195  | 120  | 107  |
| Cu | 254  | 284  | 284  | 249  | 304  | 266  | 259  | 267  | 364  | 541  | 193  | 412  | 257  | 241  | 234  | 64.4 | 247  | 332  | 326  |
| Zn | 128  | 124  | 141  | 133  | 134  | 131  | 116  | 118  | 150  | 123  | 140  | 146  | 136  | 120  | 145  | 120  | 142  | 136  | 132  |
| Ga | 25.8 | 23.1 | 26.2 | 25.8 | 25.2 | 25.7 | 25.4 | 25.5 | 24.5 | 25.7 | 25.4 | 26.5 | 27.9 | 25.5 | 27.3 | 23.5 | 26.0 | 26.6 | 25.7 |
| Rb | 3.82 | 13.3 | 43.4 | 38.5 | 52.1 | 45.7 | 53.5 | 53.1 | 22.6 | 65.1 | 70.6 | 68.9 | 58.5 | 38.8 | 46.9 | 70.3 | 23.1 | 59.7 | 58.6 |
| Sr | 882  | 870  | 830  | 580  | 1027 | 639  | 661  | 672  | 457  | 484  | 742  | 785  | 451  | 511  | 448  | 569  | 586  | 546  | 539  |
| Y  | 38.3 | 36.9 | 36.5 | 36.0 | 36.2 | 35.4 | 32.7 | 33.6 | 37.1 | 37.0 | 36.7 | 37.7 | 34.4 | 36.9 | 35.4 | 37.6 | 37.2 | 36.1 | 35.0 |
| Zr | 365  | 350  | 350  | 348  | 360  | 349  | 327  | 324  | 366  | 352  | 356  | 377  | 304  | 349  | 352  | 353  | 370  | 341  | 335  |
| Nb | 40.8 | 40.4 | 42.0 | 42.2 | 41.8 | 43.3 | 42.0 | 40.2 | 43.0 | 39.4 | 41.8 | 44.3 | 33.3 | 39.0 | 39.9 | 38.7 | 41.9 | 37.1 | 36.3 |
| Ba | 239  | 424  | 1306 | 405  | 1621 | 524  | 472  | 498  | 239  | 741  | 1065 | 1003 | 627  | 479  | 578  | 697  | 407  | 510  | 490  |
| Hf | 9.47 | 8.78 | 8.81 | 8.56 | 8.79 | 8.66 | 7.74 | 7.91 | 8.65 | 8.50 | 8.55 | 9.19 | 7.74 | 8.96 | 8.96 | 9.22 | 9.51 | 8.76 | 8.67 |
| Ta | 2.38 | 2.38 | 2.54 | 2.52 | 2.55 | 2.58 | 2.48 | 2.52 | 2.56 | 2.34 | 2.57 | 2.83 | 2.20 | 2.57 | 2.62 | 2.57 | 2.69 | 2.46 | 2.38 |
| Pb | 8.48 | 8.92 | 7.42 | 7.74 | 12.4 | 8.94 | 6.61 | 5.97 | 5.63 | 7.64 | 6.95 | 8.15 | 6.54 | 11.9 | 7.80 | 7.64 | 6.64 | 8.62 | 8.95 |
| Th | 7.12 | 6.90 | 6.84 | 6.77 | 7.03 | 6.97 | 6.70 | 6.63 | 6.58 | 6.61 | 6.57 | 6.81 | 7.21 | 8.12 | 6.49 | 8.35 | 6.97 | 6.47 | 6.25 |
| U  | 1.60 | 1.58 | 1.69 | 1.60 | 1.74 | 1.69 | 1.52 | 1.58 | 1.55 | 1.48 | 1.49 | 1.68 | 1.52 | 1.82 | 1.50 | 1.76 | 1.65 | 1.47 | 1.46 |

LOI: weight loss on ignition to 1000 °C. Mg# =  $Mg^{2+}/(Mg^{2+}+Fe^{2+})$  in atomic ratio, assuming 15% of total iron oxide is ferric.



**Table 3** Sr-Nd-Pb isotope ratios for the **analysed** volcanic rocks in the Sichuan Basin

| Sample                               | ST1-5    | YT1-1    | YT1-3    | YT1-6    | YT1-7    | ZG2-5    | ZG2-7    | ZG2-8    | 20LMD05     | 20LC06   | 20XL01   |
|--------------------------------------|----------|----------|----------|----------|----------|----------|----------|----------|-------------|----------|----------|
| Locality                             | ST1 Well | YT1 Well |          |          |          | ZG2 Well |          |          | Longmendong | Longchi  | Xinlin   |
| Rb( $\times 10^{-6}$ )               | 13.3     | 43.4     | 38.5     | 53.5     | 53.1     | 65.1     | 70.6     | 68.9     | 38.8        | 70.3     | 23.1     |
| Sr( $\times 10^{-6}$ )               | 870      | 830      | 580      | 661      | 672      | 484      | 742      | 785      | 511         | 569      | 586      |
| $^{87}\text{Rb}/^{86}\text{Sr}$      | 0.044372 | 0.151194 | 0.192215 | 0.234105 | 0.228342 | 0.389072 | 0.275352 | 0.254148 | 0.219834    | 0.357378 | 0.113896 |
| $^{87}\text{Sr}/^{86}\text{Sr}$      | 0.706884 | 0.707491 | 0.707355 | 0.706681 | 0.706694 | 0.706661 | 0.707085 | 0.707075 | 0.706865    | 0.707546 | 0.705942 |
| $^{26}\text{g}$                      | 0.000008 | 0.000007 | 0.00001  | 0.000008 | 0.000008 | 0.000008 | 0.000006 | 0.000007 | 0.000007    | 0.00001  | 0.000009 |
| $^{87}\text{Sr}/^{86}\text{Sr}(t)$   | 0.706721 | 0.706935 | 0.706648 | 0.705820 | 0.705854 | 0.705230 | 0.706072 | 0.706140 | 0.706057    | 0.706232 | 0.705523 |
| Sm( $\times 10^{-6}$ )               | 11.0     | 11.0     | 10.6     | 9.41     | 9.91     | 11.6     | 10.6     | 11.4     | 11.5        | 11.6     | 12.0     |
| Nd( $\times 10^{-6}$ )               | 51.9     | 52.1     | 52.0     | 49.5     | 50.4     | 56.0     | 52.8     | 54.0     | 54.3        | 53.7     | 56.8     |
| $^{147}\text{Sm}/^{144}\text{Nd}$    | 0.128166 | 0.127908 | 0.123307 | 0.114987 | 0.118988 | 0.125756 | 0.121209 | 0.128019 | 0.128721    | 0.130854 | 0.127975 |
| $^{143}\text{Nd}/^{144}\text{Nd}$    | 0.512530 | 0.512533 | 0.512526 | 0.512528 | 0.512528 | 0.512567 | 0.512570 | 0.512573 | 0.512507    | 0.512507 | 0.512561 |
| $^{26}\text{g}$                      | 0.000005 | 0.000008 | 0.000005 | 0.000006 | 0.000005 | 0.000004 | 0.000006 | 0.000013 | 0.000004    | 0.000004 | 0.000008 |
| $^{143}\text{Nd}/^{144}\text{Nd}(t)$ | 0.512313 | 0.512317 | 0.512317 | 0.512333 | 0.512327 | 0.512354 | 0.512365 | 0.512356 | 0.512289    | 0.512286 | 0.512344 |
| $\epsilon_{\text{Nd}}(t)$            | 0.16     | 0.22     | 0.24     | 0.55     | 0.42     | 0.96     | 1.17     | 1.00     | -0.31       | -0.38    | 0.77     |
| $T_{\text{DM}}(\text{Ma})$           | 1106     | 1098     | 1054     | 962      | 1002     | 1012     | 958      | 1028     | 1154        | 1184     | 1049     |
| $f_{\text{Sm}/\text{Nd}}$            | -0.35    | -0.35    | -0.37    | -0.42    | -0.40    | -0.36    | -0.38    | -0.35    | -0.35       | -0.33    | -0.35    |
| $^{206}\text{Pb}/^{204}\text{Pb}$    | 18.715   | 18.751   | 18.728   | 18.757   | 18.789   | 18.800   | 18.888   | 18.867   | 18.789      | 18.881   | 18.899   |
| $^{26}\text{g}$                      | 0.001    | 0.001    | 0.001    | 0.001    | 0.001    | 0.001    | 0.001    | 0.001    | 0.000       | 0.001    | 0.000    |
| $^{207}\text{Pb}/^{204}\text{Pb}$    | 15.609   | 15.613   | 15.612   | 15.611   | 15.613   | 15.617   | 15.620   | 15.621   | 15.626      | 15.629   | 15.614   |
| $^{26}\text{g}$                      | 0.001    | 0.001    | 0.001    | 0.001    | 0.001    | 0.001    | 0.001    | 0.001    | 0.000       | 0.001    | 0.000    |
| $^{208}\text{Pb}/^{204}\text{Pb}$    | 39.236   | 39.292   | 39.271   | 39.310   | 39.357   | 39.276   | 39.356   | 39.316   | 39.432      | 39.628   | 39.349   |
| $^{26}\text{g}$                      | 0.002    | 0.002    | 0.002    | 0.002    | 0.002    | 0.002    | 0.001    | 0.002    | 0.001       | 0.002    | 0.001    |
| $^{206}\text{Pb}/^{204}\text{Pb}(t)$ | 18.251   | 18.154   | 18.185   | 18.156   | 18.097   | 18.293   | 18.323   | 18.325   | 18.388      | 18.272   | 18.245   |

|                                      |        |        |        |        |        |        |        |        |        |        |        |
|--------------------------------------|--------|--------|--------|--------|--------|--------|--------|--------|--------|--------|--------|
| $^{207}\text{Pb}/^{204}\text{Pb}(t)$ | 15.585 | 15.582 | 15.584 | 15.580 | 15.578 | 15.592 | 15.591 | 15.593 | 15.606 | 15.598 | 15.581 |
| $^{208}\text{Pb}/^{204}\text{Pb}(t)$ | 38.572 | 38.500 | 38.520 | 38.440 | 38.403 | 38.533 | 38.542 | 38.597 | 38.845 | 38.685 | 38.446 |

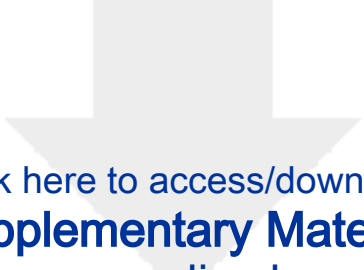
Notes:

1.  $^{87}\text{Rb}/^{86}\text{Sr}$  and  $^{147}\text{Sm}/^{144}\text{Nd}$  ratios are calculated using Rb, Sr, Sm and Nd contents by ICP-MS and measured  $^{87}\text{Sr}/^{86}\text{Sr}$  and  $^{143}\text{Nd}/^{144}\text{Nd}$  ratios by MC-ICP-MS.
2. In  $T_{\text{DM}}$  calculation, ratios of  $(^{143}\text{Nd}/^{144}\text{Nd})_{\text{DM}}$  and  $(^{147}\text{Sm}/^{144}\text{Nd})_{\text{DM}}$  took values of 0.51315 and 0.225, respectively.
3. In  $\epsilon_{\text{Nd}}(t)$  calculations, ratios of  $(^{87}\text{Sr}/^{86}\text{Sr})_{\text{CHUR}}$ ,  $(^{87}\text{Rb}/^{86}\text{Sr})_{\text{CHUR}}$ ,  $(^{143}\text{Nd}/^{144}\text{Nd})_{\text{CHUR}}$  and  $(^{147}\text{Sm}/^{144}\text{Nd})_{\text{CHUR}}$  are 0.7045, 0.0847, 0.512638 and 0.1967, respectively, while  $t = 258.5$  Ma.

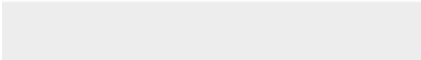

1 **Table 4** Distribution of the Emeishan basalts in the ELIP

| Zone              | Locality      | Rock type                       | Reference   |
|-------------------|---------------|---------------------------------|---|
| Inner zone        | Dali          | High-Ti basalts, low Ti basalts | Hanski et al. (2010)  |
|                   | Lijiang       | High-Ti basalts, low Ti basalts | Song et al. (2001), Zhang et al. (2006)                                       |
|                   | Binchuan      | High-Ti basalts, low Ti basalts | Song et al. (2001), Xiao et al. (2004),<br>Xu et al. (2007), Xu et al. (2001) |
|                   | Ertan         | High-Ti basalts, low Ti basalts | Song et al. (2001), Xu et al. (2001)  |
|                   | Jianchuan     | High-Ti basalts, low Ti basalts | Song et al. (2001)  |
|                   | Pingchuan     | Low Ti basalts                  | Xu et al. (2014)  |
|                   | Miyi          | High-Ti basalts                 | Xu et al. (2014)  |
|                   | Kangsi        | High-Ti basalts                 | He et al. (2010)  |
|                   | Wanmachang    | High-Ti basalts                 | He et al. (2010)  |
|                   | Shuidiqiao    | High-Ti basalts                 | He et al. (2010)  |
|                   | Longzhoushan  | High-Ti basalts                 | Xu et al. (2007)  |
| Intermediate zone | Yongsheng     | High-Ti basalts, low Ti basalts | Hao et al. (2004)   |
|                   | Dongchuan     | High-Ti basalts                 | Song et al. (2008), Xu et al. (2001)  |
|                   | Qingyin       | High-Ti basalts                 | Xu et al. (2014)  |
|                   | Qiaojia       | High-Ti basalts                 | Xu et al. (2014)  |
|                   | Weining       | High-Ti basalts                 | Xu et al. (2014)  |
|                   | Duge          | High-Ti basalts                 | Xu et al. (2014)  |
|                   | Zhaotong      | High-Ti basalts                 | Li et al. (2017c)   |
| Outer zone        | Zhijin        | High-Ti basalts                 | Lai et al. (2012), Xu et al. (2007)   |
|                   | Jinding       | High-Ti basalts                 | Xu et al. (2007)  |
|                   | Tubagou       | High-Ti basalts                 | Li et al. (2016b)   |
|                   | Baise         | High-Ti basalts                 | Fan et al. (2008)   |
|                   | Bama          | High-Ti basalts                 | Fan et al. (2008), Lai et al. (2012), Liu<br>et al. (2017)                    |
|                   | Tianyang      | High-Ti basalts                 | Fan et al. (2008), Liu et al. (2017)  |
|                   | Sichuan Basin | High-Ti basalts                 | This study  |

International standard samples values of major and trace elements and Sr-Nd-Pb isotopes are listed in it.



Click here to access/download  
**Supplementary Material**  
appendix.xlsx



No conflict of interest exists in the submission of this manuscript, and manuscript is approved by all authors for publication

I would like to declare on behalf of my co-authors that the work described was original research that has not been published previously, and not under consideration for publication elsewhere, in whole or in part.